REPORT NO. NADC-88065-60

HYDROGEN-FREE ELECTRODEPOSITION OF CADMIUM COATINGS ON HIGH-STRENGTH STEEL FOR CORROSION PROTECTION

R. Varma, T. Hoeller, and H. Shimotake
Chemical Technology Division
Argonne National Laboratory
Argonne, Illinois 60439

FEBRUARY 29, 1988

FINAL REPORT, TASK RO2201001

Approved for Public Release. Distribution is Unlimited

Prepared for
NAVAL AIR DEVELOPMENT CENTER
Warminster, PA 18974

NOTICES

REPORT NUMBERING SYSTEM – The numbering of technical project reports issued by the Naval Air Development Center is arranged for specific identification purposes. Each number consists of the Center acronym, the calendar year in which the number was assigned, the sequence number of the report within the specific calendar year, and the official 2-digit correspondence code of the Command Office or the Functional Department responsible for the report. For example: Report No. NADC-86015-70 indicates the fifteenth Center report for the year 1986 and prepared by the Systems and Software Technology Department. The numerical codes are as follows:

CODE	OFFICE OR DEPARTMENT
00	Commander, Naval Air Development Center
01	Technical Director, Naval Air Development Center
02	Comptroller
05	Computer Department
07	Planning Assessment Resources Department
10	Anti-Submarine Warfare Systems Department
20	Tactical Air Systems Department
30	Battle Force Systems Department
40	Communication & Navigation Technology Department
50	Mission Avionics Technology Department
60	Air Vehicle & Crew Systems Technology Department
70	Systems & Software Technology Department
80	Engineering Support Group

PRODUCT ENDORSEMENT – The discussion or instructions concerning commercial products herein do not constitute an endorsement by the Government nor do they convey or imply the license or right to use such products.

SECURITY CLASSIFICATION OF THIS PAGE

AD-A197711

REPORT DOCUMENTATION PAGE

1a REPORT SECURITY CLASSIFICATION Unclassified	1b RESTRICTIVE MARKINGS N/A
2a SECURITY CLASSIFICATION AUTHORITY	3 DISTRIBUTION AVAILABILITY OF REPORT Approved for public release; distribution unlimited
2b DECLASSIFICATION DOWNGRADING SCHEDULE	
4 PERFORMING ORGANIZATION REPORT NUMBER(S)	5 MONITORING ORGANIZATION REPORT NUMBER(S) NADC 88065-60
6a NAME OF PERFORMING ORGANIZATION Argonne National Laboratory 6b OFFICE SYMBOL (If applicable)	7a NAME OF MONITORING ORGANIZATION Naval Air Development Center
6c ADDRESS (City, State, and ZIP Code) Chemical Technology Division Argonne, IL 60439	7b ADDRESS (City, State, and ZIP Code) Code 6062 Warminster, PA 18974-5000
8a NAME OF FUNDING/SPONSORING ORGANIZATION 8b OFFICE SYMBOL (If applicable)	9 PROCUREMENT INSTRUMENT IDENTIFICATION NUMBER N/A
8c ADDRESS (City, State, and ZIP Code)	10 SOURCE OF FUNDING NUMBERS PROGRAM ELEMENT NO: 61153N; PROJECT NO: R02202; TASK NO: R02201001; WORK UNIT ACCESSION NO: N/A

11 TITLE (Include Security Classification)
Hydrogen-Free Electrodeposition of Cadium Coating on High Strength Steel for Corrosion Protection

12 PERSONAL AUTHOR(S)
R Varma, T. Hoeller and H Shimotake

13a TYPE OF REPORT	13b TIME COVERED	14 DATE OF REPORT (Year Month Day)	15 PAGE COUNT
Final Report	FROM ____ TO ____	1988, February 29	

16 SUPPLEMENTARY NOTATION

17 COSATI CODES			18 SUBJECT TERMS (Continue on reverse if necessary and identify by block number)
FIELD	GROUP	SUB GROUP	
11	03		Electrodeposition, pulse current, high current density pulse-nucleation, hydrogen-free cadmium, flow cell fluoborate, molten salt. (JES)
07	02		

19 ABSTRACT (Continue on reverse if necessary and identify by block number)

A new method of electroplating cadmium onto high-strength steel has been developed at Argonne National Laboratory. The method has three aspects: (1) high-rate electrodeposition by pulsed currents in a flow cell that uses a flowing electrolyte, (2) an optimized pulse-nucleation step, followed by pulse or DC current growth of the electrodeposit, and (3) the use of aqueous fluoborate electrolyte. The electrolyte flow/pulse-plating method with aqueous fluoborate provides a unique approach for high-speed, hydrogen-free cadmium plating of steel in engineering shapes and sizes.

A second method, which is based on electrodeposition from a molten salt, has also been investigated and shows promise as yet another hydrogen-free cadmium-plating technique.

20 DISTRIBUTION/AVAILABILITY OF ABSTRACT	21 ABSTRACT SECURITY CLASSIFICATION
☒ UNCLASSIFIED/UNLIMITED ☐ SAME AS RPT ☐ DTIC USERS	Unclassified
22a NAME OF RESPONSIBLE INDIVIDUAL Dr Vinod S Argarwala	22b TELEPHONE (Include Area Code) (215) 441-1122
	22c OFFICE SYMBOL NADC-Code 6062

DD FORM 1473, 84 MAR 83 APR edition may be used until exhausted
All other editions are obsolete

SECURITY CLASSIFICATION OF THIS PAGE

TABLE OF CONTENTS

		Page
ABSTRACT		1
1.0	PURPOSE	2
2.0	INTRODUCTION	2
3.0	BACKGROUND	3
	3.1 Advantages of Cadmium Coatings	4
	3.2 Hydrogen Codeposition During Electroplating - A Serious Drawback	4
	3.3 Surface and Morphological Aspects of the Electrodeposits	5
	3.4 Optimizing the Rate of Cadmium Deposition	5
4.0	ELECTRODEPOSITION FROM AQUEOUS ELECTROLYTE	6
	4.1 Overview	6
	4.2 Electrolyte Selection	7
	4.3 The Use of Additives	7
	4.4 Nucleation and Crystal Growth	7
	4.5 Pulse Plating	9
	4.6 Forced Electrolyte Convection and Pulse Current	9
5.0	EXPERIMENTAL	13
	5.1 Computer-Controlled Pulsed-Currents for Plating	13
	5.2 Computer Software for Pulse Profiles	18
	5.3 Plating Cells and Electrolytes	18
	5.4 Electrolyte-Flow Plating Cell	20
	5.5 Electrolyte Preparation Procedures	20
	5.6 Electrodeposition Procedure for Cadmium Plating from Fluoborate Electrolyte	25
6.0	EXPERIMENTAL RESULTS	27
	6.1 Electrochemistry of Cadmium Plating from Fluoborate Electrolyte	27

TABLE OF CONTENTS (contd)

	Page
6.2 Plating in Pulse Flow-Cell System	30
6.3 Current-Potential and Overpotential Rise Time	35
6.4 Nucleation and Growth Experiments	36
6.5 Pulse Plating Experiments from Stirred Electrolyte	37
6.6 Coating Evaluations	37
7.0 DISCUSSION OF RESULTS	40
7.1 Overview	40
7.2 Nucleation and Film Growth under DC or Pulse Currents	41
7.3 Cadmium DC Deposition from Fluoborate Electrolyte	50
7.4 Pulse Plating of Cadmium from Fluoborate Electrolyte	50
7.5 Preliminary Measurements of Hydrogen Codeposition	58
8.0 ELECTRODEPOSITION FROM MOLTEN SALT	62
9.0 CONCLUSIONS	64
ACKNOWLEDGEMENTS	67
APPENDIX I: Operation Manual for "Pulse Experiment" on the DEC 350 Professional Computer	68
APPENDIX II: Instrumentation and Operation Procedures for Running Computer Pulse Experiments	71
APPENDIX III: Electroplating from Alkaline-Cyanide Electrolyte	76
APPENDIX IV: Techniques for Substrate Preparation and Analysis of Electrodeposits	90
APPENDIX V: X-Ray Diffraction	96
REFERENCES	103

A-1

LIST OF TABLES

No.		Page
1	Pulse-Plating Instrumentation	14
2	Cadmium Fluoborate Bath Preparations	24
3	Effects of Plating Ssolution pH on Electrodeposition	32
4	Summary of Flow-Cell Platings	34
5	Deposition Current-Potential Data for Fluoborate Electrolyte	35
6	Overpotential Rise/Fall Times for Fluoborate Nucleation	36
7	Plating Thickness Measurements for Typical Cadmium Fluoborate Electrodeposits	40
8	Mobile Hydrogen Measurement Experiment	61
9	Eutectic Melts for Electrodeposition of Cadmium	62
10	Instrumentation Utilized in DC Plating	76
11	Cell Electrodes for DC Cadmium Cyanide Deposition	80
12	Preparation of Alkaline-Cyanide Electrolytes	80
13	Current-Potential Data for Cadmium Deposition from Cyanide Electrolyte	86
14	Cadmium Deposition Parameters From Alkaline-Cyanide Bath A	86
15	Cadmium Deposition Parameters From Alkaline-Cyanide Bath B	86
16	Cadmium Deposition Parameters From Alkaline-Cyanide Bath C	87
17	Mean Plating Thickness and Grain Size Measurements for Typical Cadmium Cyanide Electrodeposits	89
18	Major Cadmium Diffraction Peak Data	97

LIST OF FIGURES

No.		Page
1	Wiring diagram (front view) of computer operated pulse system	15
2	Wiring diagram (rear view) of computer operated pulse system	16
3	Computer programmable current-time profiles and defined parameters	19
4	Interior of electrolyte flow-cell	21
5a	Schematic of electroplating system under electrolyte flow and pulsed current	22
5b	Pulse electrolyte flow-cell plating system	23
6	Electrode assembly for electrodeposition of cadmium from fluoborate electrolyte	26
7	Cyclic voltammograms for cadmium electrodeposition from fluoborate electrolyte (with cadmium)	28
8	Cyclic voltammograms of cadmium electrodeposition from Fluoborate electrolyte (without cadmium)	29
9	Potentiostatic current-time transients for the electrodeposition of cadmium from fluoborate electrolyte	31
10	X-ray diffraction pattern of cadmium electrodeposited from fluoborate electrolyte	38
11	Optical micrograph of steel surface preparations	42
12	SEM micrograph of cadmium electrodeposited from fluoborate electrolyte on mild steel at 0.030 $A \cdot cm^{-2}$ for 10 min	43
13	SEM of cadmium electrodeposited from fluoborate electrolyte on mild steel under 0.945s nucleating pulse	44
14	SEM of cadmium electrodeposited from fluoborate electrolyte on mild steel under 0.50 $A \cdot cm^{-2}$ nucleating pulse	46
15	SEM of cadmium electrodeposited from fluoborate electrolyte under various nucleating pulses	47
16	SEM of cadmium electrodeposited from fluoborate electrolyte under various nucleating pulses	48

LIST OF FIGURES (contd)

No.		Page
17	Current-time nucleation regimes for cadmium electrodeposited on mild steel from fluoborate electrolytes	49
18	SEM micrographs of surfaces of cadmium electrodeposited from fluoborate electrolyte under initial nucleating pulse followed by DC film growth	51
19	SEM micrographs of cros sections of cadmium electrodeposited from fluoborate electrolyte under initial nucleating pulse followed by DC film growth	52
20	SEM micrographs of cadmium electrodeposited from fluoborate electrolyte under nucleating pulse followed by DC film growth . .	53
21	SEM micrographs of cadmium electrodeposited from fluoborate electrolyte (flowing at 3.5 $m.s^{-1}$) under pulse currents	55
22	SEM micrographs of cadmium electrodeposited from fluoborate electrolyte (flowing at 1.7 $m.s^{-1}$) under under pulse curents . . .	56
23	SEM micrographs of surfaces of cadmium electrodeposited from fluoborate electrolyte (flowing at 1.7 $m.s^{-1}$) under pulse currents	57
24	SEM micrographs of cadmium electrodeposited from fluoborate electrolyte on steel under cathodic pulse at various current densities.	59
25	SEM micrographs of cadmium electrodeposited from fluoborate electrolyte under initial nucleating pulse and cathodic pulsed-growth	60
26	Schematic of electrochemical cell system for molten salt deposition	63
27	Cyclic voltammograms of iron in the melt $AlCl_3$-NaCl-$BaCl_2$ (eutectic)-CdI_2 at 148.5°C	65
28	Electrochemical cell for deposition of cadmium from alkaline-cyanide electrolyte	78
29	Electrode assembly for deposition of cadmium from alkaline-cyanide electrolyte	79
30	Cadmium deposition efficiency versus current density for alkaline-cyanide baths (contd)	81

LIST OF FIGURES (contd)

No.		Page
31	Cadmium deposition potentials versus Cd^{2+}/Cd^{o} for electrodepositon from alkaline-cyanide bath A	82
32	Cadmium deposition potentials versus Cd^{2+}/Cd^{o} for electrodeposition from alkaline-cyanide bath B	83
33	Cadmium deposition potentials versus Cd^{2+}/Cd^{o} for electrode position from alkaline-cyanide bath C	84
34	SEM micrograph of cadmium electrodeposited on nickel at different current densities from alkaline-cyanide electrolyte	88
35	Hexagonal close-packed unit cell of cadmium	96
36	X-ray diffraction pattern of cadmium electrodeposited on nickel from alkaline-cyanide electrolyte at 2 $A \cdot cm^{-2}$ (0^{o}-rotation)	98
37	X-ray diffraction pattern of cadmium electrodeposited on nickel from alkaline-cyanide electrolyte at 2 $A \cdot cm^{-2}$ (90^{o}-rotation)	99
38	X-ray diffraction pattern of cadmium electrodeposited on AISI 4340 steel from alkaline-cyanide electrolyte at 15 $mA \cdot cm^{-2}$	100
39	X-ray diffraction pattern of cadmium electrodeposited on AISI 4340 steel from alkaline-cyanide electrolyte at 4.3 $mA \cdot cm^{-2}$.	101

Hydrogen-Free Electrodeposition of Cadmium Coatings on High-Strength Steel for Corrosion Protection

R. Varma, T. Hoeller, and H. Shimotake
Chemical Technology Division
Argonne National Laboratory
Argonne, Illinois 60439

ABSTRACT

A new method of electroplating cadmium onto high-strength steel has been developed at Argonne National Laboratory. The method has three aspects: (1) high-rate electrodeposition by pulsed currents in a flow cell that uses a flowing electrolyte; (2) an optimized pulse-nucleation step, followed by pulse or DC current growth of the electrodeposit; and (3) the use of aqueous fluoborate electrolyte. The electrolyte flow/pulse-plating method with aqueous fluoborate provides a unique approach for high-speed, hydrogen-free cadmium plating of steel in engineering shapes and sizes.

A second method, which is based on electrodeposition from a molten salt, has also been investigated and shows promise as yet another hydrogen-free cadmium-plating technique.

1.0 PURPOSE

The objective of the work was to electrodeposit 12.7 μm (0.5 mil) thick cadmium coatings on high-strength steel (300M or AISI 4340) at high speed without hydrogen ingress into the bulk steel. The work involving cadmium electrodeposition from alkaline-cyanide and fluoborate baths, as well as from molten salt is described. Experiments were conducted in a flow system designed to provide forced convection of the electrolyte during electroplating to facilitate high-rate plating. Results obtained with this system are described. The results of high-rate DC and pulsed current experiments are studied including the use of a nucleating pulse to initiate growth and to provide good adhesion of the coating to the substrate. Optimization of the flow and pulsed systems is shown to be essential in developing a new method for electroplating hydrogen-free cadmium on steel.

2.0 INTRODUCTION

High-strength 4340 or 300M steel components in naval aircraft are subject to abrupt mechanical failures[1,2] during service in a marine environment because of hydrogen embrittlement, stress corrosion cracking, and corrosion fatigue. A high-strength steel specimen under load may fail from the combined effects of electrochemical corrosion and stress.

Surface cracks on steel substrates may originate from localized corrosion, which may include preferred chemical attack along grain boundaries or development of internal stresses related to hydrogen-atom diffusion into the bulk. One of the proposed mechanisms[1] of hydrogen embrittlement is the stress caused by high internal pressure due to recombination of hydrogen atoms

in bulk steel to form hydrogen molecules. For corrosion resistance during service in marine environments, electrodeposition of a thin coating of cadmium onto steel has been the practice[3], particularly in military and aerospace applications. Cadmium is the most widely used coating for corrosion protection of high-strength steel components (e.g., fasteners, landing gear, springs, bearing rings) in marine environments. Cadmium out performs zinc of equal thickness in such environments by a factor of approximately two and may also be used to provide significant protection in industrial environments (i.e., SO_x/NO_x-H_2O-CO_2). Cadmium excels in lubricity, solderability, electrical conductivity, and compatibility with aluminum alloys. Additionally, its corrosion products are relatively nonbinding, and of themselves, are not detrimental to the substrate. Hence, a cadmium coating is preferred for use in the aircraft industry.

3.0 BACKGROUND

Direct current electroplating of cadmium from cyanide baths is the state-of-the-art technology practiced for corrosion protection in aerospace and naval applications. A typical plating, for example, involves electrodeposition from an alkaline-cyanide electrolyte (an aqueous solution prepared from $CdCO_3$, $Cd(CN)_2$, NaCN, and NaOH) using low current densities. Some of the drawbacks of this plating process are: (1) significant codeposition of hydrogen during cadmium plating, (2) long time periods of plating (for example, 0.5 mil thick deposits may take 10 min), and (3) environmental concerns for safe disposal of the toxic plating-waste themselves.

In our initial work, cadmium was to be electrodeposited as a fine-grain coating on high-strength steel at high rates using pulsed or direct currents

from cyanide electrolytes. Hydrogen embrittlement of the substrate due to excessive hydrogen codeposition prevailed in that process. With this result in mind, two other sources for producing dense and mechanically adherent electrodeposited cadmium coatings on steel were considered: (1) fluoborate electrolyte and (2) molten-salt electrolytes.

3.1 Advantages of Cadmium Coatings

Cadmium coatings offer anodic protection,[3] particularly in industrial environments; being anodic to iron, dissolution of the coating takes place in preference to that of the underlying steel substrate (E^o, Cd^{+2}/Cd^o = -0.4030 V vs. SHE; E^o, Fe^{+3}/Fe^o = -0.037 V vs. SHE). The flow of electrons from the dissolution of the cadmium decreases the potential of the underlying steel substrate, making it more cathodic and therefore more noble. A corrosion couple of this type becomes more significant when the cathodic area is small compared with the anodic area, as is the case of a tiny hole or crack in the cadmium coating. Cadmium coatings offer protection to the steel substrates in salt-water environments by forming a passive film of Cd(OCl)Cl which may be impervious to transport of Cl^- or H^+ ions. For all these reasons, cadmium is to be preferred as a coating in a marine environment.

3.2 Hydrogen Codeposition During Electroplating - A Serious Drawback

Cadmium coatings are usually electrodeposited from cyanide electrolytes by use of conventional plating techniques. During this process, hydrogen is codeposited, a portion of which enters the steel with the consequent deleterious effect on mechanical properties. The subsequent baking of plated steel for removal of hydrogen is not very efficient because cadmium acts as a barrier for hydrogen diffusion. Plating from other electrolytes (such as fluoborate) has been claimed[4,5] as being less prone to hydrogen embrittlement than from the cyanide bath. This study addresses this issue and provides alternatives.

3.3 Surface and Morphological Aspects of the Electrodeposits

An ideal defect-free surface, such as one without grain boundaries, generally provides less variations in local potential in an aqueous environment, and such a surface may provide improved corrosion resistance. Coatings are prone to degradation because their grain boundaries have higher free energy and are therefore susceptible to chemical attack. As grain sizes are decreased, a larger portion of the surface is at higher-free energy, but the ratio of the cathodic to the anodic areas (i.e, single-crystals to grain boundary areas) is decreased. In such a microcrystalline layer, thermodynamic stability of the layer by formation of a passive film may impede the diffusion and transport of ions such as Cl^-, OH^-, etc. and thereby decrease corrosion rates. Corrosive attack on a coating, such as cadmium, causes an electron current. This electron current provides corrosion protection to the substrate even where cracks in the coating may exist. This anodic protection is maximized by a microcrystalline cadmium layer. On the other hand, a total disappearance of all the grain boundaries, as in the formation of a continuous amorphous layer, may offer the best corrosion resistance. With no macroscopic surface-potential differences in an amorphous layer, corrosion is not kinetically favored. Where scratches or cracks are common in the electrodeposit, a microcrystalline cadmium layer, which offers anodic protection to the substrate, is better for corrosion protection.

3.4 Optimizing the Rate of Cadmium Deposition

Techniques developed at Argonne for depositing a microcrystalline cadmium layer provide high-rate electrodeposition from aqueous or molten salt electrolytes. High-rate deposition means achieving increased mass transport of Cd^{+2}-cation species across the diffusion layer. The electrochemical transport of cadmium in an electrolyte is diffusion controlled, and the rate is given by a limiting current density,

$$i_L = zFD \frac{Co}{\delta} \quad (1)$$

where

z = number of electrons required for electroneutralization of one Cd^{+2}-ion species,

F = Faraday's constant,

D = diffusion coefficient

δ = diffusion layer thickness,

and

Co = bulk concentration of Cd^{+2}-ion species.

This equation predicts that the rate of deposition can indeed be maximized by increasing the plating current density near i_L by an optimal choice of deposition parameters. High-rate cadmium deposition can be achieved by avoiding mass transfer limitation and codeposition of hydrogen at the limiting current.

4.0 ELECTRODEPOSITION FROM AQUEOUS ELECTROLYTE

4.1 Overview

Experimental parameters most important in controlling deposition rates are the overpotential η, the diffusion layer thickness δ, and the bulk concentration of the reducible cadmium species, Co.

By definition, the deposition overpotential, η, is the difference $E - E^o$, where E is the actual potential applied to the electrode and E^o is the open-circuit electrode potential for the Cd^{+2}/Cd^o couple. Appropriate high overpotentials can be applied by proper choice of galvanostatic current densities at the electrode surface. At high current densities, electroreduction of many species and complexes (including Cd^{+2} and H^+ ions)

occurs, which reduces the plating efficiencies and causes the the commonly observed hydrogen codeposition and the embrittlement of steel.

A high deposition rate for cadmium avoiding codeposition of hydrogen requires that the thickness of the electrochemical diffusion layer be reduced, that the metal-ion species be replenished by forced convection of the electrolyte, and the overpotential be kept below the hydrogen overvoltage. It became clear in the early part of this study that both pulse plating and electrolyte flow must be utilized in order to achieve high deposition rate (i.e., use of high limiting current in the deposition process). An increase in the bulk concentration may also help to augment the deposition rate. Therefore, the characteristics of the cadmium deposits may be improved by an optimal choice of experimental parameters. Some of these are discussed in detail below.

4.2 Electrolyte Selection

The hydrogen codeposition *during* cadmium electroplating on steel substrates from aqueous fluoborate electrolyte is less favored than in the case of its electrodeposition from cyanide electrolyte because of higher hydrogen overvoltage on steel from fluoborate electrolyte. Furthermore, the cyanide acts to block recombination of monoatomic H-species which enter directly into the substrate recombining to form diatomic hydrogen.

4.3 The Use of Additives

The use of additives in aqueous fluoborate plating baths may increase the throwing power for improved coating uniformity on the substrate. With the voids and edges covered, a smoother deposit is produced with additives.

4.4 Nucleation and Crystal Growth

Coatings that will exhibit adherence to the substrate and that will have the necessary fine-grained and coherent morphology require: (1) an appropriate nucleation step and (2) high-rate electrocrystallization- growth.[6]

Initial nucleation steps, which consist of formation of cadmium atom clusters of critical size distributed at a high density over the surface, are essential for providing strong adhesion of the electrodeposited layer onto the substrate. Nucleation is dependent on the density of surface sites available on the substrate, the overpotential for the nucleation process, and the time period of deposition. The density of the nuclei cluster that is formed rises exponentially with the overpotential. Uniform nucleation coverage of the substrate surface using a moderate nucleation overpotential pulse of appropriate width is desired. This event, if followed by electrocrystallization under controlled DC or pulse currents, will produce a strongly adherent electrodeposited coating of cadmium on steel.

The process of electrochemical growth of a cadmium layer on steel substrate which has been optimally nucleated generally will occur along certain crystallographic directions. In general, the preferred orientation may result in dendritic crystal growth, an undesirable result. However, proper control of the metal-cation activity in the electrolyte and the electrolyte pH, the use of additives, and a pulse profile which can be both cathodic (with high peak current) and anodic may reduce this risk, even at high current densities. This was the approach taken.

A preliminary investigation on the fundamentals of the electrocrystallization process for cadmium electrodeposition from fluoborate electrolyte provided new information; certain advantages in using this electrolyte--particularly with regard to avoiding codeposition of hydrogen--were revealed. Cyclic voltammetry and chronoamperometry analysis in conjunction with microstructural examination of the electrodeposits by optical and scanning electron microscopy were conducted to provide this information. The results

from the experiments suggested the possibility of specific control of the deposition conditions during nucleation and the initial electrocrystallization stages, both to avoid hydrogen uptake and to produce a continuous, nonporous, protective cadmium layer before further film growth takes place.

4.5 Pulse Plating

A number of studies that involve pulse-plating techniques have been reported in the literature.[7,8,9] These studies have shown that a high concentration gradient of metal-cation species across the diffusion layer at the beginning of each successive cathodic pulse can be assured by proper choice of pulse peak currents, cathodic pulse duration, rest period and/or anodic pulse, and pulse repetition rates. Bipolar pulses with appropriate cathodic and anodic currents, may be utilized to avoid formation of dendritic deposits. A nucleating pulse followed by an appropriate net cathodic pulse (i.e., periodic reverse pulse sequence) is ideally desired for cadmium plating with little chance of hydrogen embrittlement.

4.6 Forced Electrolyte Convection and Pulse Current

Forced convection or electrolyte flow near the cathode surface (so as to create turbulence) may (1) enhance the concentration gradient of metal ion-species across the diffusion layer by making the pulsating diffusion layer thinner and (2) replenish the metal-ion concentration at the diffusion layer during plating.

Theoretical considerations show that the diffusional mass transfer during electrodeposition obeys Fick's second law, i.e.,

$$\frac{\partial C}{\partial t} = D\frac{\partial^2 C}{\partial x^2} \qquad (2)$$

where C is the concentration and D is the diffusion constant. Fick's law has been solved for the initial conditions,

$$t = 0,\ x \geq 0 : C = Co \tag{3}$$

$$t > 0,\ x = 0 : D \frac{\delta C}{\delta x} = \frac{i(t)}{zF}\ , \tag{4}$$

and the following pulse conditions,

$$i(t) = i_p : mT < t \leq (m + \theta)\ T\ , \tag{5}$$

and

$$i(t) = 0 : (m + \theta)\ T < t \leq (m + 1)\ T \tag{6}$$

where Co is the initial concentration, i is the current, i_p is peak pulse current during time t_{on}, z is the number of electrons involved, F is Faraday's constant, T is a cycle period, θ is the duty cycle (t_{on}/T), and m is an integer, 1, 2, 3... .

The metal ion concentration at the surface is then

$$C(t, 0) = Co - \frac{2i_p}{zF\delta\alpha} \cdot \sum_{n=1}^{\infty}\left[\frac{1}{(2n-1)^2}\{1 + \exp[-(2n-1)^2\alpha t]\cdot\{\exp[(2n-1)^2\alpha\theta T]-1\}\}\right.$$

$$\left. \cdot \{\frac{1-\exp[(2n-1)^2\alpha mT]}{1-\exp[(2n-1)^2\alpha T]}\} - \exp\ (2n-1)^2\alpha mT]\right] \tag{7}$$

where $\alpha = (\pi^2 D/4)^2$, and δ is the thickness of the diffusion layer. The concentration of metal ion at the end of a pulse is

$$C_{on} = Co - \frac{8i_p\delta}{zF\pi^2 D} \sum \frac{1}{(2n-1)^2} \frac{1-\exp[-(2n-1)^2\alpha\theta T]}{1-\exp[-(2n-1)^2\alpha T]} \tag{8}$$

The concentration of metal ion at the end of a rest period is

$$C_{off} = Co - \frac{8i_p\delta}{zF\pi^2D} \Sigma \frac{1}{(2n-1)^2} \frac{\exp[-(2n-1)^2\alpha T]-\exp[-(2n-1)^2\alpha(T-\theta T)]}{\exp[-(2n-1)^2\alpha T]-1} \quad (9)$$

The limiting current density of DC plating is expressed by

$$i_{dl} = zFDCo\delta^{-1} \quad (10)$$

The plating current density must be kept less than i_{dl} to prevent hydrogen evolution. In the case of pulse plating, the limiting current density is defined as the current density to result in $C_{on} = 0$. Using Eq. 9, the limiting current density for pulse deposition is

$$i_{pl} = \frac{1}{\frac{8\delta}{zF\pi^2DCo} \Sigma \frac{1}{(2n-1)^2} \frac{1-\exp[-(2n-1)^2\alpha\theta T]}{1-\exp[-(2n-1)^2\alpha T]}} \quad (11)$$

Therefore, the ratio between the two limiting current densities are from Eqs. 10 and 11,

$$\frac{i_{pl}}{i_{dl}} = \frac{1}{\frac{8}{\pi^2} \Sigma \frac{1}{(2n-1)^2} \frac{1-\exp[-(2n-1)^2\alpha\theta T]}{1-\exp[-(2n-1)^2\alpha T]}} \quad (12)$$

When $T \ll 1$,

$$\frac{i_{pl}}{i_{dl}} \xrightarrow[\theta,\ T\ll 1]{} \frac{1}{\theta} \quad (13)$$

implies that the limiting current density during pulse current plating could be increased significantly, as high as 100 times if the duty cycle θ is

lowered to 0.01. For example, if a pulse condition such as t_{on} = 10 μs and T = t_{on} + t_{off} = 1 ms, is adopted (i.e., θ = 10/1000 = 0.01), the pulse limiting current density could be raised by 100 times the DC limiting current density. (The i_{dl} for the present system has been estimated to be ~1.0 A•cm^{-2}.) However, further analysis shows that when T<<1

$$\frac{i_{pl}^{av}}{i_{dl}} \xrightarrow[\theta,\ T\ll 1]{} 1 \qquad (14)$$

where $$i_{pl}^{av} = \frac{1}{T}\int_0^T i(t)dt,$$

the average pulse limiting current density could not exceed the DC limiting current density. Furthermore, as the pulse period T becomes shorter, the recovery of the surface concentration becomes insufficient. To overcome the limitation of the pulse plating, the thickness of the diffusion layer must be reduced. This reduction can be achieved effectively by the electrolyte-flow cell.

The thickness of the hydrodynamic boundary layer in a turbulent regime on a smooth flat plate can be calculated by Karman's equation

$$\frac{\delta_H}{x} = 0.376\ Re^{-1/5} \qquad (15)$$

where Re is the Reynold's number characterizing the flow rate. The diffusional boundary layer thickness is related to δ_H by Levich's equation

$$\delta = 0.6\ Sc^{-1/3} \cdot \delta_H \qquad (16)$$

where Sc is the Schmidt number. Therefore, simply substituting Eq. 15 into Eq. 16 results in

$$\frac{\delta_1}{\delta_2} = \frac{Re_2}{Re_1}^{1/5} \quad (17)$$

indicating that the diffusion boundary layer thickness can be reduced by raising the Reynolds number of the plating solution flow. For example, if the Reynolds number is raised from 1,000 to 25,000, the thickness of diffusion boundary layer would be reduced by a factor of 2. It is important that (1) the duty cycle be cut short to achieve high pulse current density, and (2) the flow rate of the plating solution be increased to approach the turbulent regime to provide an even flux of metal ionic species near the substrate surface. An optimized combination of both the pulse and high flow rate would provide high-speed electrodeposition without exceeding the limiting current density; consequently, no hydrogen codeposition would take place.

5.0 EXPERIMENTAL

5.1 Computer-Controlled Pulsed-Currents for Plating

A pulsed-current instrumentation setup capable of producing milli- and microsecond pulses with current densities up to 5 $A \cdot cm^{-2}$ was desired. Steel coupons with areas of 25 cm^2 were to be used as cathodes for deposition studies. This approach required a power supply capable of at least 100 A. To facilitate variation of any or all of the pulse profile parameters, the experiment was computer-driven. A digital storage oscilloscope with disk drive was used to record current and potential waveforms.

The components of the pulse-plating instrumentation are listed in Table 1.

Table 1. Pulse-Plating Instrumentation

Computer	DEC Professional 350 with 10-Mbyte Hard Disc Drive
Power Supplies	Transrex Programmable Cell Cycler (500 A at 8.5 V) Model ISR 2307 (Gultan Industries) with Model CU - 5000 Cooling Unit (Electro Impulse Inc.)
	Wenking High-Power Potentiostat Model HP 72 (Bank Electronik, W. Germany)
Voltage Calibrator	Model DVC 8500 (Datel)
Crate Driver	Camac Crate Model 1500 - P1 A/B (Kinetic Systems)
Switch	Double Pole - Double Throw (General Electric) Type A: 200 A, 250 V DC
Resistor	225 W, 1 Ω (Mallory)
Data Acquisition	Norland Model 3001 Waveform Analyzer with Tektronix Model 620 Monitor
	7100B Strip Chart Recorder with 2 Model 17501A Plug-in Modules (Hewlett-Packard)
Data Plotting	HP 7044A X-Y Recorder (Hewlett-Packard)
Data Storage	8-in. Floppy Disc Drive (Industrial Microsystems)
Miscellaneous	Unity Gain Buffer Amplifier 2 - 4/0 AWG Hypalon Loco Cable, 600 V (Cyprus Wire and Cable)
	Various wires, electrical connectors, and coaxial cables.

A schematic wiring diagram of the computer pulse instrumentation is given in Figs. 1 and 2. Appendices I and II give special operational procedures for the computer and experimental instrumentation, respectively. An overview of the theory for pulsed-current operation follows.

The experimenter first programs the described pulse parameters into the computer. When the computer begins execution of the program, it sends digital voltage signals to the Camac crate. The crate amplifies the signal to a 10-V full-scale range and sends an analog signal to the chosen power supply. This signal drives the current in proportion to the full-scale output of the power

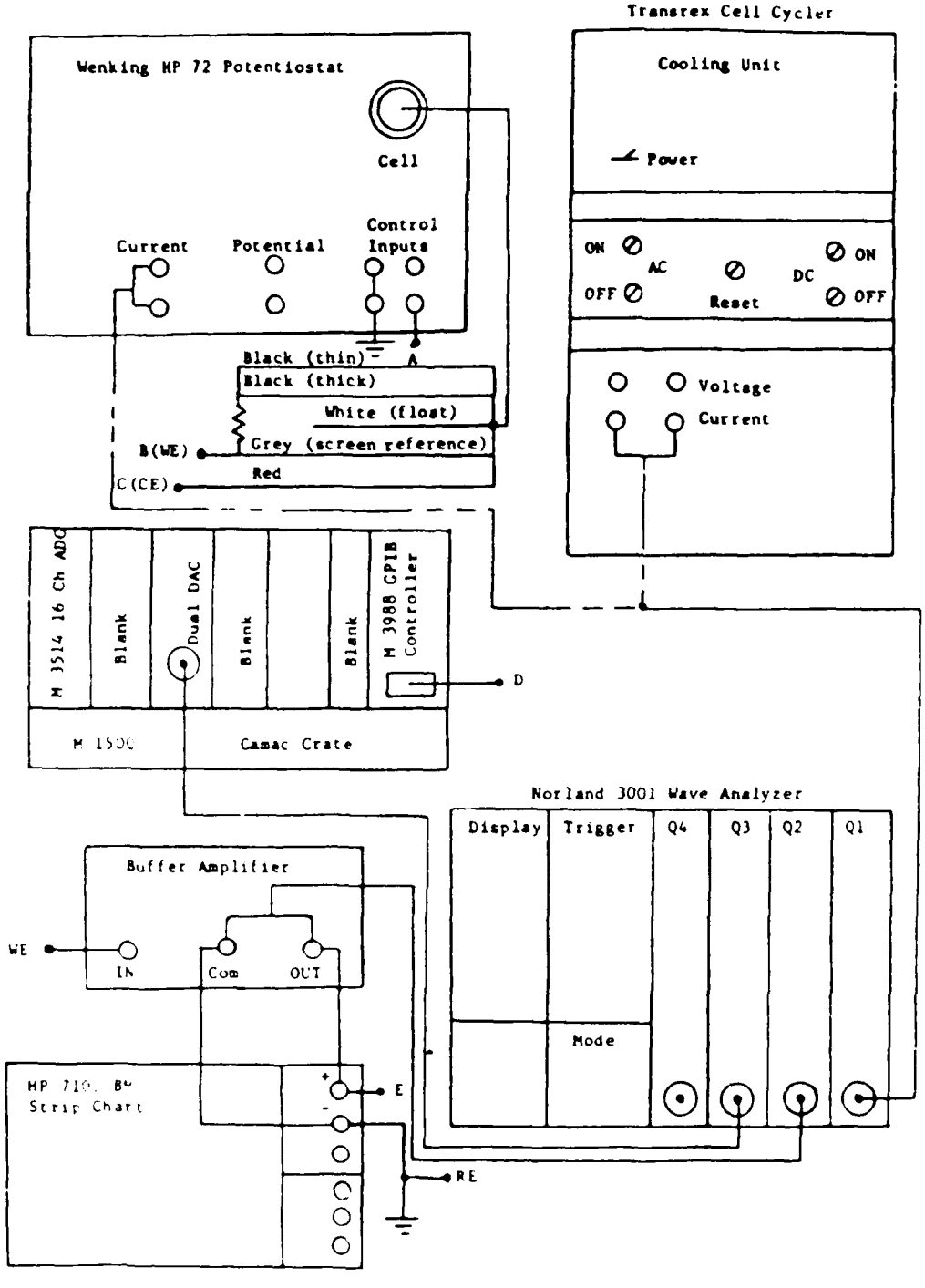

Fig. 1. Wiring diagram (front view) of computer operated pulse system.

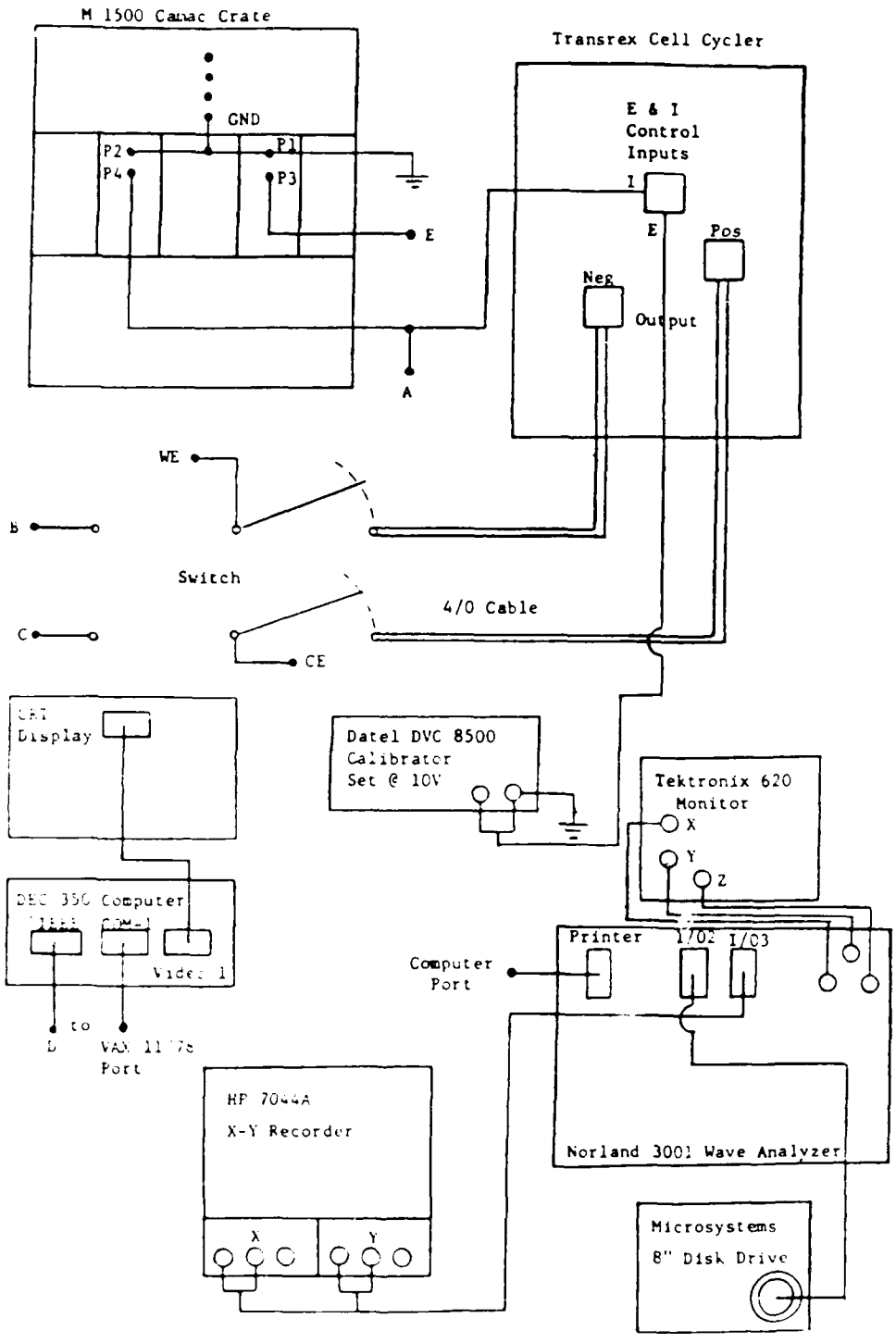

Fig. 2. Wiring diagram (rear view) of computer operated pulse system.

supply. The Wenking Potentiostat is used according to manual specifications in the controlled-current (galvanostatic) mode. With a 1-Ω current-control resistor, the Wenking Power supply may give a maximum current of 10 A at ±20 V. The Transrex power supply is rated to ±500 A at 8.5 V, but, as shunted for the experiment, it may provide 150 A at 20 V. The extra voltage (not current) is needed for controlling current through the resistive cell. To use the Transrex power supply for bipolar current pulsing, a -10 V reference voltage is supplied to the control inputs. As a result, the effective operating limits of the Transrex is 150 A at ±10 V.

Data comes from several sources--current, potential, and time measurements. The buffer amplifier monitors the reference potential of the posts on either power supply.

Data may be monitored and recorded by several methods. The Camac crate is equipped with an analog-to-digital converter which monitors the potential at the working electrode with respect to the reference electrode. In this way, the speed of data acquisition is limited to the clock rate at which the computer can process and store data on a 10-megabyte hard disc drive. For the work described herein, the read and write times to the hard disk drive limited the computer execution time to about 25 ms per data point. This relatively poor execution speed may also be attributed to software limitations; fewer programming steps may decrease this time.

The strip chart recorder is used in conjunction with the reference electrode for monitoring the working electrode potential during DC experiments. It is also used for monitoring the potential of a long nucleating pulse followed by a DC growth current.

The strip chart recorder is not adequate for recording potential during a fast current pulse. In this case a Norland 3001 Waveform Analyzer was used.

Depending on the input channel, the Waveform Analyzer has digital time resolution to 2 or 5 μs/point. Four separate channels for monitoring various waveforms are available. In this experimental setup, two channels monitor the current and potential waveforms, and a third channel is a trigger channel for capturing fast waveforms. A built-in microprocessor can be programmed to perform a wide variety of arithmetic and logical operations, such as rise-time determinations and waveform differentiations. An 8-in. floppy disc drive provides hard storage of waveforms displayed on the monitor. The operator can retrieve data by output to an x-y recorder (refer to the Norland 3001 owner's manual) or by downloading the data to the mainframe VAX 11/780 (see Appendix II). Once the data is in the VAX, publication-quality graphics can be obtained.

5.2 Computer Software for Pulse Profiles

The computer pulse program generates four types of pulses--nucleation, cathodic, anodic, and growth. By definition, the nucleation pulse is a single deposition pulse which occurs before any other pulse. It is responsible for the initial nucleation on the substrate. The cathodic (deposition) pulse and anodic (dissolution) pulse follow, and form a cycle which may be repeated. After execution of these pulse cycles, one long [growth pulse may be added. Defined by up to 12 different current, time, and repetition parameters, a combination of any of these pulse types may be used during a given experiment. The resultant waveform is called the pulse profile. Some possible pulse profiles are shown in Fig. 3. The software responsible for the pulse program is printed in the Addendum to this report.

5.3 Plating Cells and Electrolytes

Cadmium was electrodeposited on Types 4340, 300M, and 1018 steel substrates from aqueous cyanide and fluoborate electrolytes to provide a large

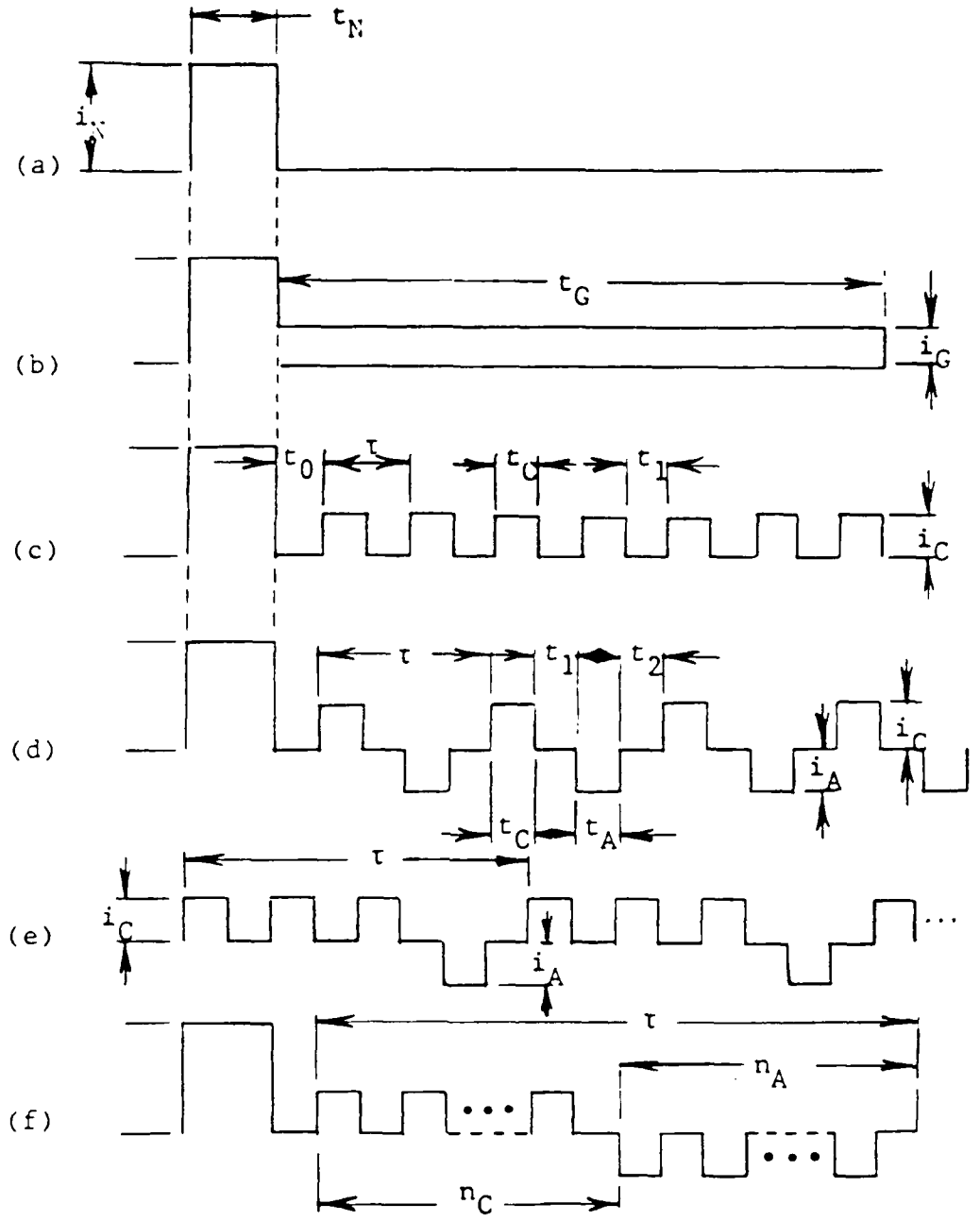

Fig. 3. Computer programmable current-time profiles and defined parameters: (a) nucleation, i_N t_N; (b) nucleation and DC growth, i_N, t_N, t_G, i_C; (c) nucleation and cathodic pulse, i_N, t_N, t_0, i_C, t_1; (d) nucleation and bipolar pulse, i_N, t_N, t_0, i_C, t_C, t_1, i_A, t_2; (e) multiple cathodic and anodic pulse; and (f) most general nucleation and bipolar pulse, parameters same as (d) including number of cathodic and anodic repeats, n_C and n_A. τ is the repeat cycle time.

number of samples for evaluation. Both electrolytes were used in a conventional cell, with an electrode assembly that was attached to a Lucite coverplate incorporating one steel working electrode (WE), two cadmium counter electrodes (CE), and a suitable reference electrode (RE). The cells and electrolytes used in the case of the cyanide plating are given in Appendix III.

5.4 Electrolyte-Flow Plating Cell

An electrolyte flow-cell was constructed from two blocks of polyethylene which, when closed, enclose a liquid-flow channel between the steel cathode coupon and cadmium anode that is separated from the cathode by 3-4 mm (Fig. 4). The other components of the system are a polyethylene tank for storing up to 10 gallons of the electrolyte, PVC piping, valves, a flowmeter, and a circulating pump. Figure 5(a) and 5(b) are respectively the schematics and a photograph of the assembled system. The electrolyte flow-cell was interfaced with a DC or pulse source for the experiments. Type 300M steel samples, 1.125 in. in diameter by 0.060 in. thick, were plated with cadmium under different current and flow conditions. The pulse generator used in this system was a Sorensen SRL-20-25 power supply and a LWD scientific minipulser.

5.5 Electrolyte Preparation Procedures

The concentrations and operating conditions of two cadmium fluoborate electrolyte preparations are given in Table 2. The prescriptions for the baths were based on the work of Lowenheim[10] and on a 1955 U.S. patent.[5]

Appropriate amounts of boric acid H_3BO_3 (Fisher, reagent), ammonium fluoborate NH_4BF_4 (Cerac/Pure, Inc., 99.5%), and cadmium fluoborate $Cd(BF_4)_2$ (Pfaltz and Bauer, aq. soln. 50.1 wt %) were weighed in clean glassware. The $Cd(BF_4)_2$ was weighed in three separate allotments and poured into a 1-L Erlenmeyer flask. The boric acid and ammonium fluoborate powders were added

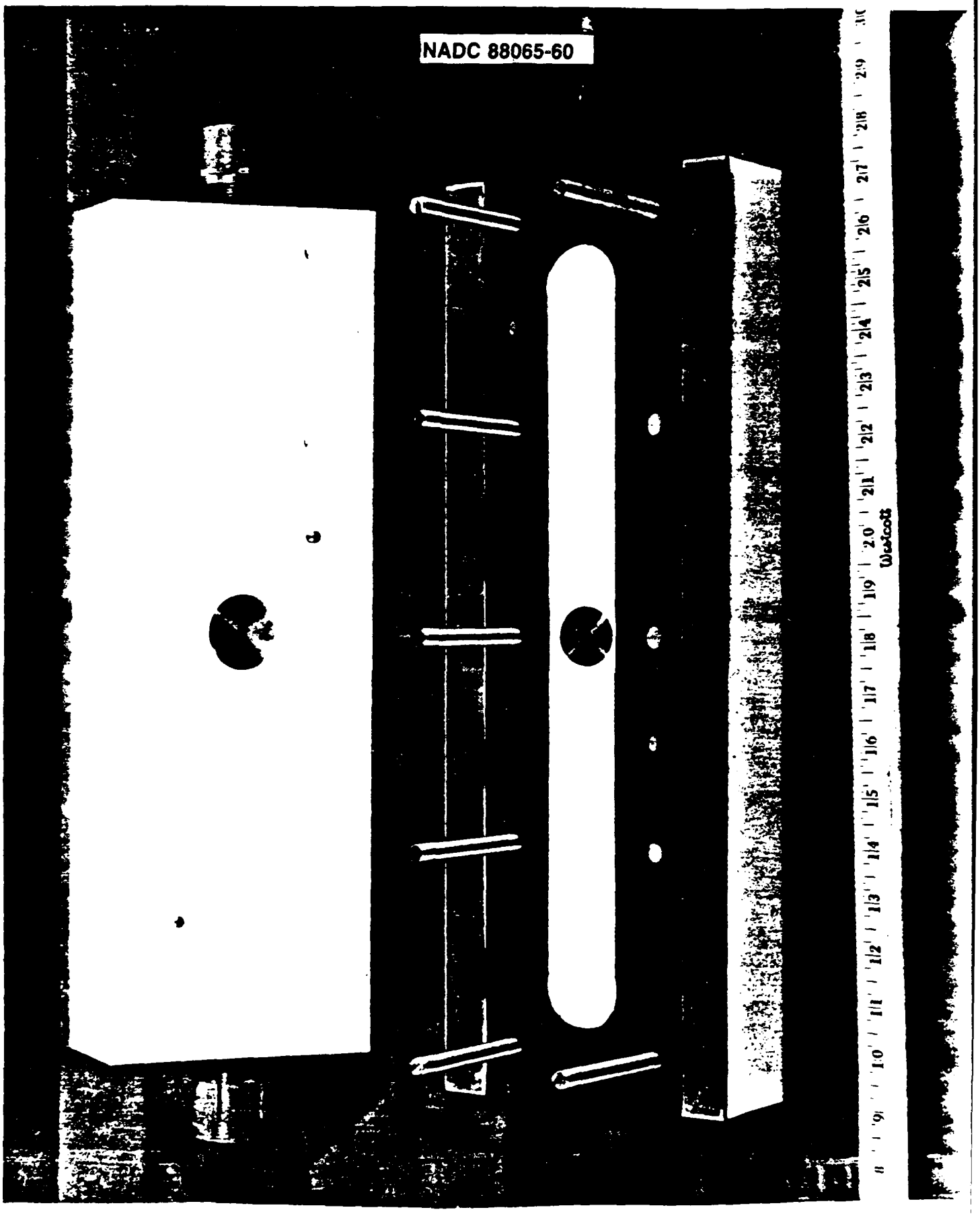

Fig. 4. Interior of electrolyte flow-cell.

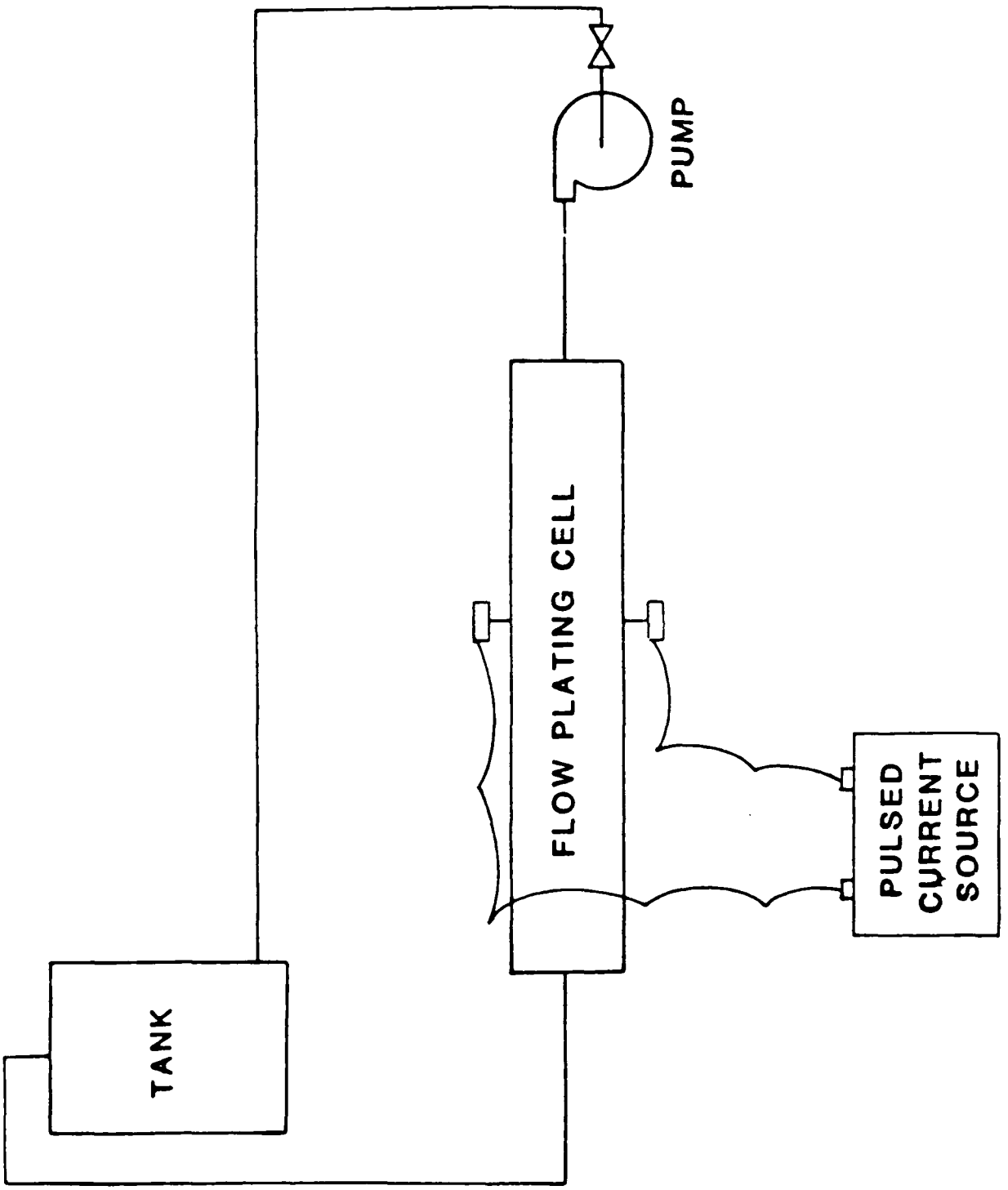

Fig. 5a. Schematic of electroplating system for electrolyte flow and pulsed-current.

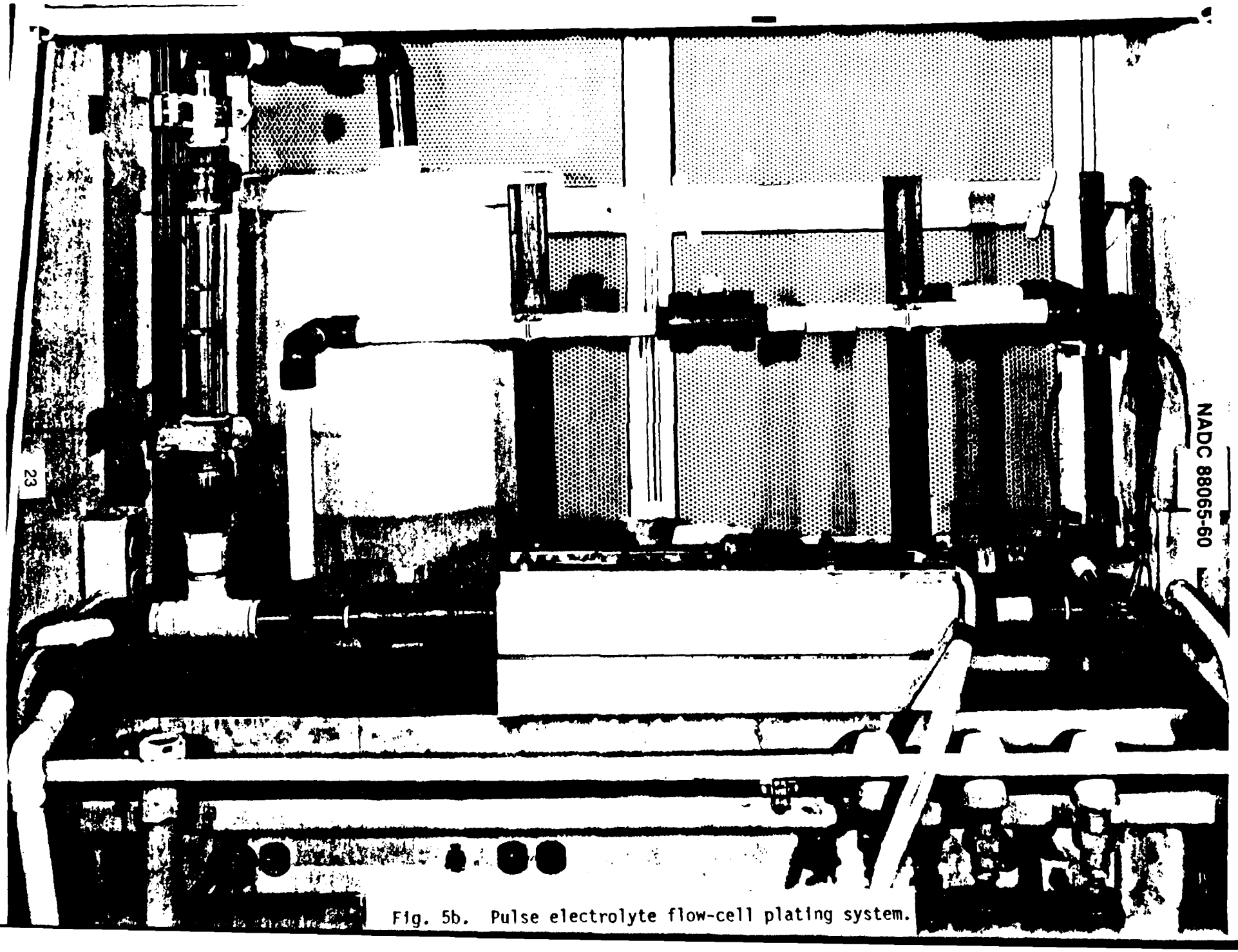

Fig. 5b. Pulse electrolyte flow-cell plating system.

Table 2. Cadmium Fluoborate Bath Preparations

	Bath 1	Bath 2
H_3BO_3, g	22.537	22.520
$NH_4(BF_4)$, g	59.937	60.031
$Cd(BF_4)_2$	407.0	242.317
Protein Colloid, 1%, ppm	40	2
pH (operating range)	3.2-3.3	2.3-2.8
Specific Resistance, Ω•cm	8.79±0.09 (STD)	7.7±0.10 (STD)
Conductivity, $\bullet(\Omega\bullet cm)^{-1}$	0.107	0.124

and dissolved with stirring and moderate heating to about 65°C. After cooling to room temperature, the pH was checked with the Beckman meter and glass pH/reference electrode. Because of interactions of the electrolyte with the glass probe, the pH measurements were not reproducible (the displayed pH value decreased). A chemical-resistant (epoxy body) Ag/AgCl combination pH/reference electrode (Cole-Palmer) was later used, and the electrode generally gave better reproducibility and stability. Because the commercial stock solution of cadmium fluoborate came with a pH that was adjusted near zero, the initial pH measurements of the preparations were much lower than desired. To raise the pH, small amounts of 10%, 20%, 33% ammonium hydroxide (Baker, analyzed reagent) or concentrated ammonium hydroxide were slowly added with stirring. With each addition of ammonium hydroxide, a white precipitate formed and gradually turned the clear bath cloudy. Additional amounts of cadmium fluoborate were added to lower the pH, which had risen higher than desired. When the desired pH had been reached, the solution was allowed to stand and was filtered through millipore 1- to 2-μm filter papers (Type RA) under vacuum.

To find the pH operating range given in Table 2, the pH of the bath was measured several times during the experiment and at its conclusion. A noticeable increase in the pH of Bath 2 occurred during the course of experiments. Daily additions of doubly distilled water were made with stirring to replace evaporation losses.

For use in the flow-cell, large amounts of cadmium fluoborate electrolyte were prepared as follows. The plating solutions used were made from distilled water containing $Cd(BF_4)_2$ (242 $g \cdot l^{-1}$), NH_4BF_4 (60 $g \cdot l^{-1}$), H_3BO_3 (23 $g \cdot l^{-1}$), and ~2 ppm animal glue (i.e., technical protein colloid). After the addition of $Cd(BF_4)_2$, H_3BO_3, and NH_4BF_4, enough distilled water was added to bring the volume up to 75% of total volume being prepared. The solution was stirred on a hot plate/stirrer for 2-4 hr before adjusting the pH.

The pH was adjusted using 20% NH_4OH, adding small amounts while stirring, and allowing the pH to equilibrate before adding more NH_4OH. A pH meter standardized at 2.00 was used to measure the pH. When the pH approached 2.0, more distilled water was added to bring the volume up to the total, since adding water increases the pH slightly. If necessary, the pH was further adjusted to pH 2.1 - 2.2 with NH_4OH.

The solution was allowed to sit overnight to help the particulate matter settle before filtering. The solution was then decanted and vacuum filtered with a Millipore 5-μm filter, changing the filter every 100-150 mL.

5.6 Electrodeposition Procedure for Cadmium Plating from Stirred Fluoborate Electrolyte

The typical electrode assembly, consisting of a 2.5 cm x 1.3 cm x 0.3 cm plate of 1018 steel as the WE with two adjacent cadmium CE (or anodes) and a RE, was fabricated and assembled in a Lucite cell-cover plate holder. The assembly, which was used for electroplating cadmium from the fluoborate electrolyte, is shown in Fig. 6. Deposition was achieved at room temperature from a magnetically stirred electrolyte.

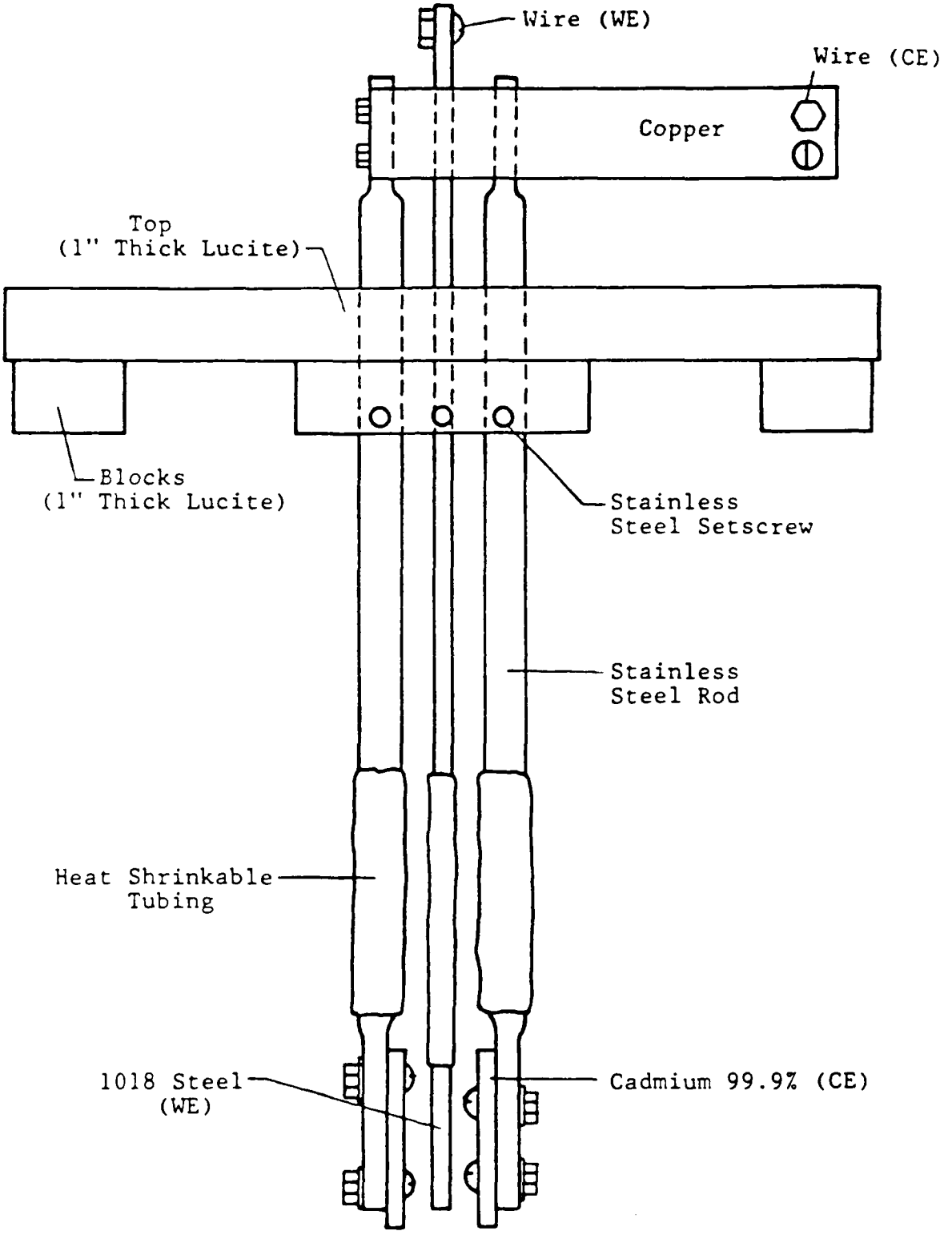

Fig. 6. Electrode assembly for electrodeposition of cadmium from fluoborate electrolyte. WE to CE distance is 4 to 5 mm (with 1 mm screw clearance).

6.0 EXPERIMENTAL RESULTS

6.1 Electrochemistry of Cadmium Plating from Fluoborate Electrolyte

The goal of this work was to achieve a basic understanding of the cadmium electrodeposition process from fluoborate electrolyte. This understanding has enabled us to develop new plating techniques which have potential in engineering applications. The fundamental studies were conducted along two lines of investigation: (1) experiments were conducted to determine the mechanism of cadmium electrocrystallization from aqueous fluoborate electrolyte and to elucidate its interconnection with the hydrogen discharge process, and (2) a theoretical study was conducted to conceptually design high-rate electrodeposition of cadmium using an electrolyte flow-cell under conditions whereby mass transfer limitations become insignificant.

The studies were conducted[11] using electrochemical techniques (e.g., cyclic voltammetry and chronoamperometry). The electrolyte was a cadmium fluoborate solution together with other additives; it was prepared with the following composition: $CdBF_4$, 241.5 $g \cdot l^{-1}$; H_3BO_3, 22.5 $g \cdot l^{-1}$; NH_4BF_4 60 $g \cdot l^{-1}$; and required NH_4OH addition to pH 2.4. Working electrodes of (a) platinum, (b) copper, (c) cadmium, (d) tungsten, (e) 4340 steel, and (f) 1018 steel (all mechanically polished to 0.5 μm Al_2O_3) were used in this study. The cyclic voltammetry and chronoamperometry measurements were conducted in fluoborate electrolyte solutions containing cadmium (Fig. 7), and also in solutions without cadmium (Fig. 8). A cyclic voltammogram obtained on different substrates including steel (Fig. 7) showed a well-defined cathodic peak at -0.9 V vs. SCE, representing cadmium electrodeposition followed by a sharp current rise. Comparison with cyclic

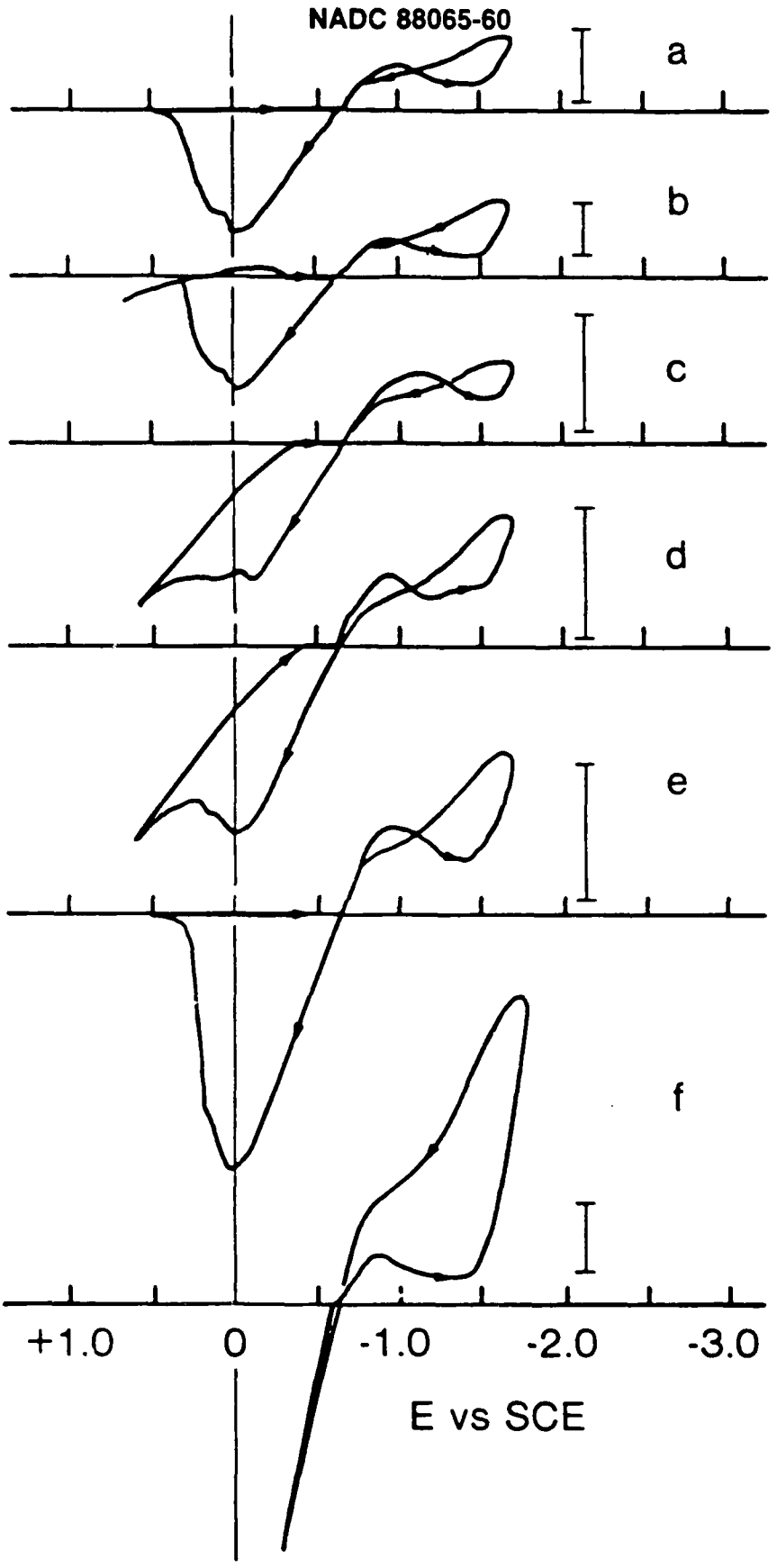

Fig. 7. Cyclic voltammograms (0.02 $V \cdot S^{-1}$) of cadmium electrodeposition from fluoborate electrolyte on (a) platinum, (b) copper, (c) cadmium, (d) tungsten, (e) 4340 steel, and (f) 1018 steel (current scale, 1 $A \cdot cm^{-1}$).

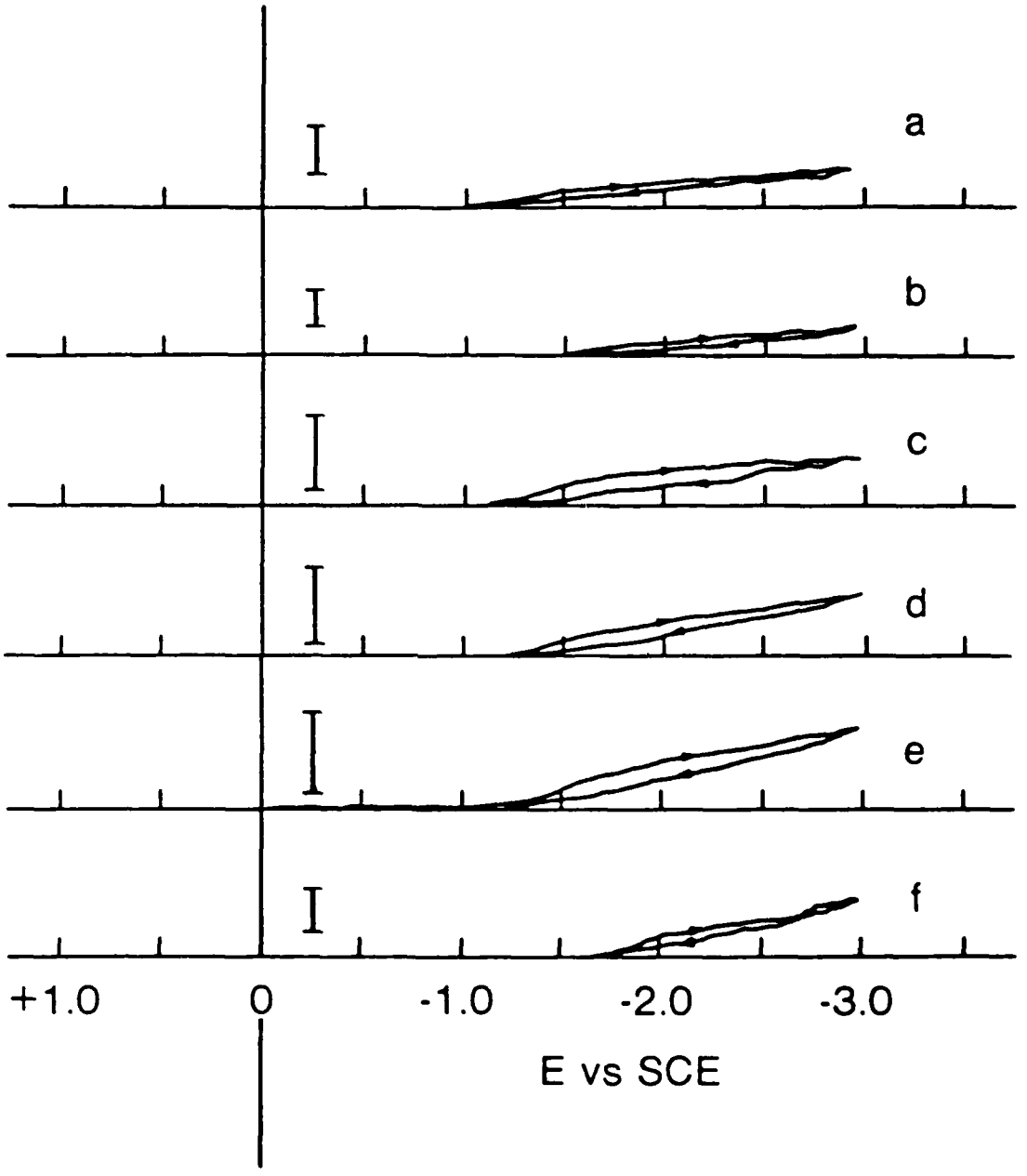

Fig. 8. Cyclic voltammograms (0.02 $V \cdot S^{-1}$) of fluoborate electrolyte without cadmium on (a) platinum, (b) copper, (c) cadmium, (d) tungsten, (e) 4340 steel, and (f) 1018 steel (current scale 0.5 $A \cdot cm^{-1}$).

voltammograms obtained with the same working electrodes but with cadmium-free electrolyte (Fig. 8), indicates that the cathodic peak (Fig. 7) corresponds closely to pure Cd^{+2}/Cd^{o} reduction without major interference from the hydrogen evolution process. The characteristics of this peak (Figs. 7 and 8), with an abrupt rising branch, slightly displaced toward cathodic values with respect to the Cd^{+2}/Cd^{o} equilibrium potential, indicate the presence of a well-defined initial nucleation stage in the electrocrystallization process. This stage was also confirmed from chronopotentiometric studies (Fig. 9), where an initial rising current branch related to the initial increase of the deposition area was obtained.

This study has indicated that the risk of hydrogen uptake is critical when the substrate is still exposed to the electrolyte during initial nucleation and growth of the cadmium nuclei. In addition, the hydrogen discharge reaction is enhanced at this stage; this enhancement is evident from the position of the final current rise, which is obtained at potentials much less cathodic than in the case of a cadmium-free solution. The potential where the rising branch starts in cadmium fluoborate solutions is approximately the same for every substrate considered (-1.5 V vs. SCE, Fig. 7); on the other hand, the hydrogen discharge from cadmium fluoborate-free solutions shows a strong dependence on the type of substrate involved (Fig. 8). This suggests that the hydrogen discharge reaction is catalyzed by some mechanism related to the presence of newly formed cadmium nuclei.

6.2 Plating in the Pulse Flow-Cell System

A large number of plating experiments using the flow-pulse system were conducted on Type 300M steel coupons (1.125-in. dia. X 0.06-in. thick) which were surface finished to 600 grit SiC paper. Copper rods, which

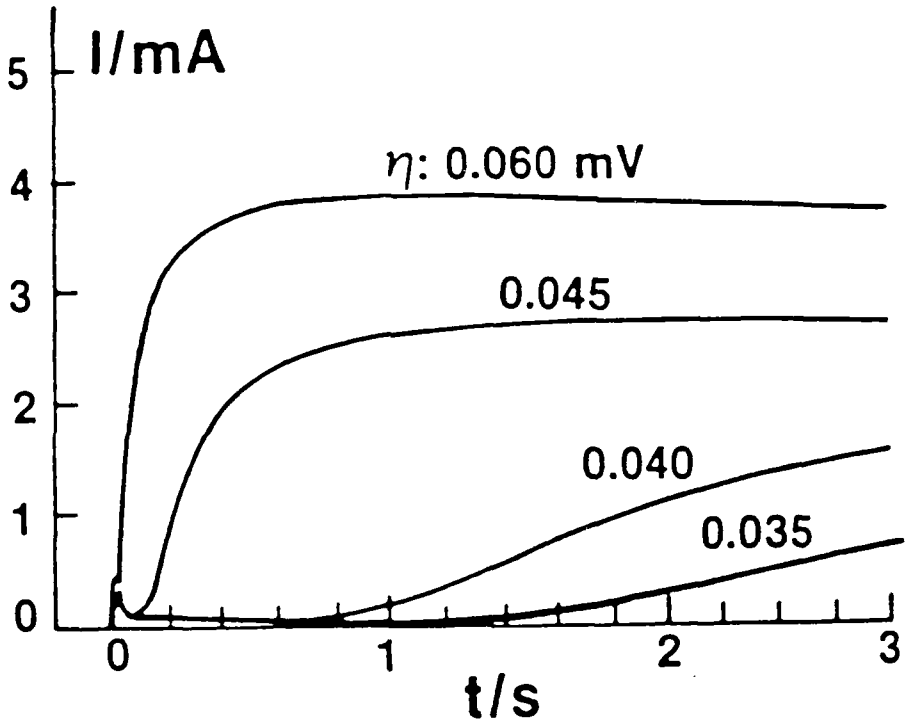

Fig. 9. Potentiostatic current-time transient for the electrodeposition of cadmium from fluoborate electrolyte. T = 25°C, substrate: platinum (0.037 cm^2)

could easily be detached, were soldered on the reverse side for an electrical connection. The anode, an oversized circular cadmium disc was positioned ~2 mm distance from the cathode. The electrolyte flow, for most of the platings reported in this work, were conducted below the turbulent regime.

Optimization of pH

To study the effect of pH on the quality of coating, seven samples were plated at different pHs. The results are summarized in Table 3. All pHs (Table 3) were measured with a pH meter standardized at pH = 4.00. The same nucleating pulse current (0.5 $A \cdot cm^{-2}$) and time (1 S) and growth current (0.03 $A \cdot cm^{-2}$) and time (10 min) were used. The optimum pH range was determined to be 2.10 - 2.20.

Table 3. Effects of Plating Solution pH on Electrodeposition

Sample	pH	Appearance
1	2.20	Metallic silvery, slightly grainy
2[a]	2.40	Metallic silvery, slightly grainy
3[b]	2.85	Grey, grainy, dendritic
4	2.10	Metallic silvery, smooth
5	2.60	Dark grey, grainy, dendritic
6	3.24	Medium grey, grainy
7	4.24	Medium grey, grainy

Solution composition: 242 $g \cdot L^{-1}$ $Cd(BF_4)_2$
60 $g \cdot L^{-1}$ NH_4BF_4
23 $g \cdot L^{-1}$ H_3BO_3
2 ppm technical protein colloid

[a]Contains only 200 $g \cdot L^{-1}$ $Cd(BF_4)_2$

[b]Contains only 150 $g \cdot L^{-1}$ $Cd(BF_4)_2$

Ten Type 300M steel samples (1.125 in. dia x 0.060 in. thick) were plated with cadmium in the flow cell under different current and flow conditions. Table 4 lists the plating conditions and the results. Three samples (FD 1, 2, and 3) were electroplated under direct currents at different flow rates. These samples showed metallic, glossy deposition, but also showed streaks on the surface, apparently caused by the stream lines in the plating solution flow. These streaks disappeared when pulse current was applied. Six samples (FP-1, 2, 3, 4, 5, and 6) were plated at a flow velocity of 0.27-3.5 $m \cdot S^{-1}$ (Re = 2000-25,600) and at current densities ranging from 1.7 to 3 $A \cdot cm^{-2}$. The pulse current was generated by a Transrex power supply controlled by the DEC computer. The pulse was limited to a minimum width of 25 ms due to the limitation of the power supply itself. The grain size of the deposits were relatively fine at high current densities and resulted in silvery grey metallic deposits.

For reference, a plating scheme involving a nucleating pulse current followed by low pulse-growth current was tested in FP-6. This scheme has been found to give the best results in a stirred plating electrolyte. However, the deposition by the flow-cell was grey and powdery, indicating coarse grain deposition. It appears that a nucleating pulse followed by DC growth is not suited for the flow-cell. Results of other experiments conducted on cadmium platings using high peak current density pulses of short duration ($t_{on} = \geq 10$ μs) and longer rest periods are discussed later in this report. The experimental results indicate the advantages of the flow-cell when combined with a pulse-current source. For example, under normal DC current, the plating of cadmium 10 μm thick would take normally 10 to 20 min. In the flow-cell, as demonstrated, it is reduced to less than 15 s, thus the production rate is increased. The danger of hydrogen

Table 4. Summary of Flow-Cell Platings

Sample No.	Density, $A \cdot cm^{-2}$	Duty Cycle	t_{on}, ms	t_{off}, ms	T, ms	No. of Pulse	Plating Time S	Flow Vel, ms	Reynolds Number (Re)	Appearance
FD-1	0.5 (strike)[a] 0.03 (growth)	DC	-	-	-	-	600	2.5	18,200	Dark grey
FD-2	0.5 (strike)	DC	-	-	-	-	600	0.7	5,100	Grey streaks
FD-3	0.03 (growth)	DC	-	-	-	-	600	0.3	2,200	White streaks
FP-1	1.7 (growth)	0.5	50	50	2800	421	1200	0.27	2,000	Silver No streaks
FP-2	1.7 (growth)	0.5	50	50	100	421	42	1.1	8,000	Silver No streaks
FP-3	2.5 (growth)	0.5	50	50	100	144	14	3.5	25,600	50% grey No streaks
FP-4	1.7 (growth)	0.5	50	50	100	210	21	3.5	25,500	Silver
FP-5	1.7 (growth)	0.25	25	75	100	365	37	3.5	25,500	White
FP-6	0.5 (strike) 0.03 (growth)	0.5	30	50	60	15,000	900	3.5	25,500	Dark grey

[a]Strike is the same as nucleating pulse.

codeposition was considerably reduced in flow-pulse plating as shown by our preliminary measurements of hydrogen in the steel coupons after deposition.

6.3 Current-Potential and Overpotential Rise Time

Current and potential measurements versus Cd^{+2}/Cd^{o} reference from the fluoborate deposition are given in Table 5. Nucleation-overpotential pulse rise times (10% to 90% peak-to-peak) and pulse fall times (90% to 10% peak-to-peak) were sharp during the deposition of cadmium from fluoborate baths; they are given in Table 6. Overpotentials (with no IR compensation) were found directly by subtracting the nucleating potential from the cadmium rest potential on the Norland waveform analyzer. For experiments at 0.030 and 0.050 $A \cdot cm^{-2}$, the overpotentials were taken from the strip chart recorder. Pulsed currents were monitored in the waveform analyzer.

For the three current densities listed in Table 6, the overpotential rise time is linear with a correlation coefficient of 0.998. Within measurement errors, this implies a purely resistive overpotential.

Table 5. Deposition Current-Potential Data for Fluoborate Electrolyte

Current Density $A \cdot cm^{-2}$	Potential[a] vs. Cd^{2+}/Cd^{o}, V; Fluoborate Deposition	Number of Independent Trials
0.030	-0.266±0.010	6
0.050	-0.423	2
0.10	-0.883	2
0.50	-4.31±0.084	8
0.96	-9.02±0.047	4

[a]Measured at end of nucleation pulse or DC growth.

Table 6. Overpotential[a] Rise/Fall Times for Fluoborate Nucleation

Current Density $A \cdot cm^{-2}$	Rise-Time (10%-90%) ms	Fall-Time (90%-10%) ms	Number of Independent Trials
0.10	0.834	0.722	1
0.50	3.63±0.174	1.40±0.247	5
0.96	7.72±0.057	3.86±0.016	4

[a]Not IR-compensated

Current and potential measurements, and rise times, given in Tables 5 and 6, show that codeposition of hydrogen during plating may be reduced by using pulse widths that are short enough so as not to exceed the hydrogen overvoltage on steel. By comparison with the cyclic voltammetry studies, deposition at up to 0.050 $A \cdot cm^{-2}$ DC from the fluoborate baths should avoid hydrogen codeposition.

6.4 Nucleation and Growth Experiments

The following experiments were conducted from a stirred electrolyte. Numerous single-pulse nucleation experiments were run from Bath 2 (pH = 2.3, Table 2) to determine the optimum initial nucleating pulse. Pulse times ranged from about 0.033 to 6.25 S at current densities from 0.030 to 1.5 $A \cdot cm^{-2}$. In many experiments, the nucleation time was varied and the current density was held fixed, and vice versa. In other experiments, the charge Q through the system was held constant at 0.25 $C \cdot cm^{-2}$, and both the time and current density were varied to keep the enthalpy of deposition constant. Based on our results, an optimal nucleating pulse on Type 1018 steel is a 0.50-$A \cdot cm^{-2}$ pulse for 0.50 S.

Direct currents of 0.030 $A \cdot cm^{-2}$ for 10 min and 0.05 $A \cdot cm^{-2}$ for 6 min were applied for growth immediately after the optimal nucleation pulses. One cathodic growth pulse at 0.030 $A \cdot cm^{-2}$ (30.1 ms on and 31.5 ms off) was

applied after nucleation. These experiments yielded semibright cadmium deposits from the low pH bath.

Standard electroplater's experiments at 0.030 $A \cdot cm^{-2}$ for 10.5 min were plated for purposes of comparison from fluoborate Baths 1 and 2 (Table 2) with no nucleation pulse. From Bath 1 (pH = 3.2-3.3), an undesirable, matte-white deposit resulted. Bath 2 yielded spotty growth with pin-size holes down to the substrate. Evidently, proper nucleation would be essential to obtain good deposits from Bath 2.

6.5 Pulse Plating Experiments from Stirred Electrolyte

Pulse plating using peak current densities from 0.10 to 3.0 $A \cdot cm^{-2}$ at about 33 ms width from Bath 1 (pH = 3.2) was not as effective as the cases in which nucleation and DC growth were used. Examination of the surfaces from pulse plating alone revealed tiny dendrites.

6.6 Coating Evaluations

X-ray diffractometry studies of representative deposits from the fluoborate baths confirmed ideal crystalline cadmium. A representative diffractometry trace of polished cadmium (polished using 0.3 μm Al_2O_3 and distilled H_2O) electrodeposited on mild steel from fluoborate Bath 2 is shown in Fig. 10. The diffractometry trace in the case of fluoborate electrolyte plating shows only slight preferred orientation, compared with those of the cyanide electrodeposits (Appendix V). The peaks of other samples were sharp, and relative heights generally did not change from a 0^{o} to 90^{o} sample rotation. The reflected intensities were stronger than any for the cyanide deposits. The slight preferred orientation with sharp, intense peaks imply polycrystalline, dense cadmium with growth oriented directly perpendicular to the substrate. The average crystallite size for the fluoborate deposition was smaller than that for the cyanide deposits based on x-ray results.

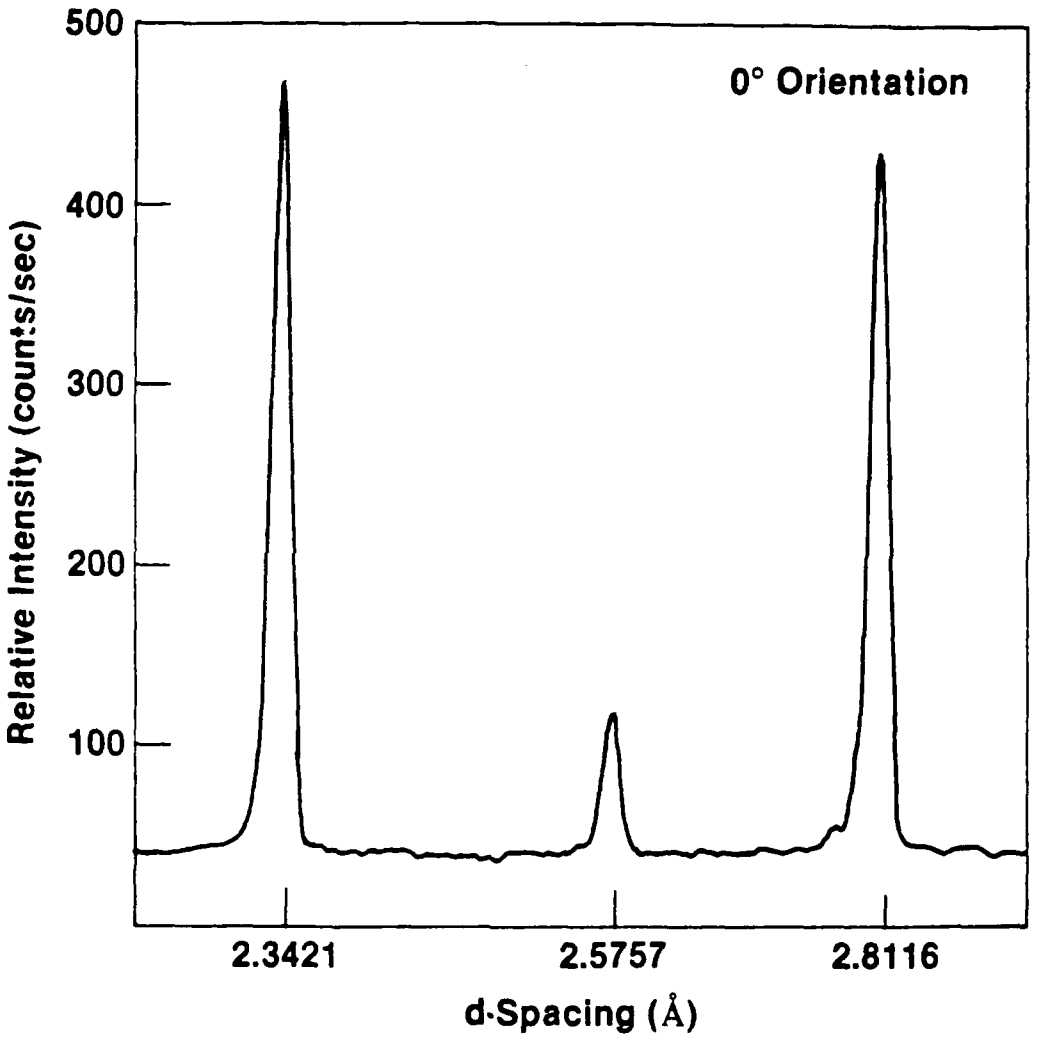

Fig. 10. X-ray diffraction pattern of cadmium electrodeposited on mild steel from fluoborate electrolyte under nucleating pulse (0.50 A•cm^2 for 0.500 S) followed by DC (0.050 A•cm^{-2} for 6 min) growth. (A similar pattern is seen at 90°C sample rotation.)

Metallography using an optical microscope provides a means for making microscopic measurements on surfaces and cross sectioned material. The microstructure of the electrodeposits at surfaces provides information on grain sizes and the relative coherence or compactness of the cadmium deposits obtained under various plating schemes. It is important to assure that the surface microstructure is pore-free and compact. The tight or strongly compact microstructure will prevent direct access of electrolyte to the metal substrate. Formation of a protective, passive film [Cd(OCl)Cl] may be more likely in this situation.

The imaging of a cross-sectioned cadmium-coated sample may provide a variety of information: (1) the nature of bonding or adherence (or tightness) of the coating to the substrate, (2) the thickness of the coating layer, and (3) in etched samples, the variation in grain-size distribution from the coating surface to the metal surface. Photomicrographs of the morphology of the cross sections have been used in this study to evaluate the adherence of the coatings on steel.

Little surface preparation was required before examining the microstructure of the cadmium coatings. In most SEM and OM examinations conducted on the surfaces, the size variations of the crystallites (which are assumed to be aggregates of grains) were observed to provide qualitative clues to the grain size.

Measurement of Coating Thickness

Measurement of cadmium plating thicknesses obtained from electrodeposition in stirred fluoborate electrolytes were made in the metallograph (at 630X) with a calibrated ocular eye piece (12.7 μm/coarse division equivalent to 1.27 μm/fine division). For good statistics, twelve measurements on each side of the cathode were made. With the

highest and lowest values discarded, an average and standard deviation for the remaining ten values on each side of the cathode were calculated. The results of these plating measurements are shown in Table 7. The large standard deviations reflect the thickness variations of the deposits near the edges. Different thickness measurements on the two sides of the cathode may have resulted from unequal spacing between the dual cadmium counter electrodes.

7.0 DISCUSSION OF RESULTS

7.1 Overview

The objectives of the research efforts were: (1) to be able to electrodeposit a 0.5-mil (or 12.7 μm) thick coating of cadmium from aqueous fluoborate on high-strength steels (300M or 4340) while avoiding hydrogen diffusion into the steel, (2) to ensure that the electrodeposit was pore-free and strongly adherent to the steel surface, and (3) to achieve deposition at high speed (mil$\cdot$min^{-1}). All three objectives were met.

Table 7. Plating Thickness Measurements for Typical Cadmium Fluoborate Electrodeposits

Experiment	Measured Plating Thickness Side 1 (μm)	Side 2 (μm)	Mean (μm)
1. Nucleation (0.50 A$\cdot$cm^{-2}, 0.500 s) + Growth (0.050 A$\cdot$cm^{-2}, 6 min)	8.5±2.2	13.4±4.4	10.9±4.9
2. Nucleation (0.50 A$\cdot$cm^{-2}, 0.500 s) + Cathodic Pulse (30.1 ms on, 31.5 ms off; 0.029 A$\cdot$cm^{-2}, 11.3 min)	8.7±2.1	7.2±2.1	7.9±3.0
3. DC Growth 0.030 A$\cdot$cm^{-2} 10 min	12.5±2.7	9.3±4.1	10.9±4.9

Significant results on coatings may be discussed suitably in the following categories: (1) nucleation-optimization studies in deposition from stirred fluoborate electrolyte, (2) pulse nucleation and film growth with DC current in deposition from stirred fluoborate electrolyte, (3) pulse-plating of cadmium in an electrolyte flow-cell, and (4) pulse plating from stirred fluoborate electrolyte.

The surface preparation steps, explained in Appendix IV, are essential for reproducibility for electrodeposited coatings of cadmium. This requirement applies equally to nucleation studies and electrocrystallization growth. Care was taken to ensure a reproducible surface in each experiment.

Photographs of a typical 4340 and 1018 steel substrate, prior to electrodeposition are shown in Fig. 11. The surfaces were mechanically polished to 600 grit SiC paper and chemically etched prior to plating.

7.2 Nucleation and Film Growth Under DC or Pulse Currents

Electrodeposits at 0.030 $A \cdot cm^{-2}$ DC current density for 10.5 min from fluoborate gave spotty growth (Fig. 12). The cross sections in Fig. 12(c and d) also showed growth inclusion where no nucleation on the substrate occurred. The spotty growth was the result of too few nucleation sites.

Effect of Varying Pulse Time and Current on Film Growth

At 0.030 $A \cdot cm^{-2}$, the overpotential appears to be insufficient for nucleation over the entire substrate.

Micrographs of nucleation at constant pulse widths of 0.945 S and variable current density are shown in Fig. 13. At 1.0 $A \cdot cm^{-2}$ and higher current density pulse, dendrite growth may be present.

Figure 13b shows better substrate coverage than does Fig. 13a. At this higher current density nearly uniform and finer coverage occurs.

|------|
0.1 mm
100 μm

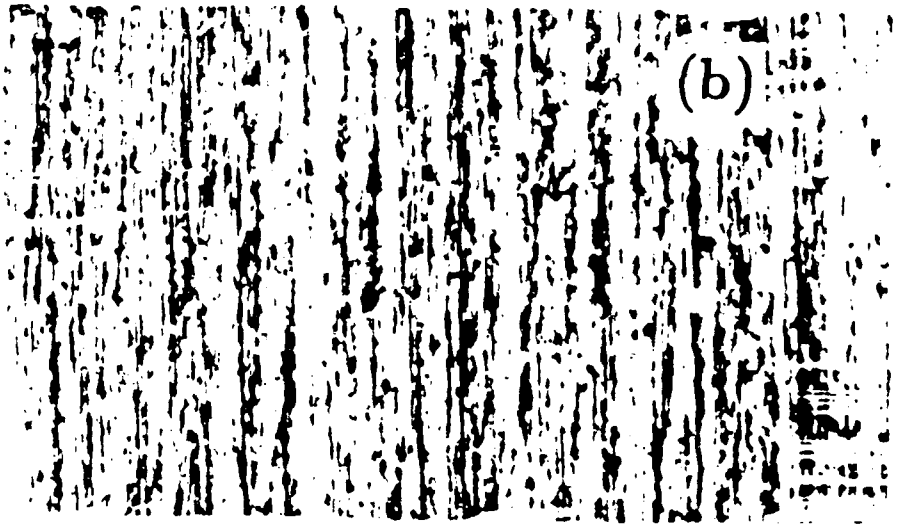

Fig. 11. Optical micrograph of steel surface preparations to 600 grade SiC paper finish followed by alkaline anodic-cleaning and acid etch, (a) 440 and (b) 1018.

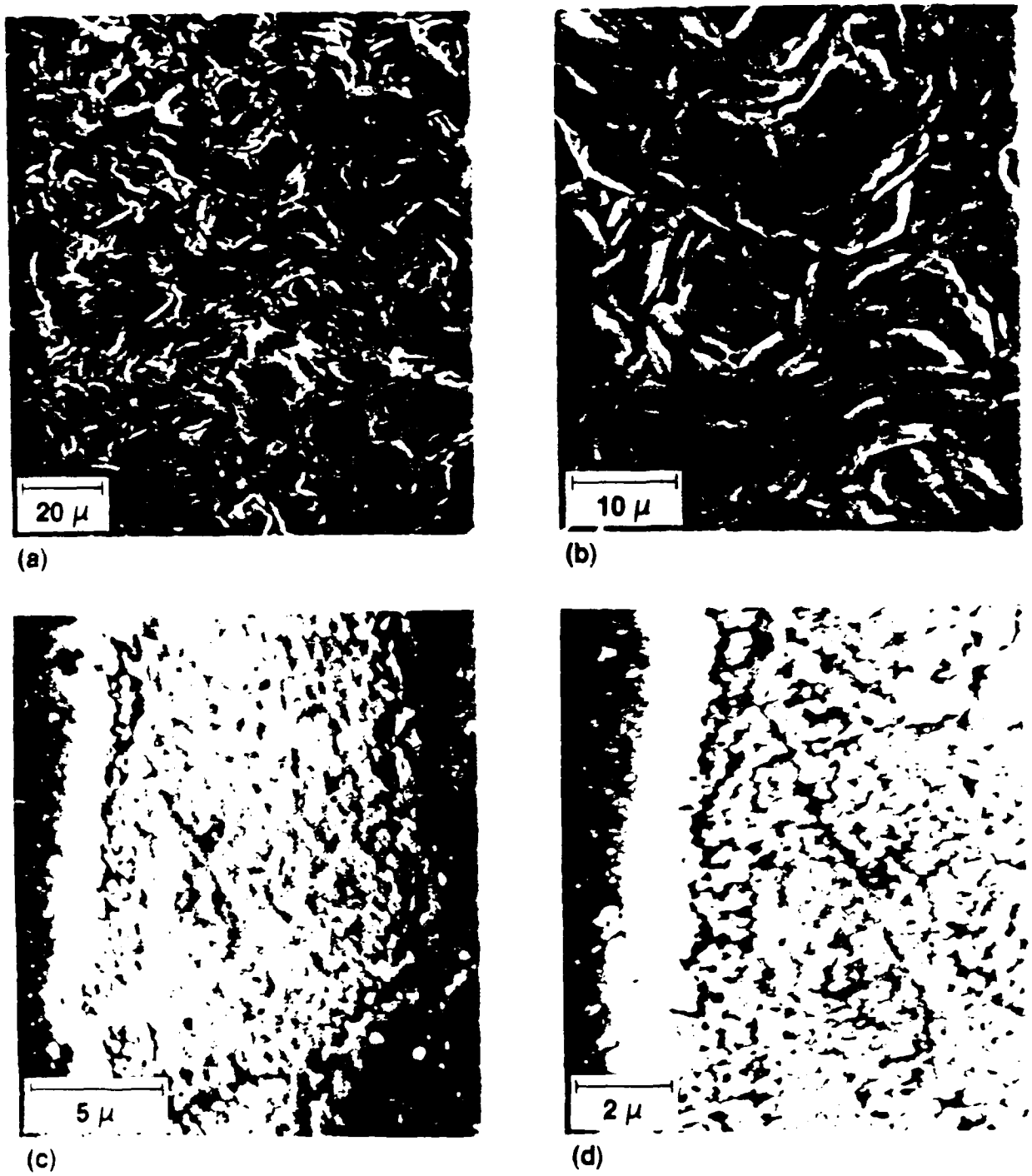

Fig. 12. SEM micrographs of cadmium electrodeposited from fluoborate electrolyte on mild steel at 0.030 A•cm^2 DC for 10 min; surface (a), and (b); cross section (c) and (d).

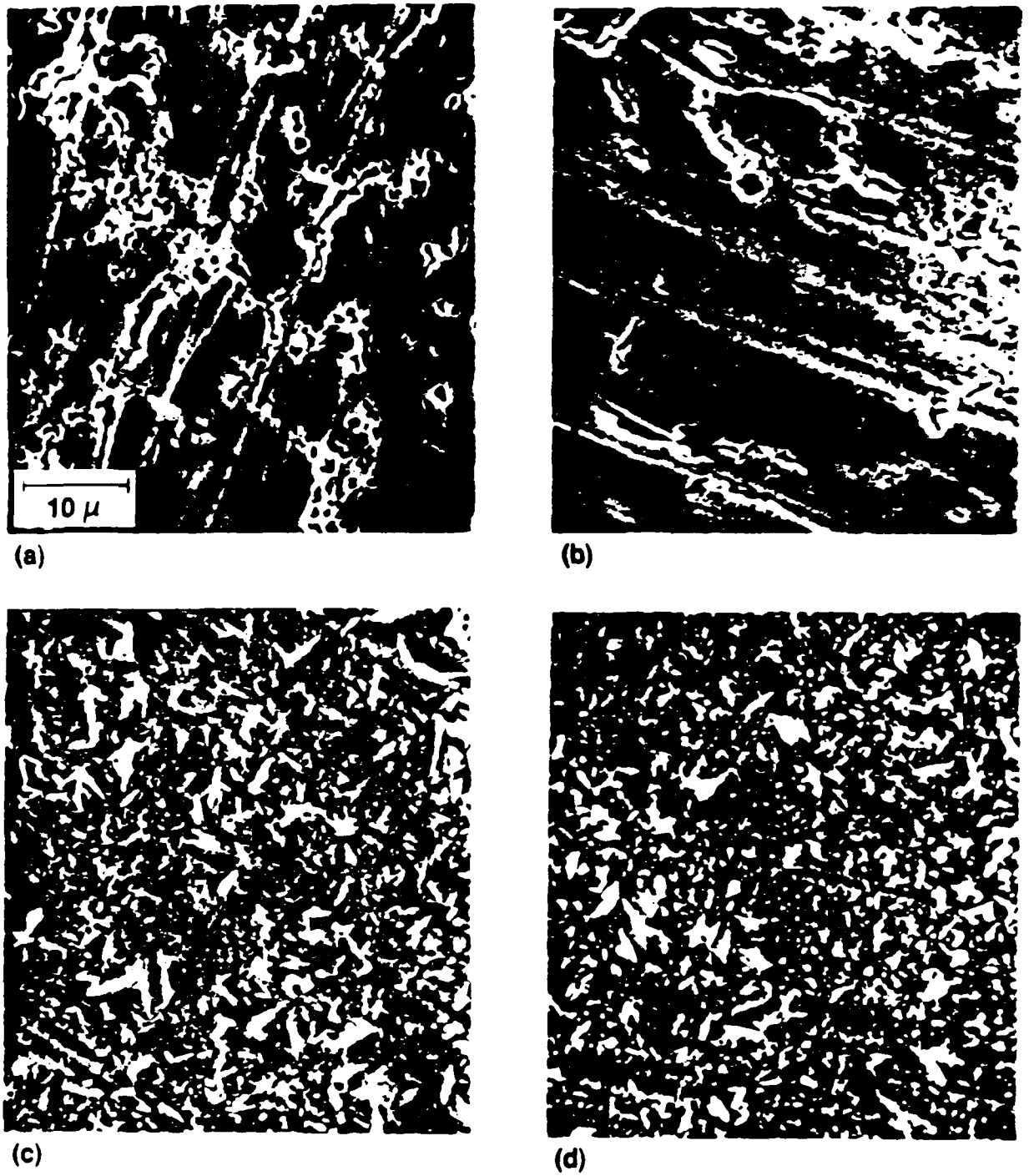

Fig. 13. SEM micrographs of cadmium electrodeposited from fluoborate electrolyte under 0.945 S nucleating pulse: effect of current density ($A \cdot cm^{-2}$); (a) 0.10, (b) 0.50, (c) 1.0, and (d) 1.5.

Micrographs of nucleation at a constant current density of 0.50 $A \cdot cm^{-2}$ and variable time width are shown in Fig. 14. These micrographs show the time development of the nucleation and initial growth process. Between 0.796 and 1.4 S, the substrate gets saturated with nuclei, and initial growth occurs. By 2.52 S, white dendrites have formed which increase in size as in Fig. 14c. This shows that at fixed current density, the nucleating pulse width must be shorter than a critical time for which dendrites form.

The effects of deposition at constant charge Q between 0.24 $C \cdot cm^{-2}$ and 0.27 $C \cdot cm^{-2}$ are shown in Fig. 15. Assuming a deposition efficiency of 100%, a deposit density for cadmium of 8.65 $g \cdot cm^{-3}$, and a charge passed of 0.25 $C \cdot cm^{-2}$, the mean deposit thickness for the micrographs shown in Fig. 15 is calculated as 0.17 μm. With approximately the same thickness, the percent coverage and relative size of the growing nuclei are indicated in Fig. 15(a-d). Fig. 15c shows the greatest percent surface coverage by nuclei of those shown in that Figure. In Fig. 16a, few, large and spotty nuclei result from a low applied overpotential. On the other hand, tiny, white dendrites have formed in Fig. 16d showing that too large of an overpotential was applied. The most desired coverage is near the conditions shown in Fig. 16c. The larger nuclei present in Fig. 16c may be the result of some initial growth.

The composite results of the nucleation studies of cadmium on mild steel from fluoborate electrolyte are summarized in Fig. 17. The area enclosed by the dashed oval is where nucleation on mild steel is expected to be good. Between the ends of the curve, corresponding to Q = 0.25 $C \cdot cm^{-2}$, the best nucleation on mild steel should occur. For Q larger than the 0.25-$C \cdot cm^{-2}$ dashed line, the nucleation is dendritic. Incomplete coverage of the substrate occurs for nucleation with Q less than 0.25 $C \cdot cm^{-2}$ At

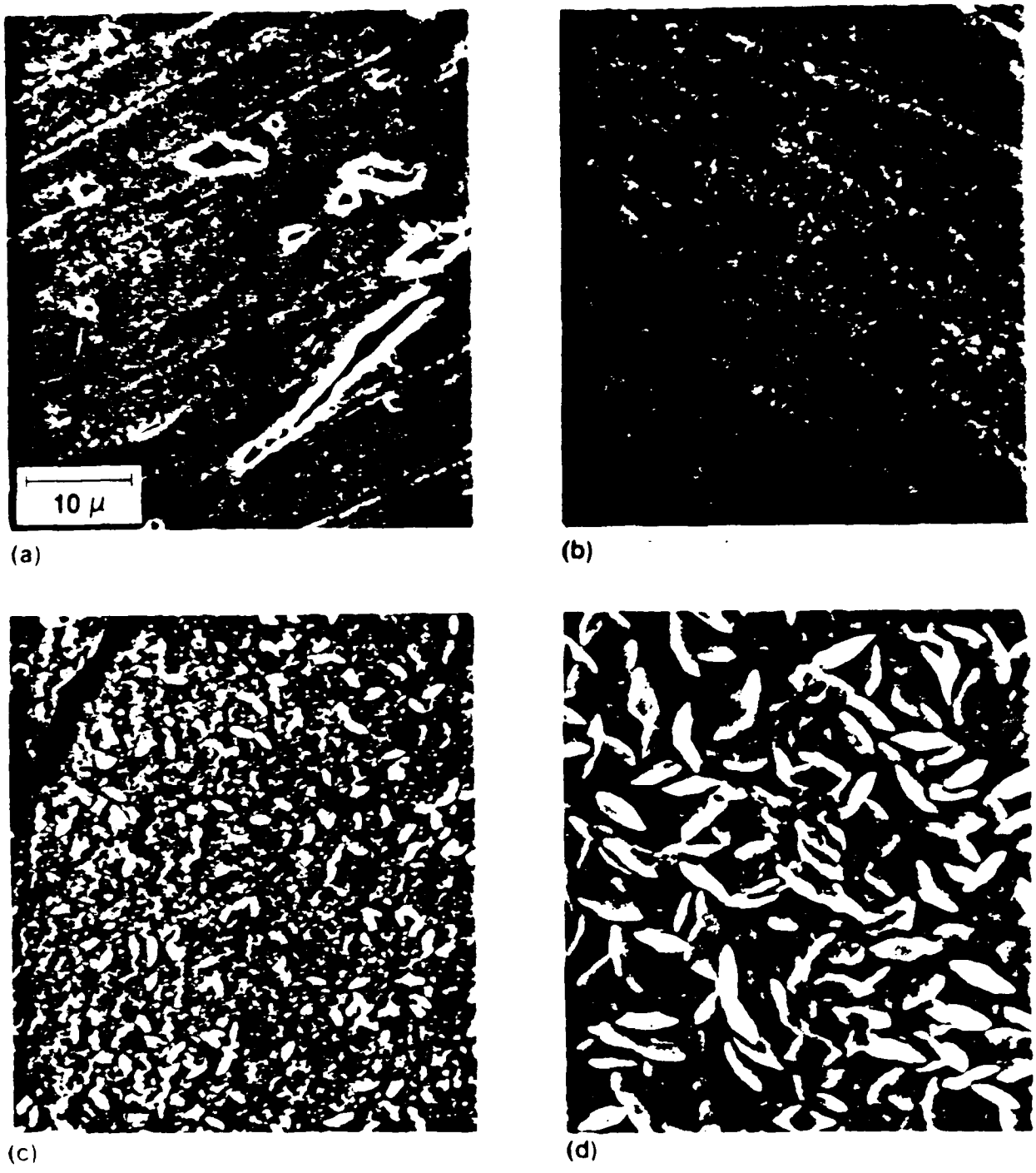

Fig. 14. SEM micrographs of cadmium electrodeposited from fluoborate electrolyte under 0.50 $A \cdot cm^{-2}$ nucleating pulse on mild steel: effect of pulse duration (in seconds): (a) 0.796, (b) 1.404, (c) 2.52, and (d) 6.25.

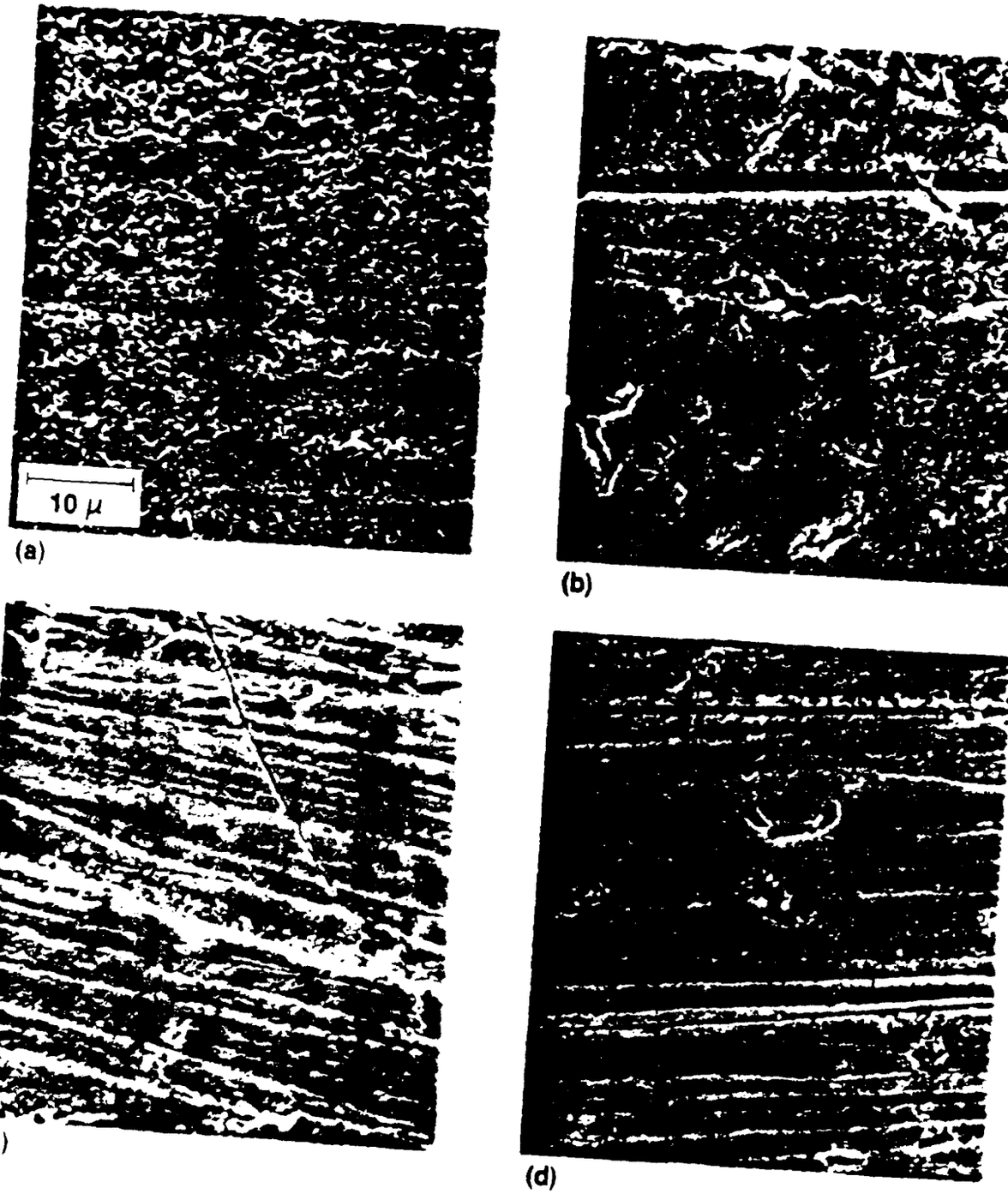

Fig. 15. SEM micrographs of cadmium electrodeposited from fluoborate electrolyte under nucleating pulse for a fixed charge density: (a) 0.030 $A \cdot cm^{-2}$ for 8.28 S, Q = 0.24 $C \cdot cm^{-2}$; (b) 0.10 $A \cdot cm^{-2}$ for 2.495 S, Q = 0.25 $C \cdot cm^{-2}$; (c) 0.47 $A \cdot cm^{-2}$ for 0.515 S, Q = 0.24 $C \cdot cm^{-2}$; and (d) 0.95 $A \cdot cm^{-2}$ for 0.2805 S, Q = 0.27 $C \cdot cm^{-2}$.

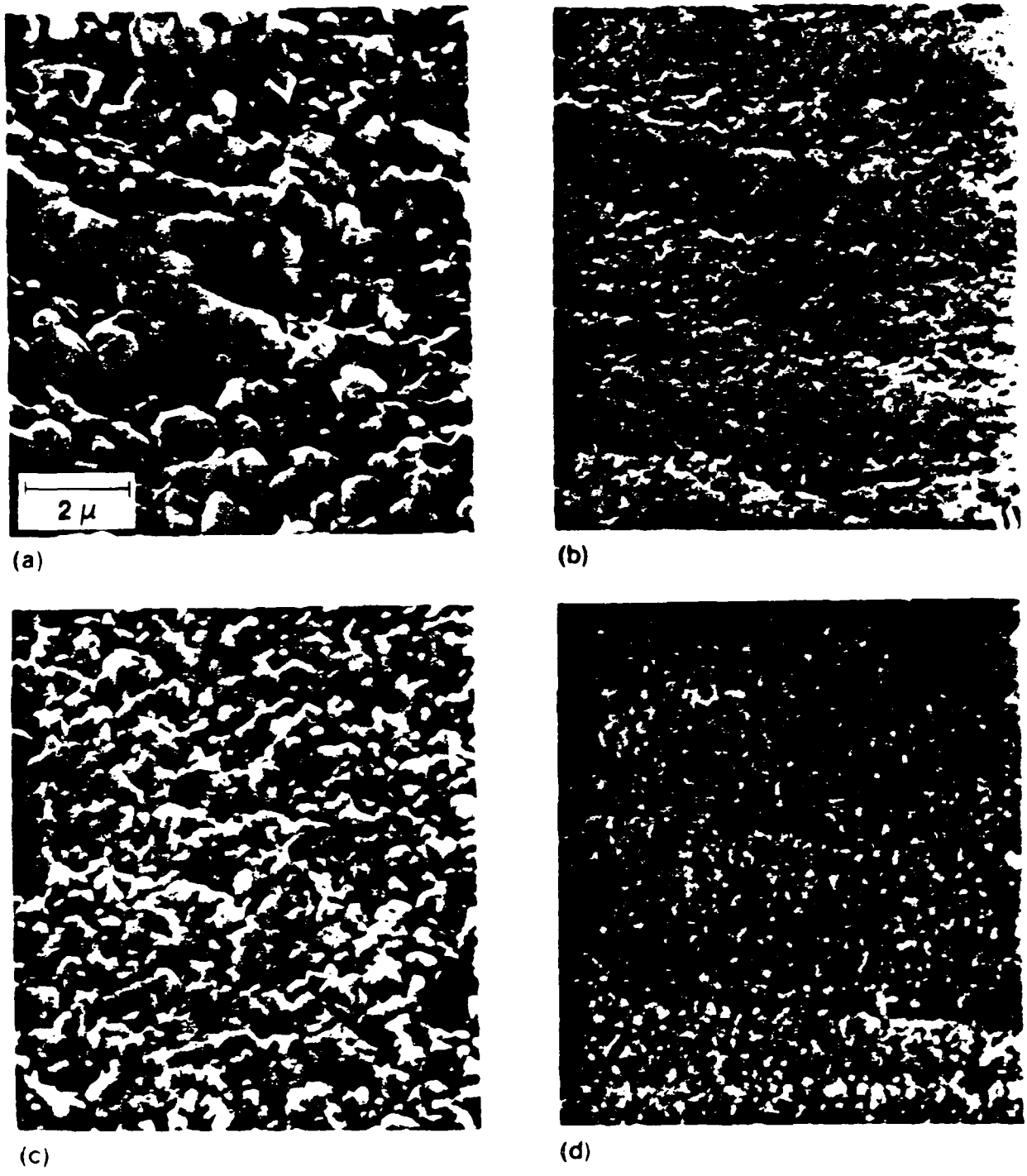

Fig. 16. SEM micrographs of cadmium electrodeposited from fluoborate electrolyte under nucleating pulse for a fixed charge density: (a) 0.030 $A \cdot cm^{-2}$ for 8.28 S, Q = 0.24 $C \cdot cm^{-2}$; (b) 0.10 $A \cdot cm^{-2}$ for 2.495 S, Q = 0.25 $C \cdot cm^{-2}$; (c) 0.47 $A \cdot cm^{-2}$ for 0.515 S, Q = 0.24 $C \cdot cm^{-2}$; and (d) 0.95 $A \cdot cm^{-2}$ for 0.2805 S, Q = 0.27 $A \cdot cm^{-2}$.

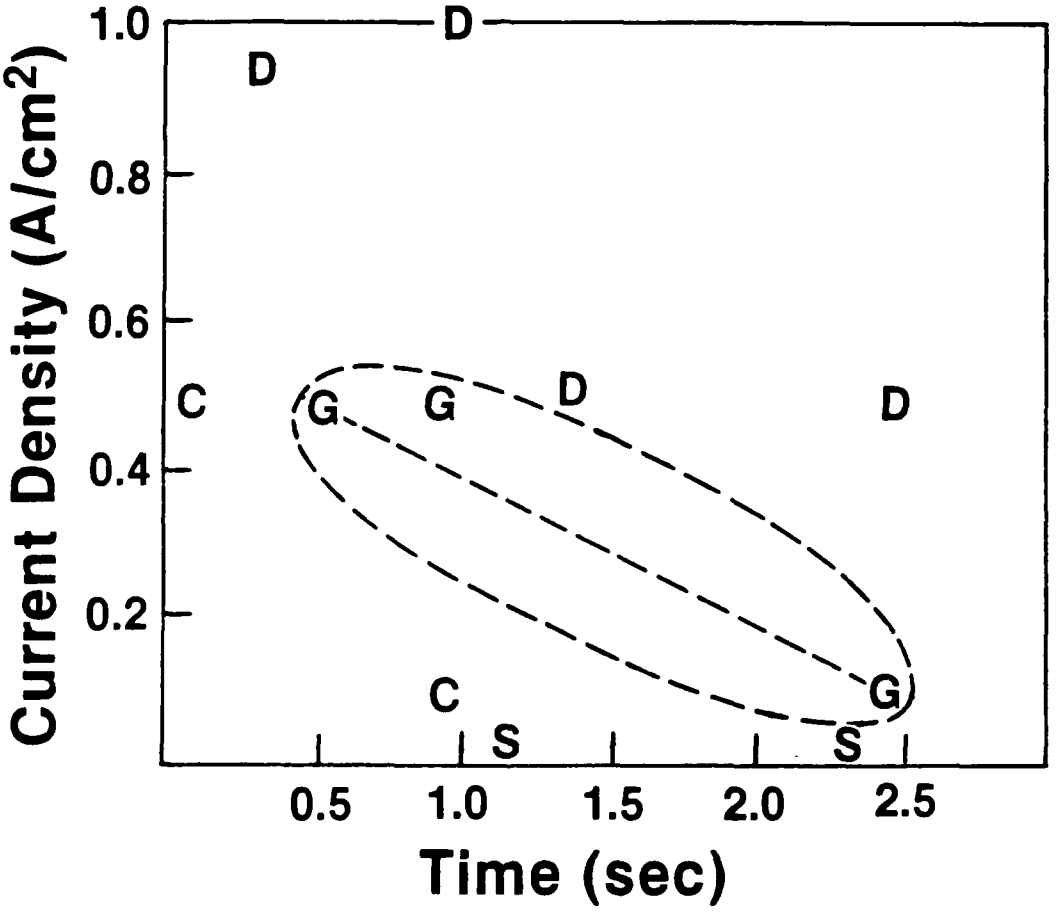

Fig. 17. Current-time nucleation regimes for cadmium electrodeposited on mild steel from fluoborate electrolytes; Key: G = good nucleation, D = dendritic, C = poor coverage, S = spotty or sponge-like.

current densities smaller than 0.030 $A \cdot cm^{-2}$, the nucleation is spotty regardless of the deposition time.

7.3 Cadmium DC Deposition from Fluoborate Electrolyte

The best deposits resulted from nucleation and growth under DC or pulse. Micrographs of the surfaces and cross sections of typical nucleation and DC growth electrodeposits are shown in Figs. 18, 19, and 20. All of the surface micrographs, (Fig. 18) show a tight, crystalline grain structure. The cadmium-steel interfaces given in Figs. 19b and c show tight interfaces. These were from nucleation (Fig. 19b) at 0.50 $A \cdot cm^{-2}$ for 0.500 S. But for nucleation at 0.10 and 0.96 $A \cdot cm^{-2}$, which is expected to be poor, (Figs. 19a and d), a slight darkening along the interface can be observed. Adhesion of the cadmium may be poorer in these cases.

With growth currents of 0.030 $A \cdot cm^{-2}$ and 0.050 $A \cdot cm^{-2}$ for 10 min or less, dendrite growth was avoided. The nucleation in each case ensured proper growth and tight interfaces, implying strong adhesion. With X-ray diffraction giving ideal powder photographs, the electrodeposits in Fig. 20 were the best cadmium deposits produced from a stirred fluoborate electrolyte.

7.4 Pulse Plating of Cadmium from Fluoborate Electrolyte

The work done in this area can be discussed in two parts: (1) pulse-plating from an electrolyte flow-cell, and (2) pulse-plating experiments from stirred aqueous electrolyte.

The electrodeposition of a 0.5-mil (12.7 μm) thick layer from fluoborate electrolyte on steel substrates required extensive surface preparation, which is described in detail in Appendix IV.

Electrodeposition of Cadmium by Pulse Flow-Cell System:

The pulse plating in an electrolyte flow-cell has provided, for the first time, hydrogen-free cadmium coatings on 300M steel. The plating speed in a flow-cell using pulse regimes with high cathodic peak current is

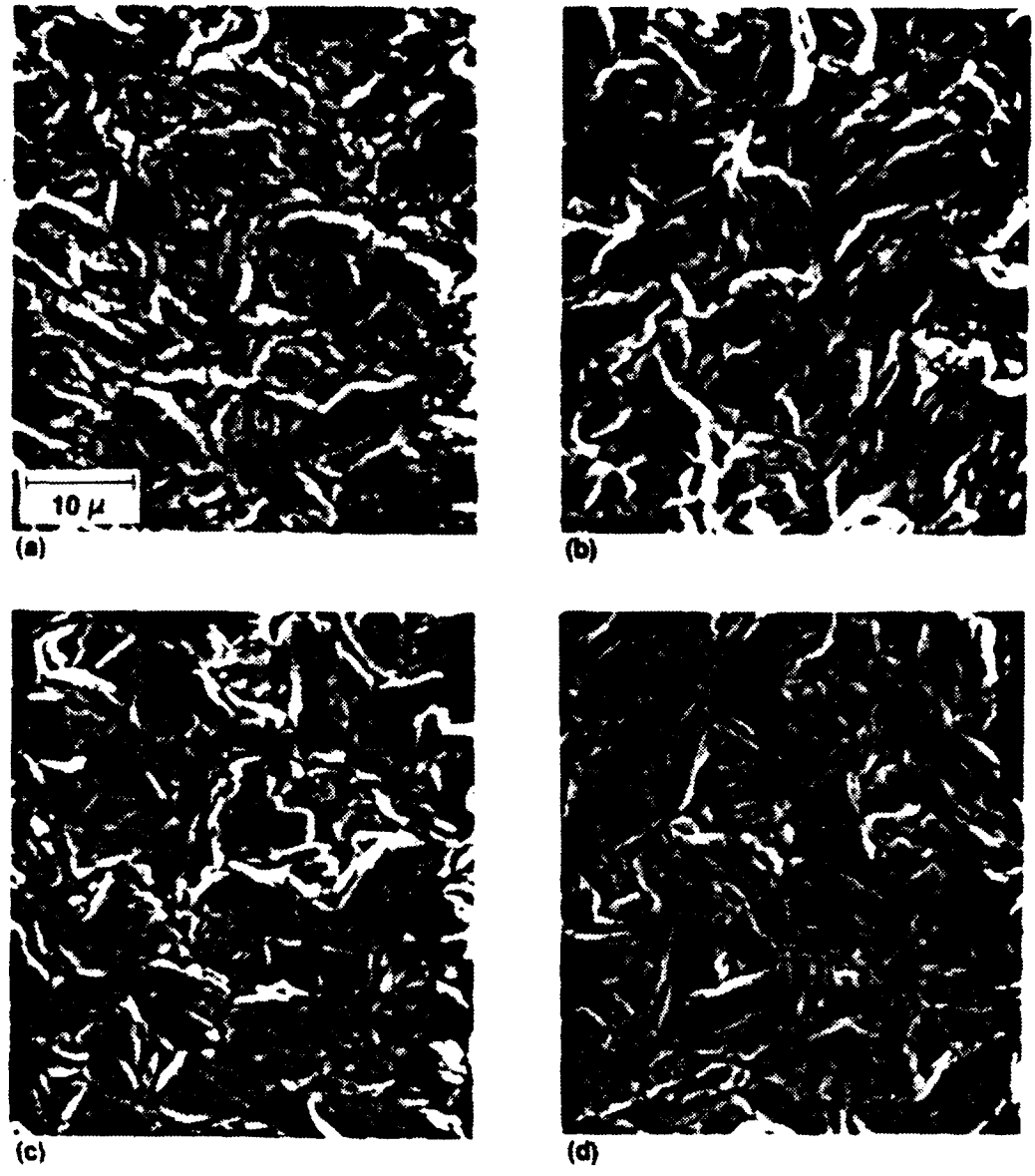

Fig. 18. SEM surface-micrographs of cadmium electrodeposited from fluoborate electrolyte under an initial nucleating pulse followed by DC film growth: (a) nucleation (0.10 $A \cdot cm^{-2}$ for 0.94 S) and growth (0.030 $A \cdot cm^{-2}$ DC for 10 min), nucleation (0.50 $A \cdot cm^{-2}$ for 0.500 S) and growth (0.030 $A \cdot ^{-2}$ DC for 10 min), nucleation (0.50 $A \cdot cm^{-2}$ for 0.500 S) and growth (0.050 $A \cdot cm^{-2}$ DC for 6 min), nucleation (0.96 $A \cdot cm^{-2}$ for 0.942 S) and growth (0.030 $A \cdot cm^{-2}$ DC for 10 min).

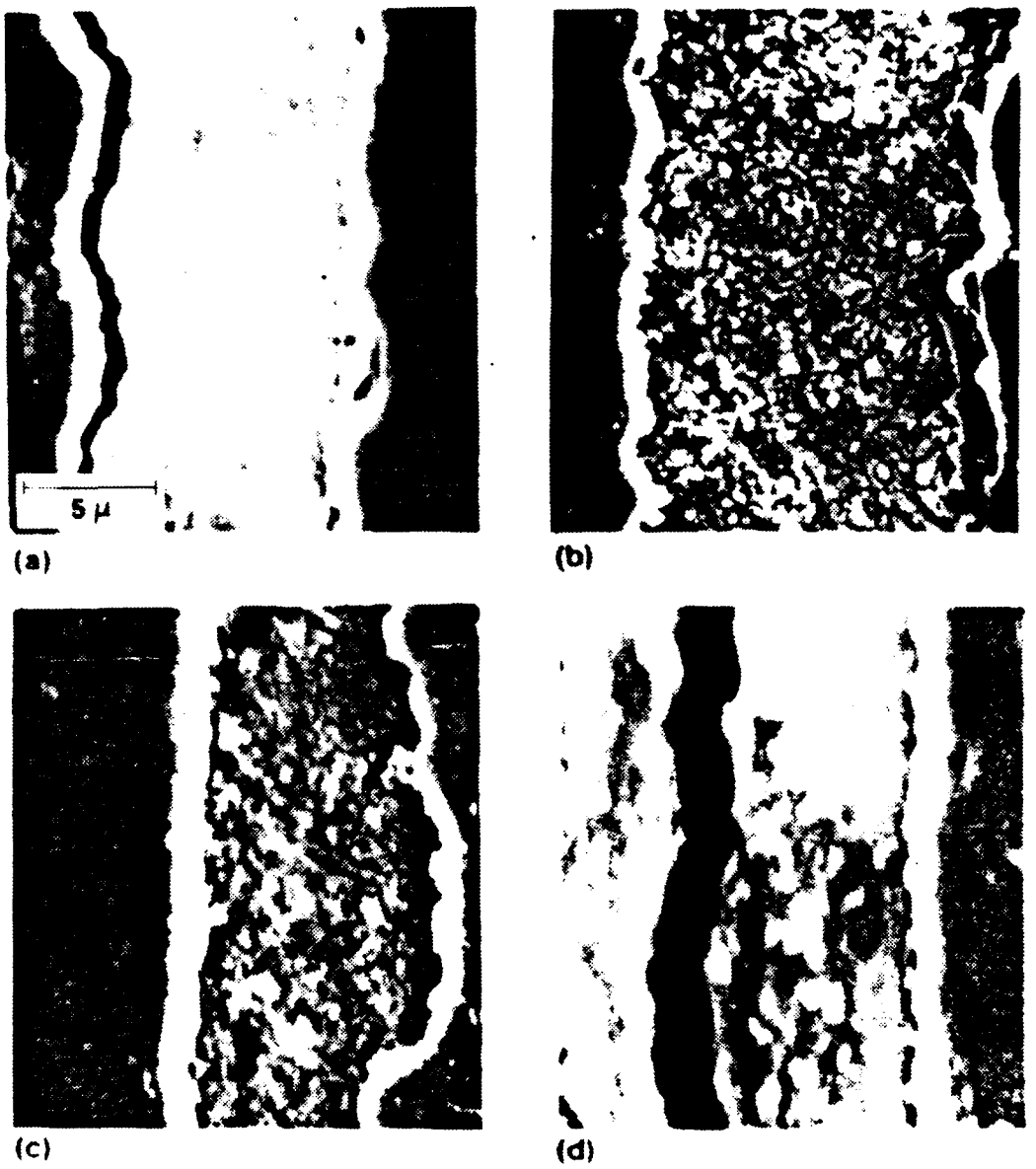

Fig. 19. SEM micrographs of cross sections of cadmium electrodeposited from fluoborate electrolyte under an initial nucleating pulse followed by DC film growth: (a) nucleation (0.10 $A \cdot cm^{-2}$ for 0.94 S) and growth (0.030 $A \cdot cm^{-2}$ DC for 10 min), nucleation (0.50 $A \cdot cm^{-2}$ for 0.500 S) and growth (0.030 $A \cdot^{-2}$ DC for 10 min), nucleation (0.50 $A \cdot cm^{-2}$ for 0.500 S) and growth (0.050 $A \cdot cm^{-2}$ DC for 6 min), nucleation (0.96 $A \cdot cm^{-2}$ for 0.942 S) and growth (0.030 $A \cdot cm^{-2}$ DC for 10 min).

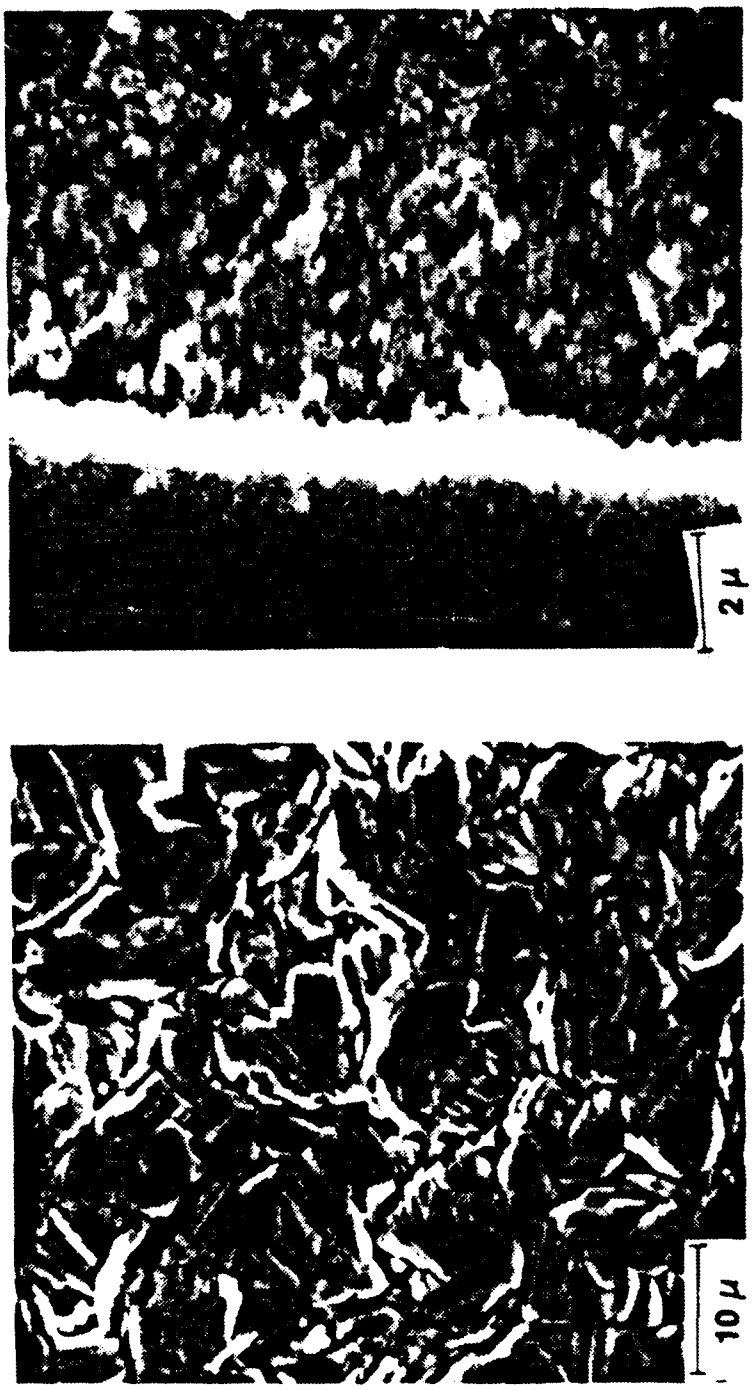

Fig. 20. SEM micrographs of cadmium electrodeposited from fluoborate electrolyte under nucleating pulse (0.50 A•cm^{-2} for 0.500 S), followed by DC growth (0.050 A•cm^{-2} for 6 min); (a) surface; (b) cross section.

about one hundred and twenty (120) times faster than the corresponding DC coatings (i.e., 5 seconds compared with about 10 minutes). Also, keeping the cathodic peak current at about 1 $A \cdot cm^{-2}$ with t_{on} of 0.1 ms and t_{off} of 1 ms, several good-quality (i.e., strongly adhering, silvery in appearance, and compact) coatings free of hydrogen codeposition were produced. This result is certainly of significance.

A number of microstructural aspects of the electrodeposits produced under pulse and electrolyte flow conditions provide keen insight into the process of cadmium electrodeposition from fluoborate electrolyte and must be explored. The scanning electron micrographs of electrodeposits obtained at a peak pulse current of 1 $A \cdot cm^{-2}$ under the action pulses of various widths, unequivocally indicate (Fig. 21) that finer grains are produced with progressively less coulombs or shorter pulses. Fine-grained electrodeposited layers (~12.7 μm thick) of cadmium are obtained by using short cathodic pulses, separated by long rest periods and moderate peak currents. The results are vividly illustrated in Figs. 22 and 23.

Pulse Plating from Stirred Fluoborate Electrolyte

Cadmium was electrodeposited on Type 1018 steel plate placed between two oversized cadmium anodes (separated by 3-4 mm) in stirred fluoborate electrolyte using the computer-driven pulse plating system. The disadvantage of this system was the inability to provide a pulse with narrow width; this problem is attributed to the processing speed of the DEC-350 system. The minimum time parameter for cathodic, anodic, or rest period of any pulse profile could only be 33 ms. Experimentally, this imposed a severe restriction on the microstructure of the coatings achievable using the system. However, a few experiments were done to provide information. These will be discussed in that context.

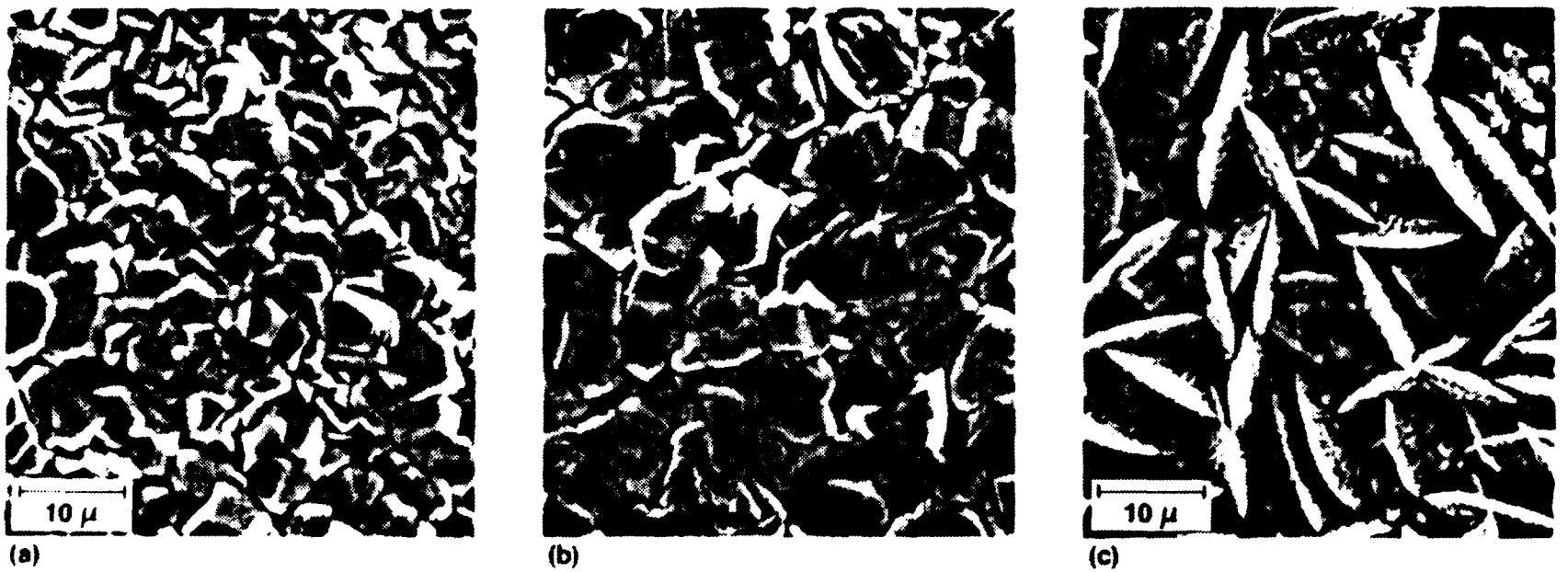

Fig. 21. SEM micrographs of cadmium electrodeposited from fluoborate electrolyte (flowing at a rate of 3.5 $m \cdot s^{-1}$) and under peak pulse current of 1 $A \cdot cm^{-2}$: (a) on-time 0.1 ms and off-time 10 ms, (b) on-time 5 ms and off-time 20 ms, and (c) on-time 40 ms and off-time 40 ms. The photographs show that dense and fine polycrystalline deposits can be obtained by fast pulses with sufficient off-time.

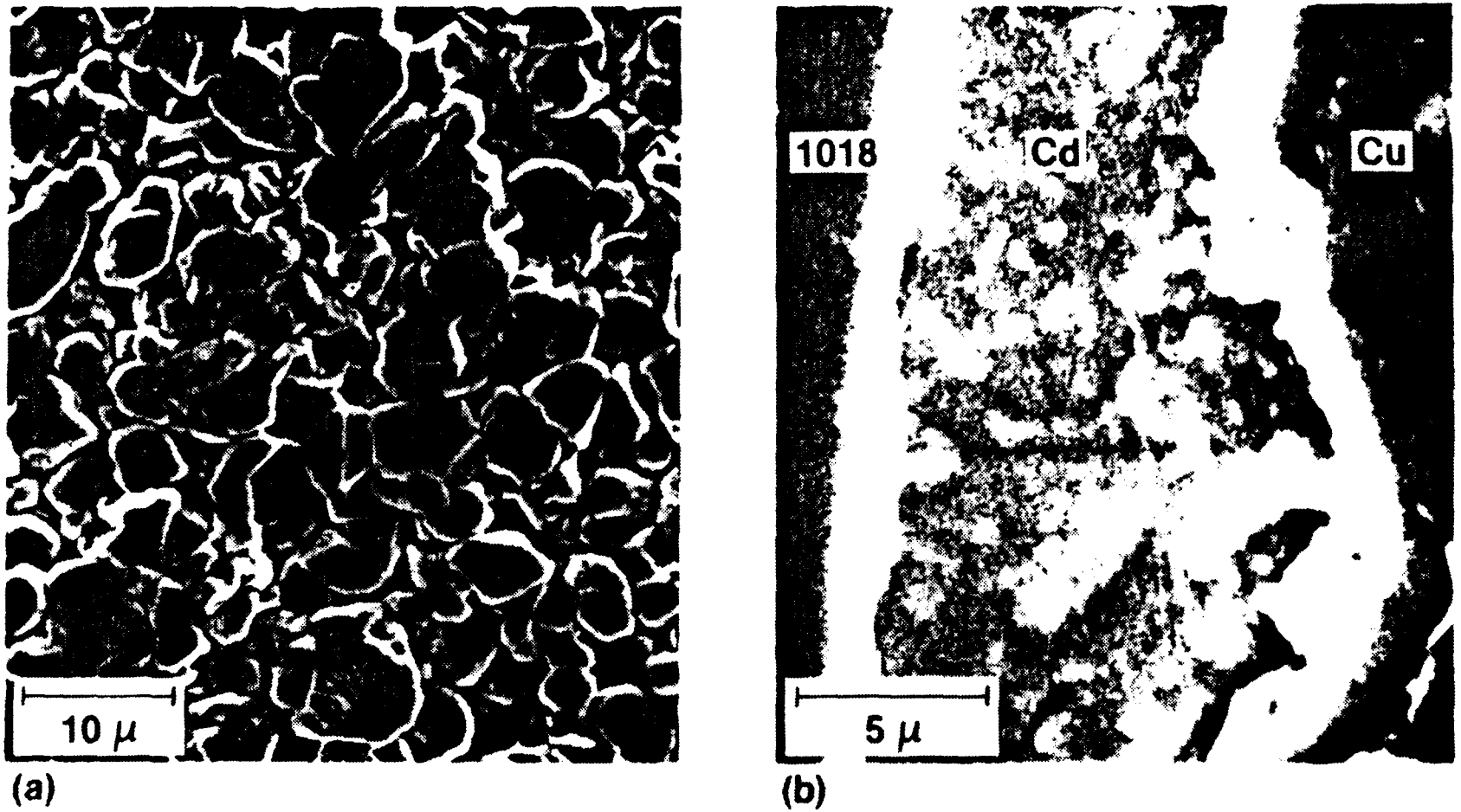

Fig. 22. SEM micrographs of cadmium electrodeposited from fluoborate electrolyte flowing at a rate of 1.7 $m \cdot s^{-1}$ and under pulse current of on-time 0.1 ms and off-time 10 ms with peak current of 1 $A \cdot cm^{-2}$; (a) surface, and (b) cross section.

Fig. 23. SEM micrographs of cadmium electrodeposited from fluoborate electrolyte flowing at a rate of 1.7 $m \cdot s^{-1}$ and under pulse current of on-time 0.05 ms and off-time 1.0 ms with peak current of 1.0 $A \cdot cm^{-2}$; (a) surface and (b) cross section.

In the stirred solution, the crystallite size of cadmium electrodeposition increases with an increase in the value of Q (or coulombs of charge transferred at the electrode-electrolyte interface) for the same t_{on} cathodic pulse width and sufficiently long rest periods t_{off}. This correlation is clearly shown in Fig. 24 and can be rationalized on the basis that crystal growth is promoted by an increase in the energy made available for the growth process.

An interesting result emerged from using an optimized nucleating pulse followed by crystal growth under pulse currents with t_{on} = 33 ms. Because of wide pulse width, the activity of Cd^{+2} species available at the substrate surface reaches steady state quickly (Fig. 25), and this promotes epitaxial growth. Even though the deposition provides strong adherence, the surface topology is dendritic. A pulse width in the μs range is more useful, as shown in the previous results.

7.5 Preliminary Measurements of Hydrogen Codeposition

One of the critical requirements of the project (namely, avoidance of hydrogen codeposition) has been satisfied. The 300M coupons plated with a 12.7-μm (0.5-mil) thick cadmium coating from aqueous fluoborate electrolyte (with pH optimized and protein colloid added) at 1 $A \cdot cm^{-2}$ peak pulse current with t_{on} = 5 μs, t_{off} = 1.0 ms, were examined for bulk permeation by mobile hydrogen.

Hydrogen which may have diffused into the samples during the DC and the flow-cell experiments were measured electrochemically using the Barnacle-cell[12] technique developed at Naval Air Development Center (NADC). The samples removed from the electroplating unit were quickly swabbed with an ammonium nitrate solution soaked in Texwipe and abraded with Scotch-Brite. After rinsing with water and methanol, the sample was dried and

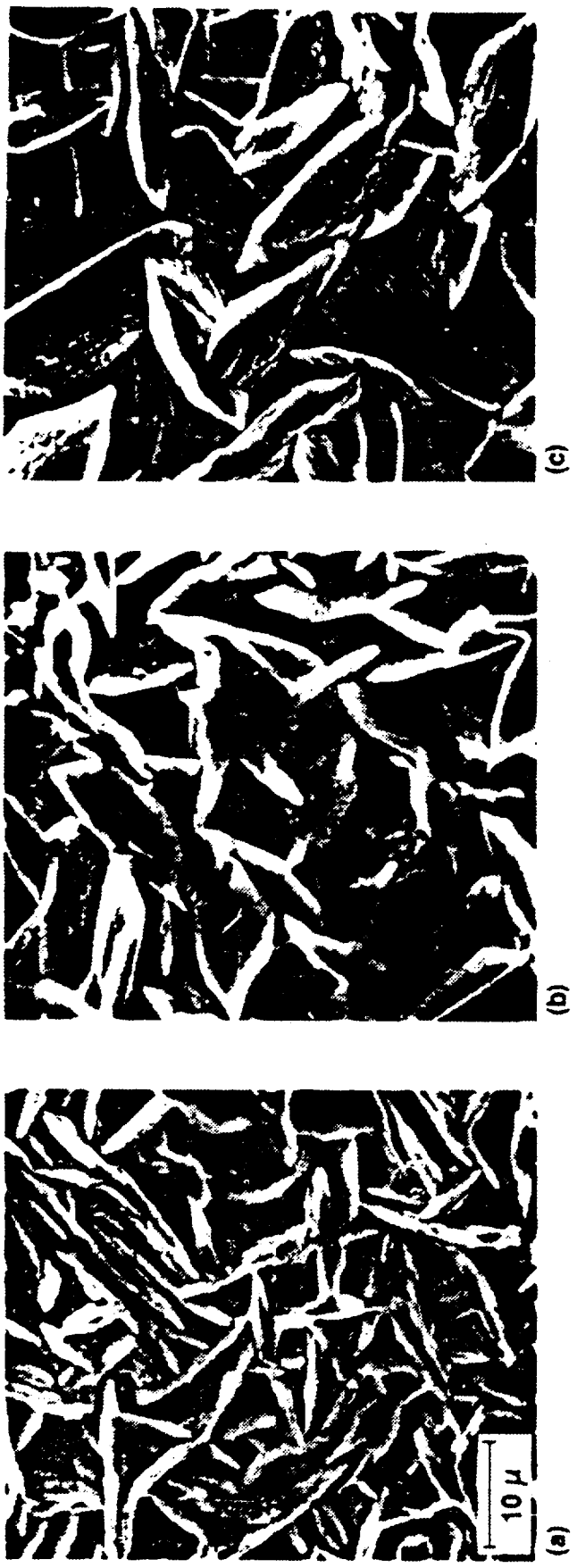

Fig. 24. SEM surface micrographs of cadmium electrodeposited on mild steel under cathodic pulsing: (a) peak current = 200 $mA \cdot cm^{-2}$, t_{on} = 33 ms, t_{off} = 1.0 S, (b) peak current = 0.96 $A \cdot cm^{-2}$, t_{on} = 33 ms, t_{off} = 2.25 S, and (c) peak current = 1.7 $A \cdot cm^{2}$, t_{on} = 43.8 ms, t_{off} = 2.5 S.

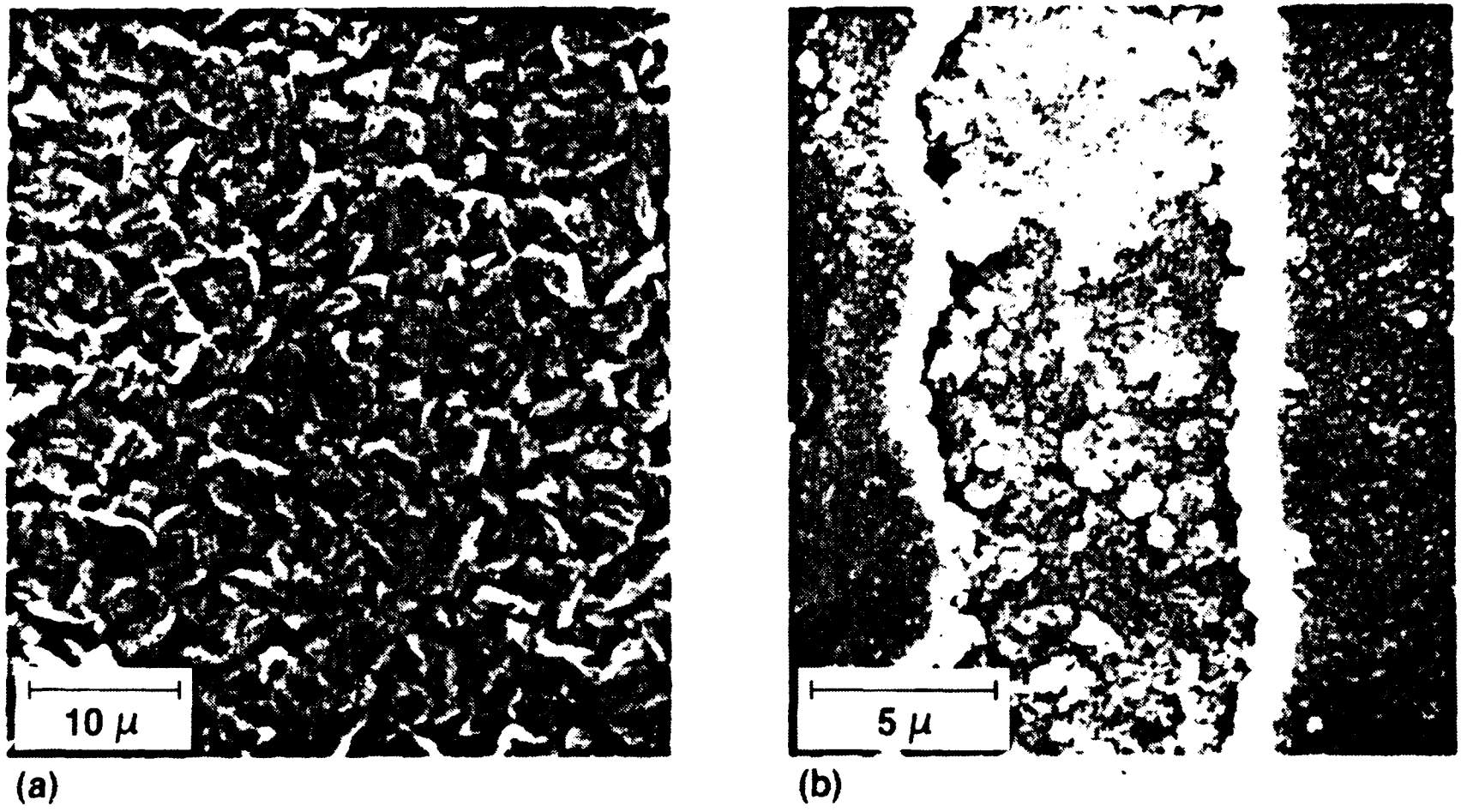

Fig. 25. SEM micrographs of cadmium electrodeposited from fluoborate electrolyte under initial nucleating pulse (0.50 $A \cdot cm^{-2}$ for 0.500 S) and 0.030 $A \cdot cm^{-2}$ cathodic pulse (t_{on} = 30.1 ms, t_{off} = 31.5 ms) growth for 11.3 min; (a) surface and (b) cross section.

mounted in a barnacle cell comprising a nickel oxide electrode and a 0.02 M NaOH solution in a Teflon container; measurements followed immediately to avoid ambient hydrogen diffussion loss. Using a 10-kΩ precision resistor (Vishay) as a shunt, current due to mobile hydrogen was measured with a Keithley 614 electrometer. The hydrogen rate was taken at the end of a 30 min run. The results are summarized in Table 8 and indicate that there was little measurable mobile hydrogen deposited in the steel substrate during the plating.

The 4340 coupons coated with the same thickness of cadmium with 0 5 $A \cdot cm^{-2}$, nucleating pulse followed by 0.030 $A \cdot cm^{-2}$ DC growth was subjected to the same examination. Both sets of measurements were compared with measurements on a blank, unplated steel specimen.

Table 8. Mobile Hydrogen Measurement Experiment

Steel	Blank,[a] $\mu A \cdot cm^{-2}$	Type of Plating	Plated Samples,[b] $\mu A \cdot cm^{-2}$
300M	0.410	Pulse	0.578
"	0.420	"	0.500
4340	0.30	DC	0.308
"	0.42	DC	0.440

[a]Annealed at 190°C for 48 h.

[b]Cd removed by ammonium nitrate solution, before plating sample was heated at 190°C for 48 h.

Note: Not enough samples were taken here to draw definite conclusions.

8.0 ELECTRODEPOSITION FROM MOLTEN SALT

Electrodeposition of cadmium from molten salt was conducted in two stages: (1) suitable molten salts were chosen and (2) electrodeposition of cadmium from a $AlCl_3$-NaCl-$BaCl_2$; (3.5-34.0-2.5 mol %, m.p. 50°C) eutectic-CdI_2 melt appeared most promising and was further investigated. Other melts investigated were CdI_2-KI-NaI (42.1-42.6-15.3 mol %, m.p. 180°C) and $AlCl_3$-KCl-NaCl (60-14-26 mol %, m.p. 90°C) eutectic-CdI_2. Those molten electrolytes selected for investigation of cadmium plating are given in Table 9. Special facilities such as dry boxes (with the absence of moisture and oxygen), electrochemical instrumentation, and electrodeposition apparatus were set up and used during the research.

Experiments were conducted in a helium-purified glove box which was equipped with furnace wells (7 cm dia. and 40 cm deep) that were evacuated to accommodate the electrochemical cell. Type 4340 steel coupons were finished to 600-grade SiC paper before the electrodeposition experiments. A typical electrochemical cell is shown in Fig. 26. Cyclic voltammograms with a 4340 steel working electrode, a cadmium anode, and a cadmium

Table 9. Eutectic Melts for Electrodeposition of Cadmium

Molten Salt Electrolyte	Composition mol %	Melting Point (°C)	Solubility mol %
$AlCl_3$-NaCl-KCl	66-20-14	110.1	$CdCl_2$
$AlCl_3$-NaCl-KCl	66-20-14	110.1	$CdCl_2$ (0.5)
CdI_2-KI-NaI	47.1-42.6-10.3	180	
$AlCl_3$-NaCl-$BaCl_2$	63.5-34-2.5	50	CdI_2 (0.3)
$AlBr_3$-KCl	72-28	80	CdI_2 (<0.03)

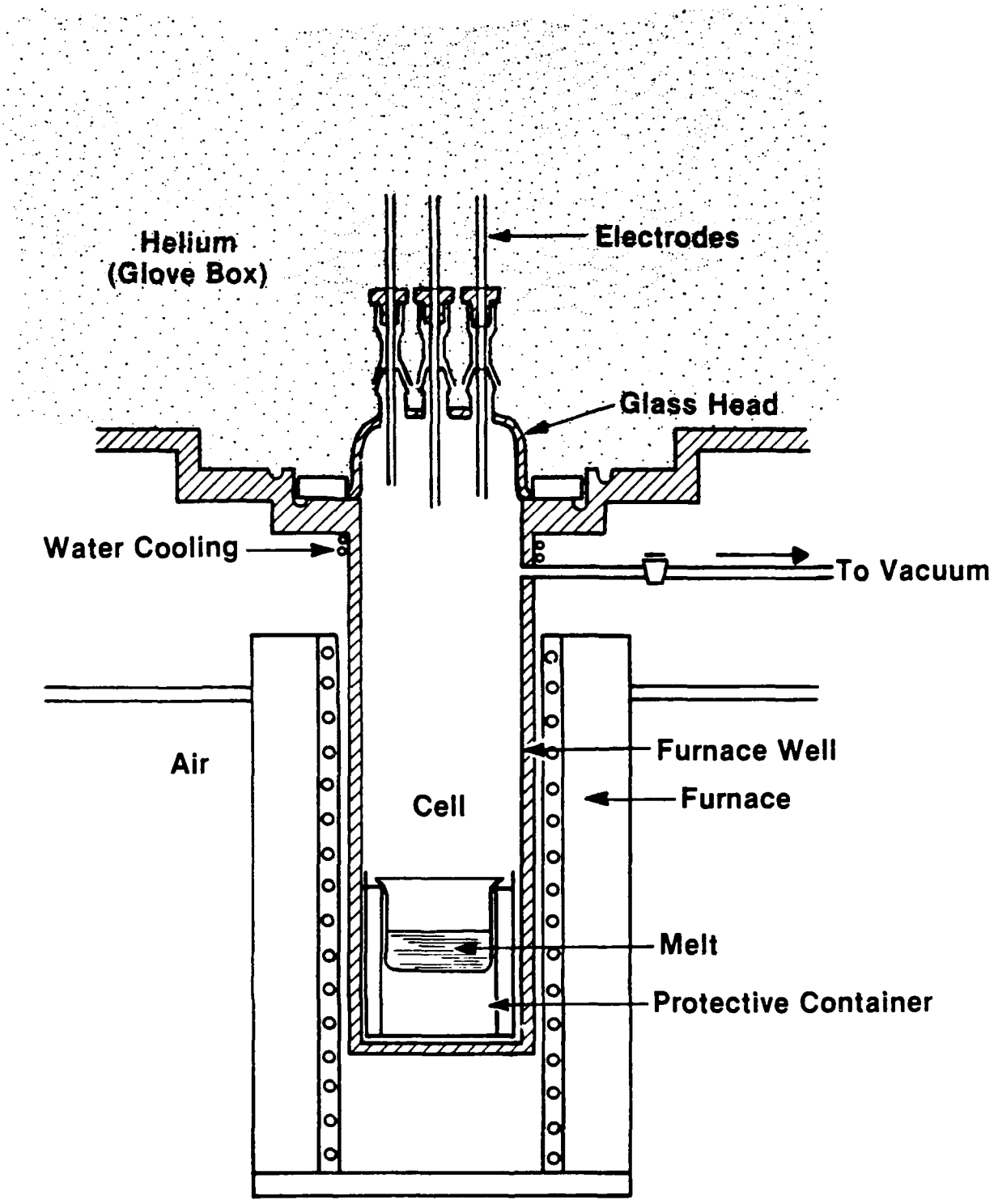

Fig. 26. Schematic of electrochemical cell system for cadmium deposition from molten salt.

reference were obtained to verify if electrodeposition of cadmium was feasible. A cyclic voltammogram from one typical melt is shown in Fig. 27. The figure shows that cadmium can be electrodeposited onto 4340 steel from the melt.

9.0 CONCLUSIONS

A new process for rapid electrodeposition of strongly adherent coatings of cadmium on high-strength 300M and 4340 steels from aqueous fluoborate electrolyte, without hydrogen codeposition, has been developed. This has been achieved by pulse-plating in an electrolyte flow-cell. In the electrolyte flow-cell, the fluoborate solution is circulated through a narrow channel, where a steel disk sample is placed facing a cadmium counter electrode. The flow rate can be adjusted from 0 to 56 $m \cdot s^{-1}$. Since a high flow velocity near the interface reduces the thickness of the diffusion boundary layer, the limiting current density can be increased. When the flow-cell is combined with a pulse current source, the limiting current density can be further increased. In addition, the pulse current will provide high throwing power, resulting in dense deposits and uniform leveling over bumps and protrusions.

Hydrogen-free electroplating of cadmium on high-strength steel from fluoborate electrolyte is feasible. A combination of a nucleating pulse of 0.50 $A \cdot cm^{-2}$ for 0.5 S and fast pulses or a DC growth current density of 0.050 $A \cdot cm^{-2}$ provides the best results, with good coverage and adhesion of void-free coatings. Initial measurements of some samples of both the DC and flow-cell/pulse experiments showed that no measurable mobile hydrogen was absorbed in the steel substrate during the plating. The softness of

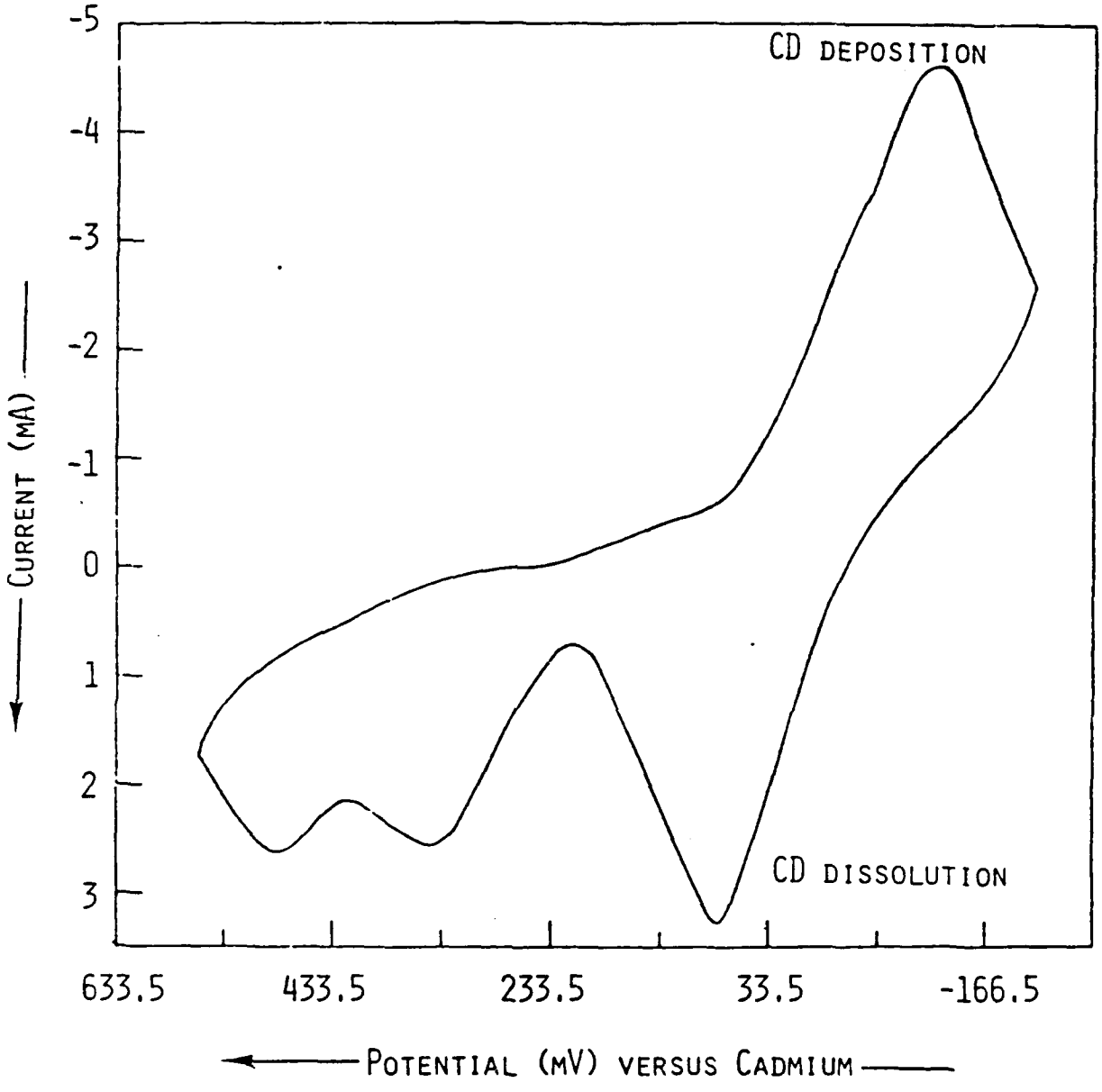

Fig. 27. Cyclic voltagram at 5 mV/s on iron in 63.3 mol % $AlCl_3$-NaCl-$BaCl_2$, CdI_2 at 148.5°C.

these deposits revealed little hydrogen embrittlement of the cadmium deposit itself.

A comprehensive study should be directed toward improving the throwing power of the fluoborate electrolyte by studying the effect of various additives. The next phase of the work should be related to optimization of variables to provide a final recommendation to the Navy for engineering scale-up.

ACKNOWLEDGMENTS

We thank Mr. M. Sloan for his help in running the flow-cell experiments. Many of the micrographs and substrate-surface preparations were prepared by M. Dupont and we acknowledge his contributions.

Some experiments on cadmium deposition from molten salts were conducted by Rajeeva Agarwal as part of his doctoral thesis. We acknowledge his contributions.

Ben Tani conducted the x-ray diffraction and SEM analyses work. For his cooperation we grateful.

We acknowledge Paul Nelson for valuable technical discussions.

T. Hoeller would like to personally thank Prof. Wesley Mathews, Jr., Georgetown University, Dept. of Physics for his critical review of a portion of this manuscript which constituted his Master's thesis in Physics, (Georgetown University, 1985). We also want to thank Dr. Don Vissers for consultations.

Technical discussions with Dr. V. Agawarala from Naval Air Development Center, Warminster, Pennsylvania have been most appreciated in conducting this project. We are grateful to NADC for funding provided for the research.

APPENDIX I

Operation Manual for "Pulse Experiment" on the DEC 350 Professional Computer

To initiate the pulse experiment program, the "Pulse Experiment" is chosen from the "Additional Applications" screen on the DEC 350 display. The title of the experiment and comments may be typed on the screen according to the prompts. After the last comment is entered, an additional <RETURN> causes the screen to display the form defining the pulse program. The cursor prompts for inputs at each field on the form. Movement between fields is initiated with <TAB> and <BACKSPACE> keys for the forward and reverse directions, respectively. By default, the Full Scale Current and Voltage settings are "10,000." When using the Transrex Power Supply the "Full Scale Current" must be changed to "50,000."

Time on the pulse program is calibrated in ticks, where 1 tick equals 15.625 ms (corresponding to a frequency of 64 Hz). The "time per tick" is a scaling factor chosen by the experimenter at the field labeled "Ticks." It will be an integral multiple of 15.625 ms. For example, with an entry of "2" for a scaling factor, the tick will be assigned a time 31.25 ms for all time entries following the "Cathodic" and "Anodic" pulse widths. Then, by setting "2" (for example) in the "Cathodic Pulse Width" field, the actual pulse width will be 2 times 31.25 ms (not 2 times 15.625 ms) and so forth.

The length of the experiment is dependent on inputs to "Cycles to Average," "Cycles to Skip," and "Number of Passes," in addition to "Cycle Time" displayed on the screen.

By definition, a cycle is the execution of zero or more cathodic-rest pulses followed by zero or more anodic-rest pulses. The number of cathodic or anodic pulses in each cycle is entered at "Pulses" on the screen. For example, if the cathodic "Pulses" are "3" and the anodic "Pulses" are "1" then three cathodic-rest sequences are executed, followed by one anodic-rest sequence. The total pulses per cycle is simply "4." The time to execute this cycle is displayed on the screen as the "Cycle Time."

The "Cycles to Average" tells the computer how many cycles are used to time-average data. The "Cycles to Skip" tells how many cycles to continue running the experiment without logging data. The computer will acquire data first and then skip the specified number of cycles.

The sum of the number of "Cycles to Average" and "Cycles to Skip" constitutes a "Pass." As each new pass occurs during operation, the computer will acquire and then halt data acquisition according to the settings at "Cycles to Average" and "Cycles to Skip." The time for one pass is simply the number of cycles per pass times the time per cycle displayed on the screen. If the total experimental running time is known, the number of passes can be determined by dividing the experiment time by the time per pass. (Note: the input to "Total Passes" as well as the inputs to "Cycles to Average" and "Cycles to Rest" must be integers.) A practical upper bound of no more than 100 passes should be made in a given experiment.

Another method to determine the total number of passes is from the total number of pulses. As before, the total number of pulses/pass is the number of pulses/cycle times the number of cycles/pass. The number of passes the operator would set is the number of total pulses divided by the number of pulses/pass. Either method of setting up the length of a pulse

experiment is satisfactory. As a check, the operator should ensure the accuracy of the "Total Passes" setting by checking for consistency between the total time and total pulse method.

The operation of the computer pulse program to form the various pulse profiles is as follows.

To produce a nucleating pulse, only the time in ticks and the amplitude corresponding to the "Nucleating Pulse" should have nonzero entries. All other fields should have "0" entries.

A DC current can be obtained by specifying a time in seconds and an amplitude following the "Growth" display. Again, all other entries must be "0."

A nucleating pulse followed by a DC current is obtained by a combination of entries to the "Nucleation" and"Growth" fields with no cathodic or anodic pulsing.

A pulse experiment is programmed as follows. The width of the pulse is specified in ticks. From the known cathode surface area and desired current density, the amplitude of the pulse current is entered. A "0" entry for either the anodic or cathodic pulse amplitudes will, in effect, be a "Rest" pulse of the duration set on the pulse width. The number of cathodic pulses (pulse-rest) to execute before the anodic pulse-rest sequence is set by the entry at "Pulses." Rest times and/or current pulses may be set to zero. The cathodic or anodic pulse can be skipped entirely by entering "0" for "Pulses." As noted above, use of this feature is necessary to produce the nucleation and growth pulses.

A combination of any or all of these pulses may be used at one time. For instance, a nucleating pulse followed by a sequence of cathodic or anodic pulses is possible. With the pulse program, virtually any pulse profile can be generated.

APPENDIX II

Instrumentation and Operation Procedures for Running Computer Pulse Experiments

A. Operation Procedures Prior to Experimentation

Prior to experimentation, each instrument should be set as follows.

1. Transrex Power Supply:
   a. Turn the 440-V circuit breaker power supply on.
   b. Turn on the main power switch to the cooling unit. (Note: the "Door Ajar" light goes out.)
   c. Press the "Reset" button. (Most of the front panel lights will go out.)
   d. Press the AC "ON" button. The AC "ON" bulb will light.
   e. Press the DC "ON" button. The DC "ON" bulb will light.
      Note: To help reduce leakage current to the cell, the DC "ON" button should only be pressed just prior to experimentation.
   f. Between experiments, the cooling unit may be turned off. In that case begin instructions at step b.
   g. Daily shut-off requires each of the preceding steps to be performed in reverse order.
2. Wenking High Power Potentiostat: Initial setup and operation is according to manual specifications (Figs. 1,2) for controlled current operation.
3. Dec 350 Professional Computer: The desired pulse is programmed into the computer as previously described in Appendix I.

4. Norland 3001 Waveform Analyzer: The user must become familiar with the basic controls necessary for obtaining and displaying waveforms on the Tektronics monitor. The operator is urged to consult the "Introduction" in the Norland 3001 Waveform Analyzer owner's manual. To trigger the analyzer for capturing the (1) initial nucleating pulse or (2) any subsequent pulse of similar width and height, such as would occur during cathodic pulsing, simply adjust the "Acquisition Trigger" controls as follows.
   a. Make a dummy cell consisting of a short circuit (i.e., 1 Ω resistor) in place of the electrochemical cell.
   b. Program the computer to run the desired pulse through the dummy cell. Display the current pulse on the waveform monitor.
   c. Obtain a *moving* display by momentarily flipping the "Release" toggle switch.
   d. Display only the channel Halves (H1, H2) or Quads (Q1, Q2, Q3, Q4) which are on (active) by pressing the keystrokes DPLY <H1 and/or H2, Q1 and/or Q2 and/or Q3 and/or Q4> vs. T/F. The "Active," "Range," and "Bias" controls should be set so that the waveform is properly displayed and not chopped. When this happens, a red diode will light near the "Bias" Control." The Wenking outputs 0.2 V at the full-scale current chosen on the "Range Selector Switch." The Transrex gives 50 $A \cdot V^{-1}$ at its current monitoring terminal. This information will aid in setting the "Range Controls" for the current pulse. Voltage levels input into the

waveform channels are generally not known until the experiment is run. As a general rule, a 0.50 $A \cdot cm^{-2}$ pulse will almost go off scale on the 5-V potential range. The "Bias Level" controls may be raised or lowered to increase the peak range.

e. Push "Triggered Hold" followed by "Periodic Hold." The display should now flash at a rate dependent on the "Sample Interval" setting. If it is not flashing, then proper triggering is not occurring. As a check, the channel where the trigger input is connected should be made "active" by turning the knob towards that channel. All other trigger knobs on the remaining three channels must be in the off position, or else the error "TRIG O/LAP" is displayed.

f. With External Triggering "OFF," Slope set to "(-)," and Coupling to "A.C.L.F. Rej." (middle position), adjust the "Sample Interval" toggle switch and the "Delay Full Screen" to get the waveform filling the screen and properly centered. For example, a 33-ms pulse may be captured with a 3/8 delay at 50 μs/pt. Following these steps, the waveform analyzer is ready to capture the first nucleating pulse during the experiment.

B. Operation Procedures for Running the Pulse Experiment.

With all of the instruments ready for operation according to the procedures above, the running of the actual experiment is as follows.

1. Push "Release" followed by "Triggered Hold" on the waveform analyzer if capturing of the first pulse is desired. Remember that the triggering acquisition and mode should be set as previously determined to record the entire first pulse.
2. Close the switch to the proper power supply.
3. Activate the power supply for controlled current operation. For the Wenking power supply, turn the "Operator Selector" switch to "I." On the Transrex cell cycler, simply push "DC ON."
4. With the pulse preprogrammed on the computer screen, pressing <Return> on the computer begins the experiment. Note: Steps 2-4 should be done in rapid succession to avoid leakage or galvanic corrosion currents to the cell.
5. During the experiment more waveforms on the analyzer may be captured by depressing "Release" followed by either "Manual Hold" or "Triggered Hold."
6. At the end of the experiment, the computer shuts off the current and displays the word "Done." To avoid leakage currents or corrosion of the deposit, the power supplies are shut off and the switch is opened as soon after the experiment as possible.
7. Hard-copy output may be obtained from the data acquired by the DEC 350 computer or the Norland Waveform Analyzer. The computer stores data at the rate of about 25 ms/pt. The resulting time-averaged data over a pass is stored on the 10-Mbyte hard disc drive. The file name given to the data is the title assigned to that experiment. To retrieve the data for plotting through the VAX 11/780, the user must log into his account using the DEC 350

Computer as a terminal. When the command GETFILE [filename.dat] is typed, a copy of "filename.dat" from the DEC 350 will be made in the VAX directory. Now the command PLOTDATA [filename.dat] will initiate the plotting on the specified printer. The major drawback to this method of data acquisition is the 25 ms/pt. speed. For higher time resolution, the data in the Waveform Analyzer is much more desirable for plotting.

The steps for downloading the data from the Norland Waveform Analyzer to the VAX are as follows. The hardware connection from the waveform analyzer to the VAX may be found in Bldg. 205 in room A-125. Following the "$" prompt, the command NEWFILE [discfilename] is entered on the VAX. The command PRINT [ARRAY] (found in the "Print Section" of the Norland owner's manual) is then executed on the waveform analyzer. A raw data file named "discfilename.raw" is now loaded on the VAX. The "RAW-TO-DAT" software program processes the raw file to a form usable by the DISSPLA plotting program. The processed file is stored separately as "discfilename.dat" Now a suitable FORTRAN program, written for DISSPLA, plots the waveforms.

APPENDIX III

Electroplating from Alkaline-Cyanide Electrolyte

Described here are results of high DC current density experiments involving deposition of cadmium from alkaline-cyanide electrolytes. Cyanide plating was found to be accompanied by hydrogen codeposition. This was a more serious problem than with the fluoborate electrolyte.

Experimental

The equipment used for electroplating cadmium from alkaline-cyanide baths at constant current densities up to 5 $A \cdot cm^{-2}$ required a 5-A DC galvanostat with a $\pm$20 V output. A multimeter and a strip chart recorder with a standard calomel reference electrode were two instruments that were used to monitor the cell current and the deposition potential. A complete listing of the equipment and accessories is given in Table 10.

Table 10. Instrumentation Utilized in DC Plating

Model 371 Potentiostat/Galvanostat (Princeton Applied Research)
Model 178 Electrometer Probe (Princeton Applied Research)
Model 7100B Strip Chart Recorder (Hewlett-Packard)
2 Model 17501A Plug-in Modules (Hewlett-Packard)
Model 8000A Digital Multimeter (Fluke)
1-Ω, 200- to 225-W Adjustable Resistor (Mallory)
10-A, 100-mV Shunt (Empro)
1:1 High-Impedance Amplifier
Model PT 320 Analytical Balance (Mettler)
Model 4812 Magnetic Stirrer/Hot Plate (Cole-Parmer)

A simple electrochemical two-electrode cell arrangement for cadmium plating from cyanide electrolyte is shown in Fig. 28. An optimized dual counter electrode arrangement is shown in Fig. 29. Various electrode configurations along with reference electrodes used in the alkaline-cyanide platings are described in Table 11. Surface preparation of Type 4340 steel was performed according to the procedure given in the Appendix IV. Prior to electrodeposition, the nickel electrode was mechanically polished with 600-Grade SiC paper and chemically etched with a solution of 15 mL HCl in 100 mL ethanol for 30 seconds.

The composition of the three different cyanide electrolytes used is given in Table 12. Fresh NaOH pellets were initially dissolved into a known volume of triply distilled water. Weighed amounts of $Cd(CN)_2$, CdO, $CdCO_3$, and NaCN were added while the solution was magnetically stirred and heated to below boiling (60-70°C) for 30 minutes. The pH and conductivity of solutions were measured. The electrodeposition of cadmium from cyanide electrolytes was conducted using direct current that varied from 0.10 to 5 $A \cdot cm^{-2}$. The electrolyte bath was kept at 25-30°C and the solution was constantly stirred.

Experimental Results

The nature of the electrodeposits from the alkaline-cyanide baths were found to be dependent on the electrode configurations (Table 11, Figs. 28 and 29), and the electrolyte (Table 12). Figure 30 is a plot of cathode efficiency as a function of current density for each bath. The deposition efficiencies observed in Fig. 30 were found to be poor because of hydrogen codeposition on the electrode surface. Measured with respect to Cd^{+2}/Cd^{o}, deposition potential-time plots are given in Figs. 31-33 for electrodeposits from Baths A-C, respectively. These overpotentials

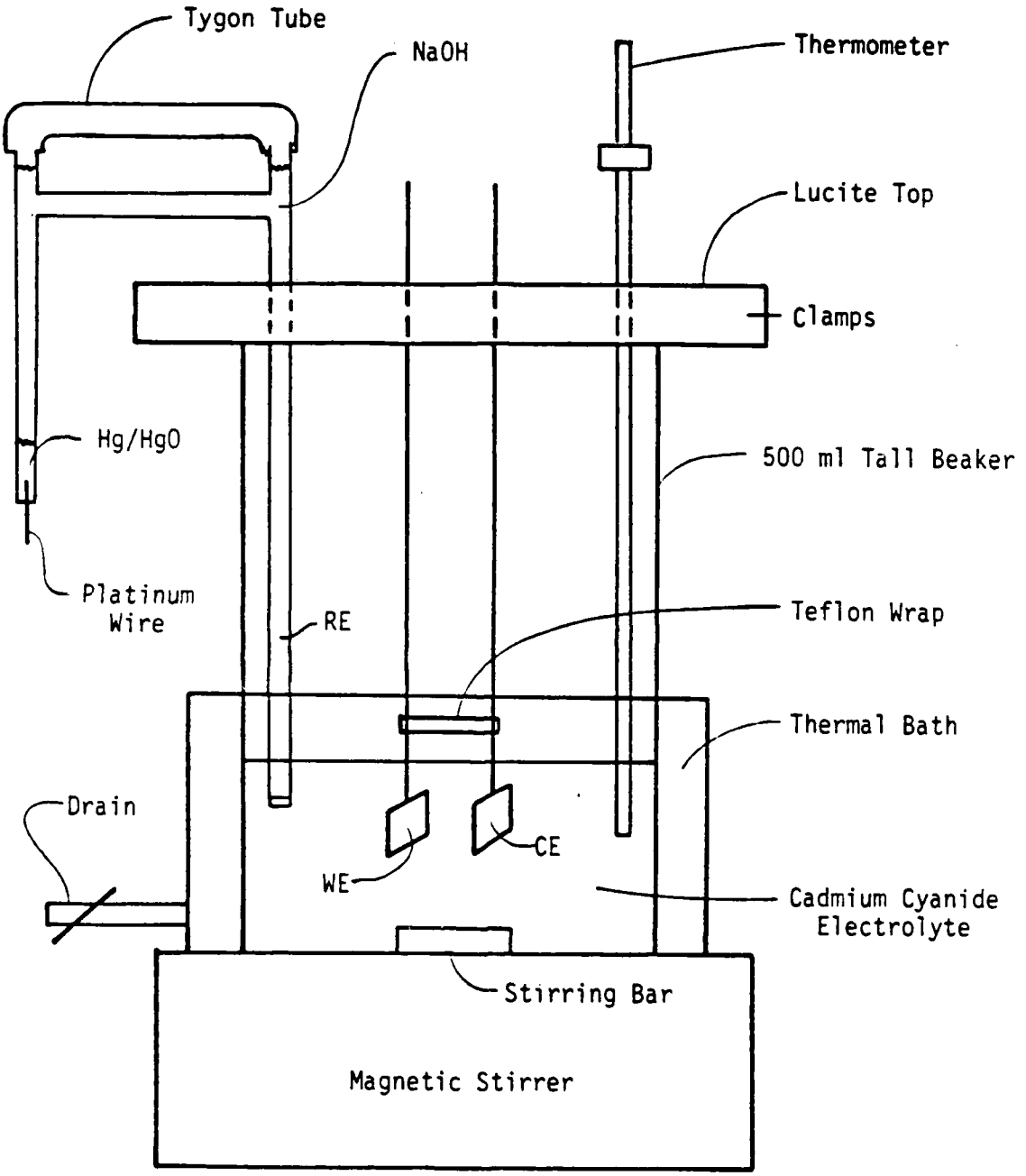

Fig. 28. Electrochemical cell for deposition of cadmium from alkaline-cyanide electrolyte.

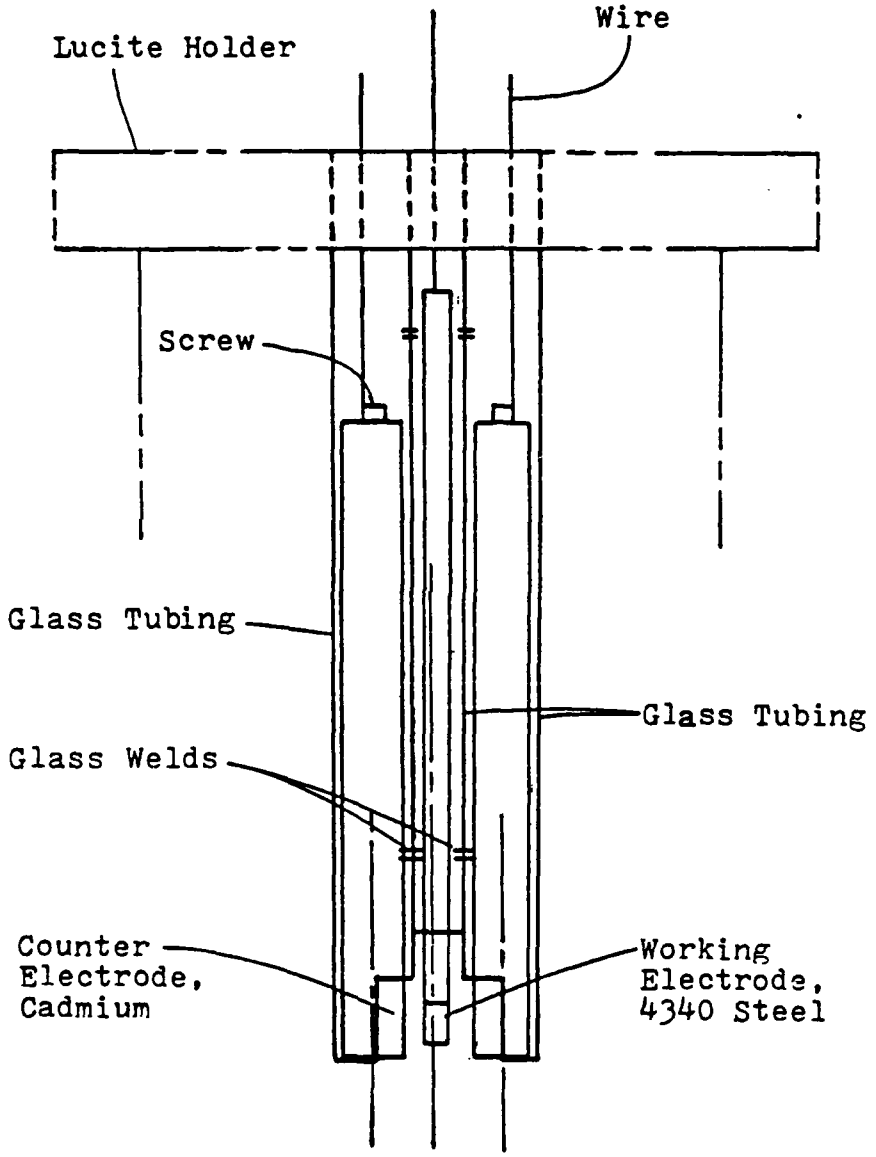

Fig. 29. Electrode assembly for electrodeposition of cadmium on AISI 4340 steel from alkaline-cyanide electrolyte (WE to CE distance is ~3 mm).

Table 11. Cell Electrodes for DC Alkaline-Cyanide Deposition

Cyanide Electrolyte Preparation	Working Electrode (WE)	Counter Electrode (CE)	Reference Electrode (RE)
A	1 cm x 1 cm x 50 mil Ni or Ni plated Cu (Area = 1 cm^2)	1 cm x 1 cm x 50 mil Ni	Hg/HgO
B	1 cm x 1 cm x 0.3 cm AISI 4340 Steel (Area = 1 cm^2)	1 cm x 1 cm x 50 mil Ni	Hg/HgO
C	0.5 x 0.5 x 0.25 cm^2 AISI 4340 Steel (Area = 0.88 cm^2)	Two 8 mm diameter 99.9% Cd rods	Hg/HgO

Table 12. Preparation of Alkaline-Cyanide Electrolytes

	Bath A "Dull" Deposit	Bath B "Bright" Deposit	Bath C "Bright" Deposit
CdO (g)	3.700	14.952	15.778
$CdCO_3$ (g)	0.360	1.442	1.560
NaCN (g)	19.139	95.742	96.614
NaOH (g)	1.080	4.152	4.772
Final Volume (mL)	500 ($\pm$5%)	1000 ($\pm$5%)	1000 ($\pm$5%)
pH	13.3	11.8	11.88
Specific Resistance ($\Omega \cdot cm$)	12.4	5.5	7.03 $\pm$0.05
Conductivity $(\Omega \cdot cm)^{-1}$	80.6 x 10^{-3}	164 x 10^{-3}	147$\pm$1.5 X10^{-3}
Moles CN^-: Moles Cd	6.58:1	7.99:1	7.99:1
Cd concentration $(g \cdot L^{-1})$	16.1	32.0	32.1

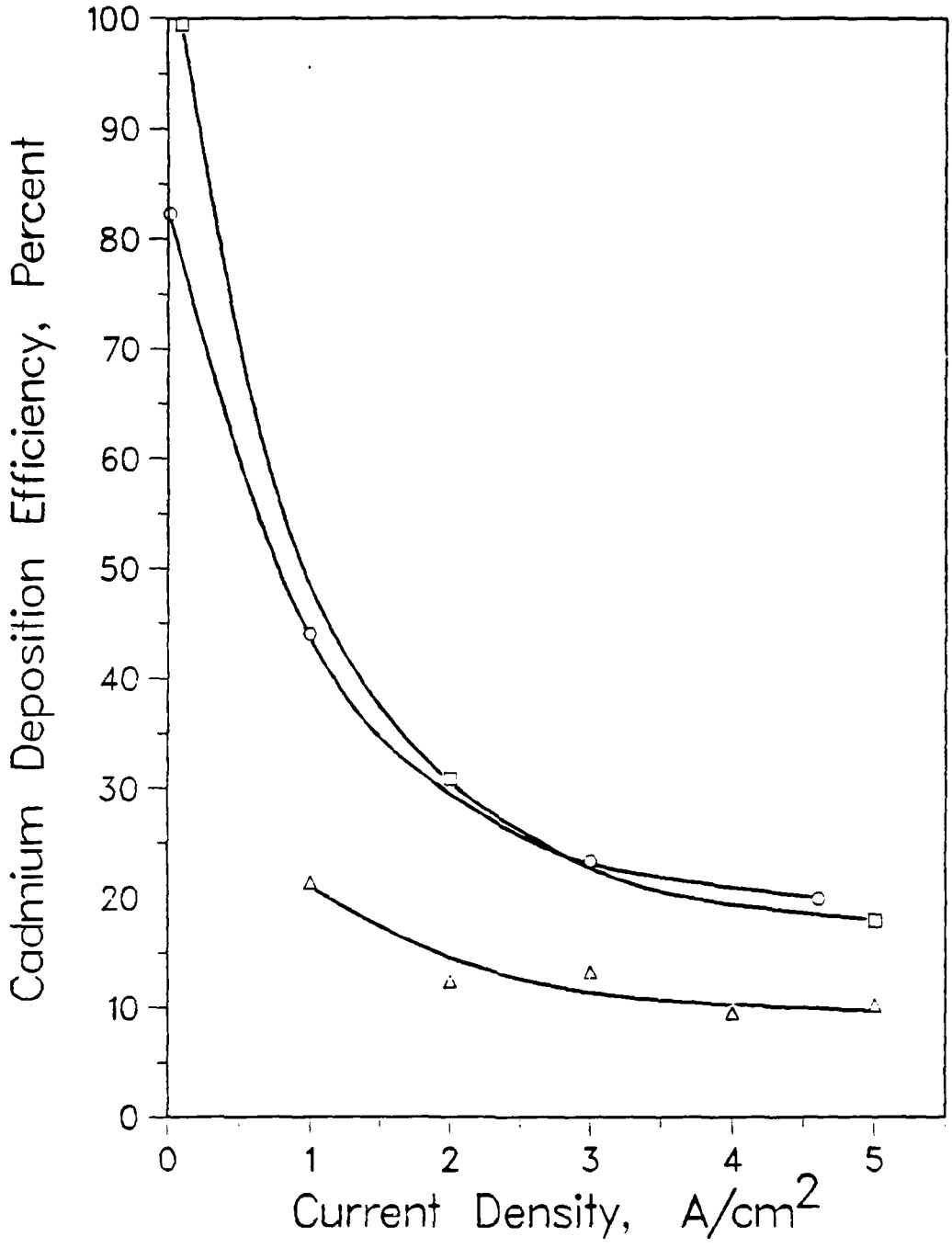

Fig. 30. Cadmium deposition efficiency versus current density for three alkaline-cyanide baths:

32 g•L^{-1}Cd; CE = Cd (Bath C)
32 g•L^{-1}Cd; CE = Ni (Bath B)
16 $\pm$ 4 g•L^{-1}Cd; CE = Ni (Bath A)

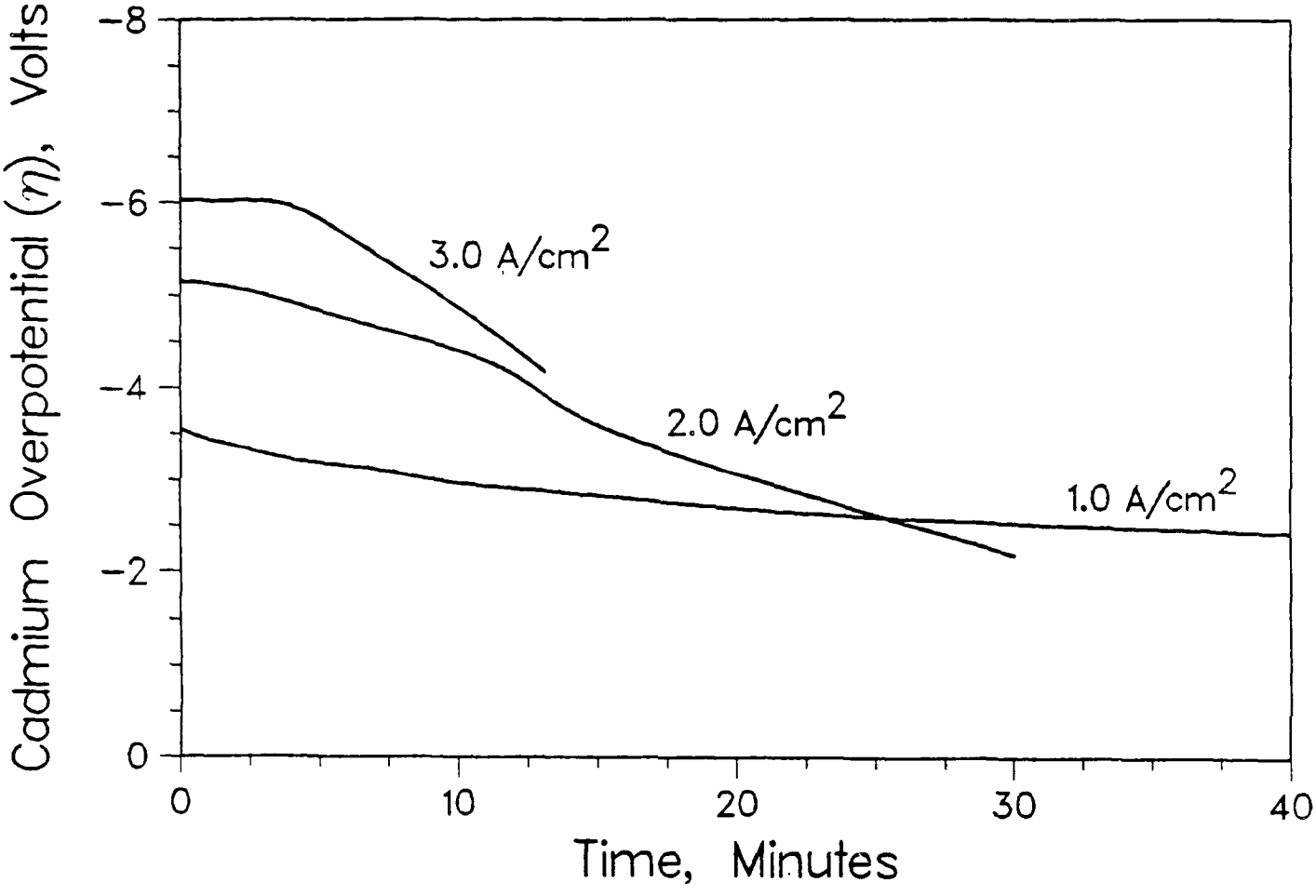

Fig. 31. Deposition potential versus Cd^{2+}/Cd^{o} reference for cadmium electrodeposition from alkaline cyanide electrolyte (16 $\pm$ 4 $g \cdot L^{-1}$ Cd, Bath A).

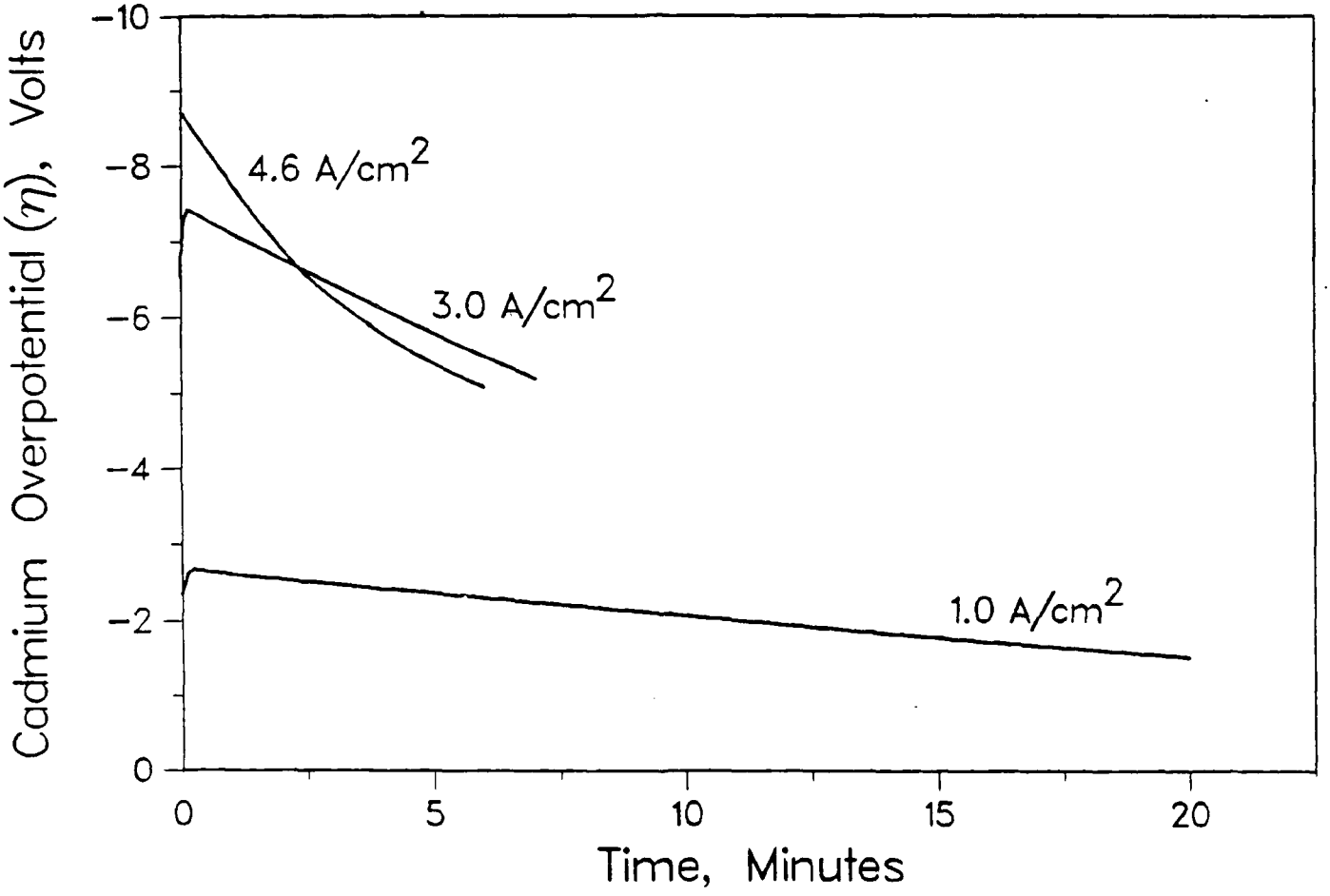

Fig. 32. Deposition potential versus Cd^{+2}/Cd^{o} reference for electrodeposition of cadmium from alkaline cyanide electrolyte (32 $g \cdot L^{-1}$ Cd, Bath B).

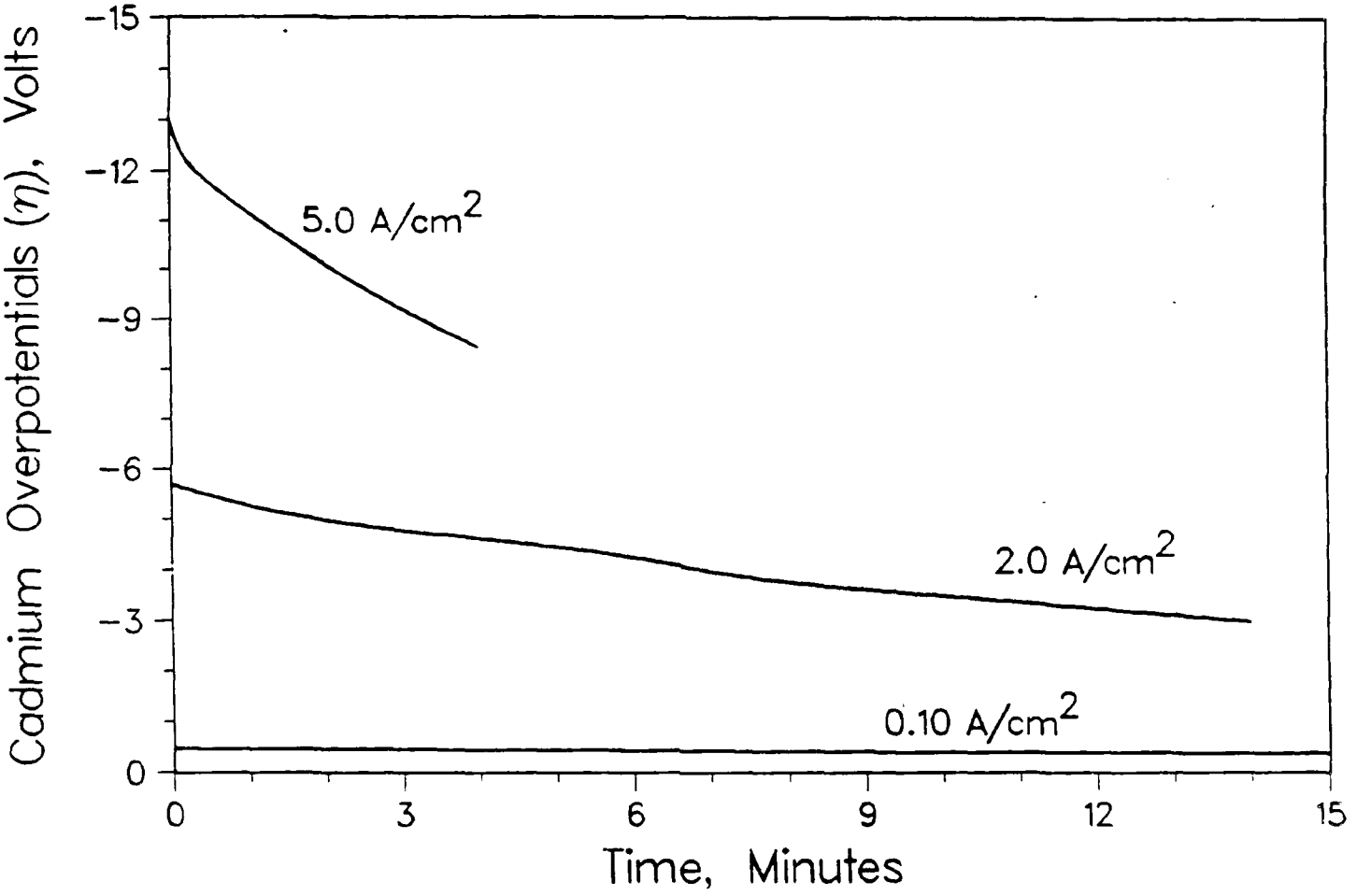

Fig. 33. Deposition potential versus CD^{2+}/Cd^{o} reference for electrodeposition of cadmium from alkaline cyanide electrolyte (32.1 $g \cdot L^{-1}$, Bath C).

were taken from strip chart recordings and are not compensated for cell IR drop. Current-overpotential data for deposition potentials versus Cd^{2+}/Cd^{o} extrapolated to time = 0 are found in Table 13. The current densities listed are the portion of the total current due to cadmium deposition corrected from the plating efficiencies in Fig. 30.

In successive plating experiments from the same electrolyte, (Tables 14-16) the cadmium concentrations were determined by subtracting the weight of deposit from the original cadmium concentrations (weight) present in the cell. All other cadmium concentrations listed, with the exception of Sample B4, are those from experiments with fresh electrolyte preparations.

It is apparent from Fig. 30 that doubling the cadmium concentration from 16 to 32 $g \cdot L^{-1}$ doubles the cathode deposition efficiency at constant current density. Twice as many dischargeable cadmium ions or complexes are available at the diffusion layer for electrodeposition; therefore, the rate of cadmium deposition is doubled. At all cadmium concentrations, the cathode efficiency decreases rapidly with current densities up to about 1 $A \cdot cm^{-2}$ and then begins to level off at 5 $A \cdot cm^{-2}$. At high current densities, mass transport and diffusion control limit the rate and amount of cadmium deposition. The larger the bulk concentration of cadmium near the diffusion layer, the higher the efficiency, regardless of mass transport limitations even at high current densities. Even the use of a soluble cadmium anode increases the efficiency at low-to-moderate current densities.

Deposition Overpotential and Concentration

From Figs. 31-33 it is observed that, at constant current densities of 1 and 2 $A \cdot cm^{-2}$, the deposition potential versus Cd^{2+}/Cd^{o} for cadmium concentrations of 16 $g \cdot L^{-1}$ is more negative than for those of 32 $g \cdot L^{-1}$.

Table 13. Current-Potential Data for Cadmium-Deposition from Cyanide Electrolyte

Cadmium[a] Current Density, $A \cdot cm^{-2}$	Potential vs. Cd^{2+}/Cd^{o},[b] V
0.023	-0.10
0.099	-0.42
0.44	-2.27
0.62	-5.39
0.70	-7.43
0.71	-8.31
0.90	-12.54

[a]Total current corrected for the cadmium deposition efficiency in Fig. 30.

[b]Determined from a linear extrapolation to time = 0 in Figs. 31, 32, and 33.

Table 14. Cadmium Deposition Parameters From Alkaline-Cyanide Bath A

Sample	A1	A2	A3	A4	A5
Current Density, $A \cdot cm^{-2}$	1.0	2.0	3.0	4.0	5
Plating Time, min	45.0	30.0	20.0	12.2	13.0
Cd Concentration, gL^{-1}	16	14	16	20	14
Weight of Deposit, mg	337	261	227	164	231
Calculated Thickness, μm	390	302	320	190	267
Efficiency, %	21.4	12.4	13.2	9.5	10.2

Table 15. Cadmium Deposition Parameters From Alkaline-Cyanide Bath B

Sample	B1	B2	B3	B4	B4
Current Density, $A \cdot cm^{-2}$	0.015	1.0	3.0	4.3	4.6
Plating Time, min	975	20.0	7.0	6.0	5.0
Cd Concentration, $g \cdot L^{-1}$	32.0	32.0	32.0	31.0	32.0
Weight of deposit, mg	424	308	171	196	160
Calculated Thickness, μm	490	356	185	227	185
Efficiency, %	82.3	44.0	23.3	21.1	19.9

Table 16. Cadmium Deposition Parameters From Alkaline-Cyanide Bath C

Sample.....	C1 (Control)	C2	C3
Current Density, $A \cdot cm^{-2}$...	0.10	2.0	5.0
Plating Time, min.....	139	14	4.0
Cd Concentration, $g \cdot L^{-1}$...	32.1	32.1	32.1
Weight of Deposit, mg.....	423	264	110
Calculated Thickness, μm..	559	350	145
Efficiency, %.....	99.4	30.8	17.9

Assuming equivalent IR drops between the cell electrodes in both baths, greater concentration polarization with 16 $g \cdot L^{-1}$ Cd may be responsible for the higher deposition potentials. The slopes of the potential-time curves also show rapid increase toward less-negative values at higher current densities. This increase in deposition potential towards less negative values may be due to increasing surface area with dendrite growth at current densities of 1 $A \cdot cm^{-2}$ or more.

Effect of High DC Current Density on Growth

A surface micrograph of cadmium deposited at 2, 3, and 4 $A \cdot cm^{-2}$ is shown in Fig. 34. At these current densities the growth was nodular and porous. For the highest current density shown, finer nodular growth occurred with higher density per unit substrate area, giving the deposit a smoother appearance. The growth shown in Fig. 34 is typical for deposition at high overpotentials.

Measurement of Plating Thickness

Measurements of cadmium plating thicknesses from cyanide electrolytes were made using an Ultraphot II Metallograph with a grating ruled to 0.01 mm. The appropriate scale photograph was then used to make at least

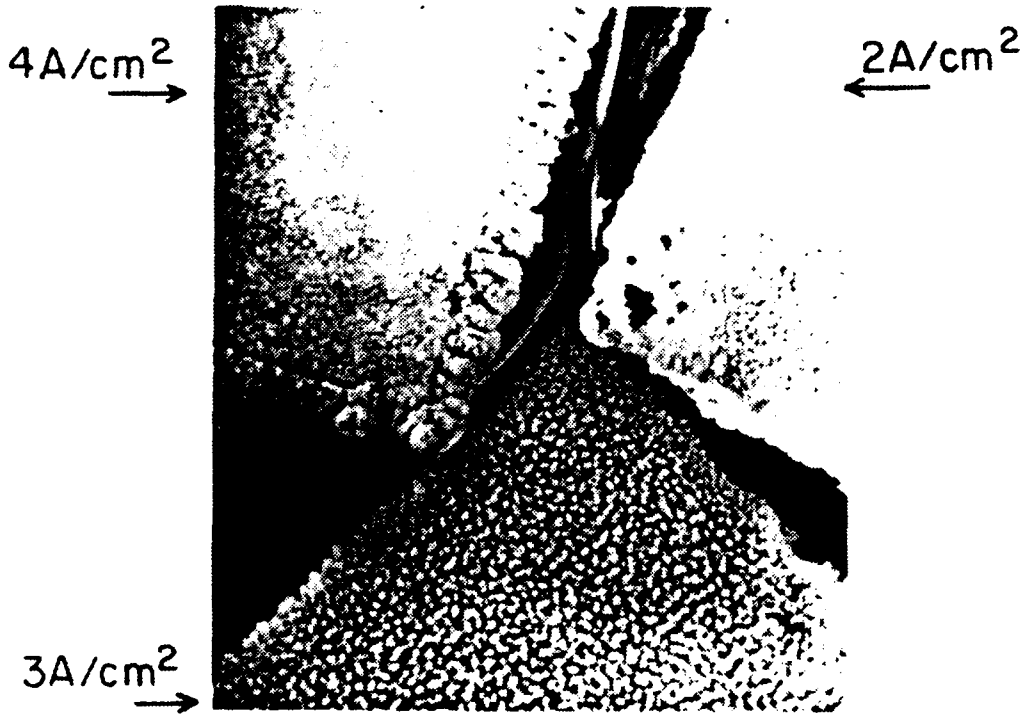

Fig. 34. SEM micrograph of cadmium electrodeposited on nickel at different current densities from alkaline-cyanide electrolyte.

eight coating thickness measurements at various places on the micrographs themselves. Where dendritic growth occurred, the thickness was measured from the substrate to the dendrite tips themselves. An average thickness and standard deviation were calculated for each picture. Different magnifications of the same cross section were not generally averaged together. Example thickness measurements, which are given in Table 17, show the porosity caused by current densities greater than 1 $A \cdot cm^{-2}$. At 0.10 $A \cdot cm^{-2}$ dense deposits of moderate grain size were obtained to a plating thickness of about 12.7 μm.

Table 17. Mean Plating Thickness and Grain Size Measurements for Typical Cadmium Cyanide Electrodeposits

Current Density ($A \cdot cm^{-2}$)	Plating Measured (μm)	Thickness Calculated (μm)	Mean Grain Size (μm)
0.1	35[a]	-	8.5
1.0	185	277	b
2.0	293	281	b
3.0	434	188	b
4.0	199	190	b
4.6	242	184	b
5.0	196	267	b

[a]Density and thickness measured from substrate to first growth inclusions in deposit.

[b]Dendritic growth; mean grain size not determinable.

APPENDIX IV

Techniques for Substrate Surface Preparation and Analysis of Electrodeposits

Substrate-Surface Preparation

To ensure tight adhesion of the cadmium deposits to the substrate and to reduce bath contamination, the mild-steel (Type 1018) cathodes were cleaned, prior to electrodeposition, as follows:

(1) Degreasing with trichlorotrifluoroethane.

(2) Anodic cleaning with either of the following:

Solution 1: Cyanide Solution

Sodium hydroxide	180 $g \cdot L^{-1}$
Sodium cyanide	120 $g \cdot L^{-1}$
Chelating agent (EDTA)	80 $g \cdot L^{-1}$
Current Density	30 $mA \cdot cm^{-2}$
Cleaning Time	2 min
Temperature	40°C

Solution 2: Commercial Alkaline-Cleaner

Kemtex 195 PG (MacDermid of Bristol, Inc.)	80 $g \cdot L^{-1}$
Current Density	60 $mA \cdot cm^{-2}$
Cleaning Time	2 min
Temperature	80°C

(3) Distilled water rinse.

(4) Acid dip in 1:1 solution of HCL to distilled water for 30 s.

(5) Distilled water rinse.

(6) Methanol rinse followed by drying with an air gun

(7) Immediate immersion in plating bath for use.

Preparation of Cross Sections of Plated Samples

In order to view grain structure and coating thickness, cross sections of the plated samples were made. A summary of the cross-sectioning and mounting procedure is as follows:

Copper Coating

Through observation, it was noted that rounding of the cadmium cross section occurred during grinding and polishing. To prevent rounding, the plated samples were coated in an electroless copper solution containing

Copper (II) sulfate $CuSO_4 \cdot 5H_2O$	30 $g \cdot L^{-1}$
Sodium potassium tartrate $KNaC_4H_4O_6 \cdot 4H_2O$	100 $g \cdot L^{-1}$
Sodium hydroxide NaOH	50 $g \cdot L^{-1}$
Sodium carbonate Na_2CO_3	32 $g \cdot L^{-1}$
Formaldehyde, 37% HCHO	29 $g \cdot L^{-1}$

The soaking time was 1-2 h to give a several micron thick layer of copper as a protective coating.

The plated sample was cut from the working electrode using a hack saw. The sample was mounted in an Isomet low-speed saw (Buehler Ltd.) to obtain a cross section with an average cutting time of three hours. This cut created a smooth surface which was then ready for grinding and polishing.

Mounting

The inside of a 1.250-in. dia mounting cup was coated with a releasing agent (Buehler Ltd.) and allowed to dry. As many as three cross-sectioned

samples, standing on edge, were placed in the cup. Twenty grams total of a 4:1 ratio of epoxy resin to hardener (LECO Corp.) was added to the cup. Copper balls were placed in the mounts to distinguish the samples. To remove trapped air bubbles, the epoxy was deaerated at room temperature in a vacuum desicator jar for 3-5 minutes. Each mount was labeled and allowed to harden for 6-8 h. After hardening, the mounts were individually labeled using a vibratory marker.

Grinding and Polishing

The surface to be viewed was ground using a Whirlimet Automatic Grinder/Polisher (Buehler Ltd.) Beginning with 80 grit SiC disks and working up to 600 grit, the surface was ground using water for a lubricant for 2-3 min. on each paper. Samples ground through 600-grit SiC were wiped dry with Kimwipes and viewed optically for uniformity of scratches. Those that had uneven or random scratch patterns were reground following the same procedure.

Polishing the sample was accomplished by a Syntron Lapping-Polishing Machine (Syntron Corp.) in a solution of 0.3-μm Al_2O_3 polish and kerosene. Those samples prepared properly through 600 grit SiC were polished for a minimum of one hour. The mounts were removed, rinsed in toluene, placed in 50 mL Pyrex beakers, immersed in toluene, and ultrasonically cleaned for 3-5 minutes (Cole-Parmer Ultrasonic Cleaner). The mounts were rinsed in toluene, methanol, and then dried with an air gun.

Etching

Before OM and SEM could be performed, the properly polished samples were chemically etched to reveal the grain structure. Electron diffraction studies have shown that grinding and polishing completely destroy the crystalline state several atomic distances below the surface. This metal layer (referred to as disturbed metal) possesses a higher free energy than the plastically

deformed metal layer below. In order to see the grain structure below, the disturbed metal layer must be removed through etching.

A chemical etchant preferentially attacks the disturbed metal, which is at high free energy, and the disturbed metal is easily removed. But when the etchant attacks the metal below this disturbed layer, the grain boundaries, which are at high free energies, are preferentially attacked. In an optical microscope with backscattered illumination, the grain boundaries appear as dark lines because they are light-scattering sources.

The etchant suitable for cadmium is Nital, a solution of nitric acid dissolved in pure ethanol. To optimize the etching, different etching times were tried using 1% HNO_3 dissolved in ethanol. Times exceeding five seconds produced a good cadmium-steel interface for SEM but produced a three-dimensional interface which was difficult to view by OM. The better etching times used were less than five seconds, which resulted in distinct cadmium-steel interfaces for both OM and SEM.

Etching was performed by dipping a cotton swab in the etchant and wiping the substrate in rapid strokes. The etchant was stopped by rinsing immediately in distilled water followed by methanol and drying with an air gun.

Optical Microscopy Instrumentation and Procedure

A Carl Zeiss Ultraphot II Research Metallograph was used for OM. A collimated white light source with a 7-A filament current supplied the bright-field illumination. A VG9 green filter (546 nm) corrected the lighting for chromatic aberration, which helped to increase image contrast. A simple polarizer rotatable to 360° allowed for phase contrast microscopy. Micrographs were made on 4 in. x 5 in. Kodak Polapan Type 52 film. The available magnifications were 630X, and 50X through 250X in 50X increments.

In most cases where the cadmium had no edge protection, rounding of the cadmium cross sections made focusing difficult at magnifications over 250X.

Scanning Electron Microscopy

For studying topography of both the cross sections and electrodeposited surfaces at higher magnifications and better resolution than optically possible, SEM was performed. The purpose of looking at the cross sections under SEM was to examine the tightness of the cadmium-substrate interface Microscopy of the deposited surfaces was done to examine crystallinity in surface growth as well as to estimate the relative grain size of the deposits. This was very important in the optimizing plating procedures.

A JEOL 35U scanning electron microscope was used. The range of the magnifications was 10X to 180,000X. Resolutions from 15 nm to 7 nm at a working distance of 39 mm to 15 mm, respectively, were possible. Sample mobility was provided by planar translation and angular tilt. Again, micrographs were made on 4 in. x 5 in. Kodak Type 52 film. An energy-dispersive x-ray spectrometer (EDXS) permitted elemental analysis over a specified spot less than 5 μm in diameter. An Ortec EEDS II computer analyzer system identified the EDXS data and reduced it qualitatively for CRT display. Before insertion into the SEM chamber, gold was chemically vapor-deposited with a Hummer II for 2 minutes (10 mA peak pulse-current) on all of the mounted cross section samples. This provided the necessary surface conductivity for SEM imaging of secondary electrons. Depending on the sample and preparation, maintaining good focus at 9000X on the cross sections was difficult. Where adhesion of the cadmium was poor, a grey spot on the micrograph was noticeable.

With the substrate in electrical contact with a holder, micrographs of the cadmium deposited surfaces were taken. Substrates from some nucleation

pulses were covered with gold to improve image resolution at 10,000X magnification. A working distance of 15 mm (not the standard 39 mm) and a 30° tilt were used in these instances. In most other nucleation samples, the substrate was tilted to 60° (working distance = 39 mm) in order to improve the image.

APPENDIX V

X-Ray Diffraction

Introduction

X-ray diffraction provides the simplest method for determining crystal structures and identifying compounds. For example, the crystal structure of cadmium, whose unit cell is shown in Fig. 35, is hexagonal close packed (hcp). The hcp structure has the tightest packing factor possible, with ideally 74% of the unit cell occupied by atoms. In the hcp system, the Miller-Bravais indices (hkil) are the reciprocals

$$\frac{1}{a}, \frac{1}{b}, -\frac{1}{a} + \frac{1}{b}, \frac{1}{c}$$

of the intersection of the real a, b, and, c axes with the crystallographic planes. The third index, i, is dependent on the first two by the relation $i = -(h + k)$. The indices listed in Table 18 specify the planes of strongest intensity for x-ray diffraction from hcp cadmium. The symmetry of the diffraction pattern and the relative spot intensities provide a positive means for crystal identification.

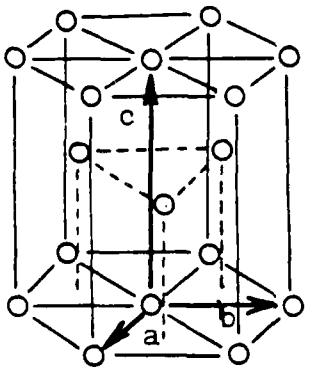

Fig. 35.

Hexagonal close-packed unit cell, c/a = 1.633 (ideally), $\angle$ ab = 120°.

Table 18. Major Cadmium Diffraction Peak Data

2θ (degrees)	d-spacing (A)	Relative Intensity I/Io	Miller-Bravais Indices, (hkil)
31.83	2.809	65	0002
34.74	2.580	32	1010
38.35	2.345	100	1011
47.81	1.901	32	1012

Debye-Scherrer Method

In order to determine the composition of the electrodeposited material, Debye-Scherrer x-ray powder diffraction was made on electrodeposits from both cyanide and fluoborate baths. Debye-Scherrer powder diffraction revealed large crystallites from the cyanide plating baths.

On the other hand, representative deposits from the two fluoborate baths showed ideal crystalline cadmium[13] powder photographs with α_1, α_2 resolution. This results from ideally sized crystallites which, at high Bragg angles, cause a geometrical splitting in the diffracted beam. Crystallites giving a powder photograph of this type are in the range of sizes 0.1 to 10 μm.[14]

X-Ray Diffractometry

In addition to powder diffraction studies, X-ray diffractometry was used to study diffraction peak height and half-widths (width at half height) of cadmium from both electrolytes. This was done to determine crystallite size of electrodeposits and preferred orientation.

Typical diffractometer traces for cadmium plated from alkaline cyanide Bath A (16 $g \cdot L,^{-1}$ Cd) and Bath B (32 $g \cdot L,^{-1}$ Cd) are shown in Figs. 36 through 39. Within instrumental and measurement errors, the d-spacing location of the peaks are those of cadmium (Table 18).

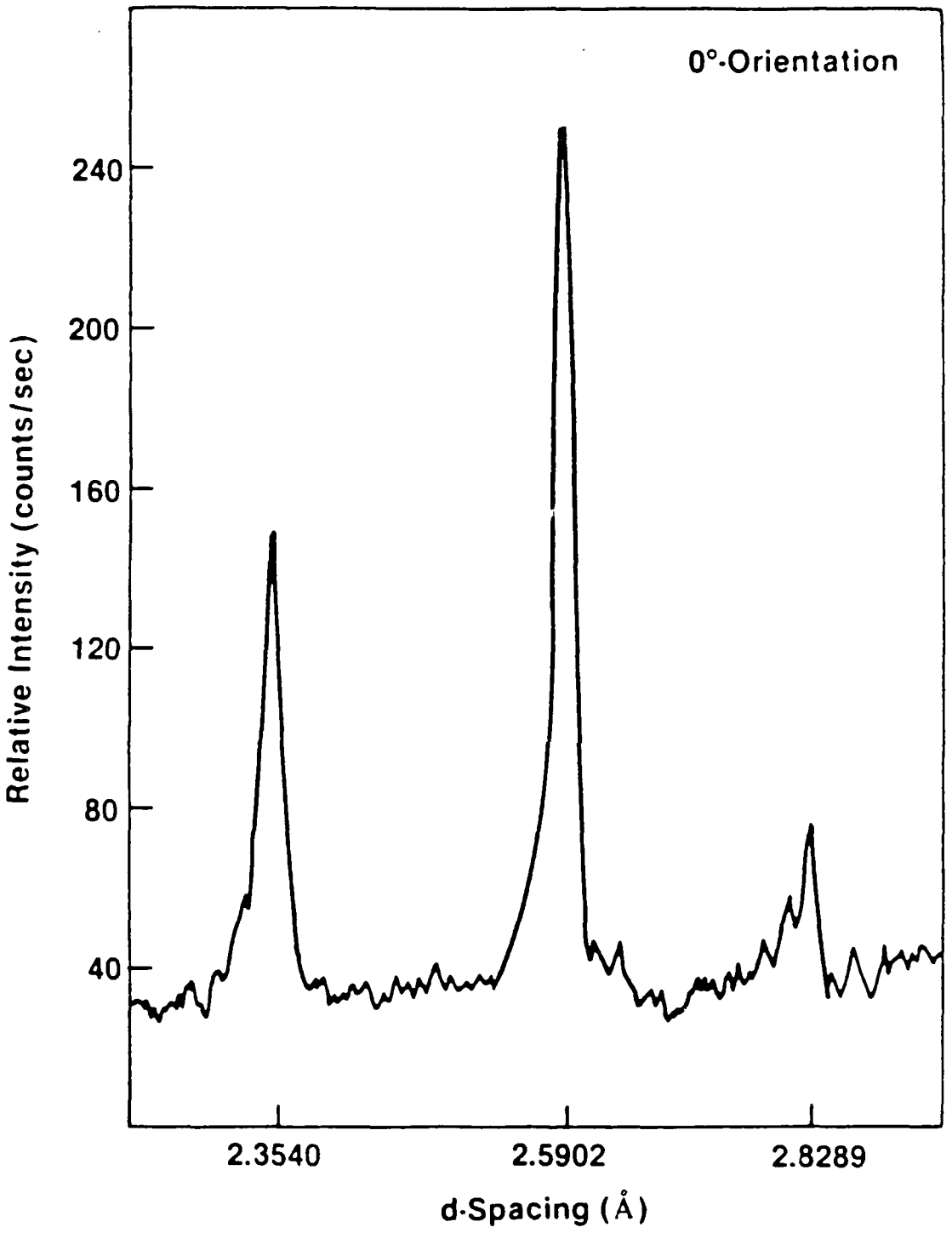

Fig. 36. X-ray diffraction pattern of cadmium electrodeposited on nickel from alkaline-cyanide electrolyte at 2 $A \cdot cm^{-2}$ DC (0^{o}-rotation).

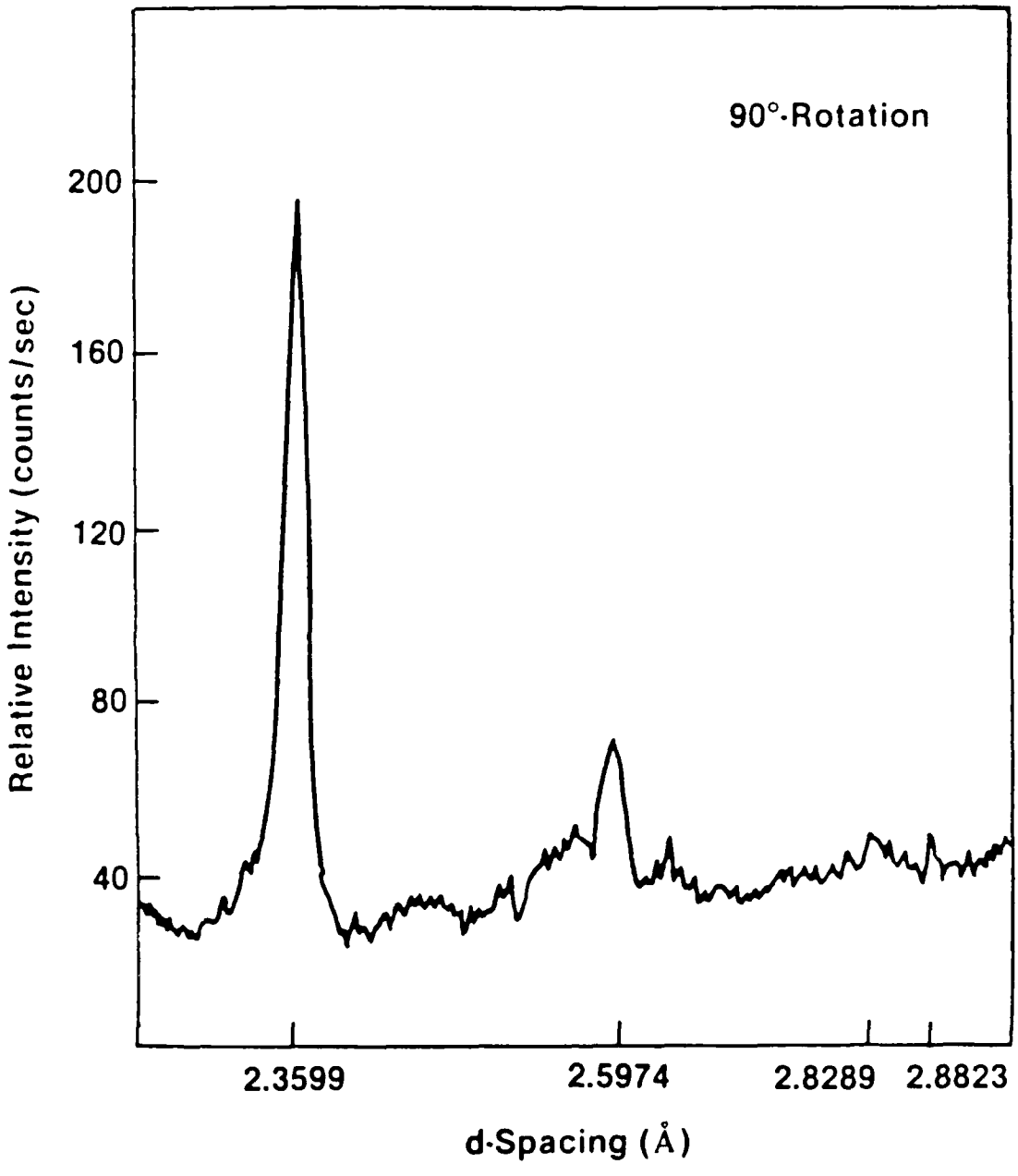

Fig. 37. X-ray diffraction pattern of cadmium electrodeposited on nickel from alkaline-cyanide electrolyte at 2 $A \cdot cm^{-2}$ DC (90^{o}-rotation).

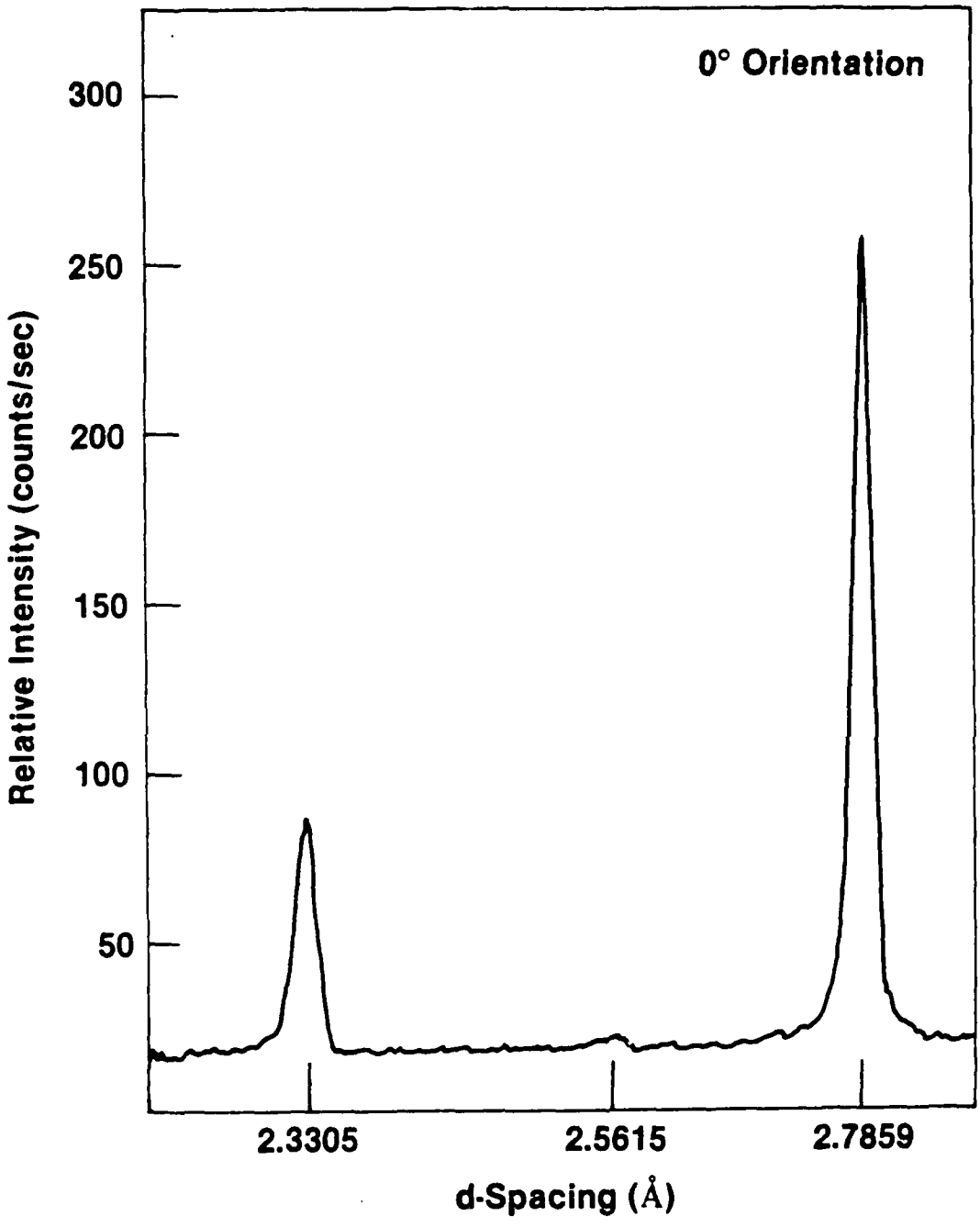

Fig. 38. X-ray diffraction pattern of cadmium electrodeposited on AISI 4340 steel from alkaline-cyanide (32 $g \cdot L^{-1}$ Cd) electrolyte at 15 $mA \cdot cm^{-2}$, (0^{o}-rotation). A similar pattern is seen at 180^{o} sample rotation.

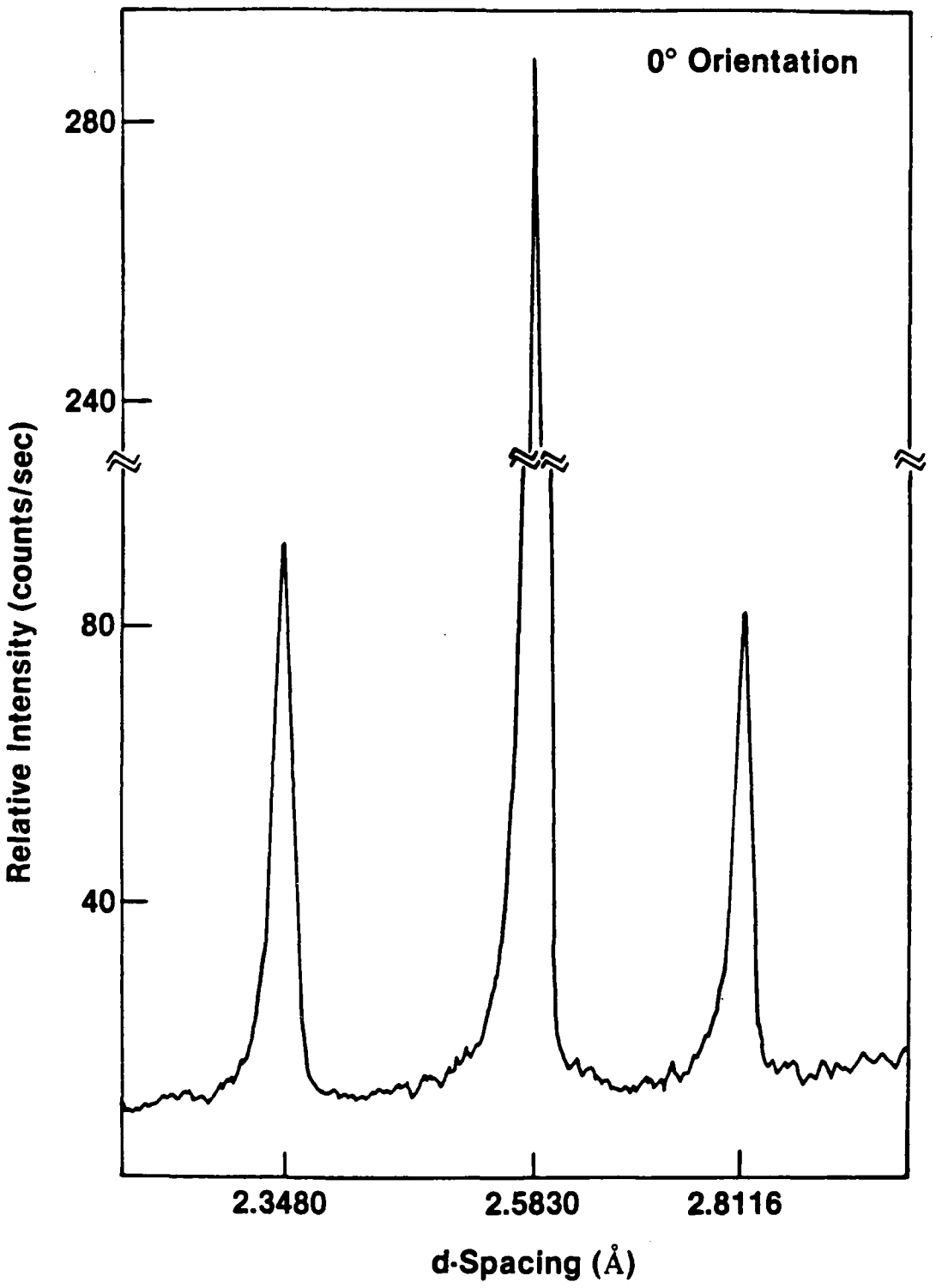

Fig. 39. X-ray diffraction pattern of cadmium electrodeposited on AISI 4340 steel from alkaline-cyanide electrolyte (31 $g \cdot L^{-1}$ Cd) at 4.3 $A \cdot cm^{-2}$.

The diffraction trace of each sample was run twice. After the first trace, the sample was repositioned and rerun at 90° or 180° rotation of the sample about a line normal to the center of its surface. Preferred orientation was evident from samples at all current densities from cyanide baths A and B. It is likely that some hydroxide was present, especially at higher current densities, where "burning" of the deposit may have occurred. Even the control electroplater's sample, plated at 15 $mA \cdot cm^{-2}$, shows preferred orientation.

Preferred orientation may result from the high current density, uniform electric field, and lack of inhibitors--all of which cause large (single-crystal) growth. Optical microscopy of the surface of the deposits from the cyanide electrolytes showed needle and plate-shaped large crystals growing perpendicular to the substrate. On the average, the needlelike or treelike growth had a definite orientation with growth on a preferred crystallographic plane. This result gives evidence that the preferred orientation was from the crystal growth and shape.

References

1. C. G. Interrante, "Basic Aspects of the Problems of Hydrogen in Steels," Am.Soc. of Metals, Proceedings of First Internat'l. Conf. on Current Solutions to Hydrogen Permeation in Steels, Washington, DC (1982) pp. 3-17.

2. H. H. Lee and M. M. Uhlig, "Corrosion Fatigue of High Strength Steels," Metal Trans. 3, 2949 (1972).

3. G. Wrangler, An Introduction to Corrosion and Protection of Metals, publisher, 19, pp. 108-119.

4. S. J. Ketcham, A Handbook of Protective Coatings for Military and Aerospace Equipment, NACE Publications, No. TPC 10, 43-48 (1983).

5. T. E. Such, Electroplating and Metal Finishing, 14, 115 (1961).

6. U.S. Patent 2,703,311, March 1 (1955).

7. T. Vargas, "Electrocrystallization of Chromium from Molten Salts," Ph.D. Thesis, University of London (1984).

8. K. I. Popov, M. D. Maksimovic, and B. M. Ocokoljic, "Fundamental Aspects of Pulsating Current Metal Electrodeposition: I. The Effect of Pulsating Currents on Surface Roughness and Porosity of Metal Deposits," Surface Technology, 99-109 (1983).

9. K. K. Popov, M. D. Maksimovic, and S. S. Djokic, "Fundamental Aspects of Pulsating Current Metal Electrodeposition: III. Maximum Practical Deposition Rate," Surface Technology, 14, 323-333 (1981).

10. I. Ohno, L. T. Lan, and S. Haruyama, Denki Dagaku, 52(11), 752 (1984).

11. F. A. Lowenheim, Electroplating, McGraw-Hill Book Co., Inc., New York, Table 17-7, Bath H, p. 406 (1978).

12. C. S. Barrett and T. B. Massalski, Structure of Metals (Pergamon Press, New York, 1980), 3rd revised ed., pp. 118-162.

13. Powder Diffraction File, Inorganic Phases (International Centre for Diffraction Data, 1984), File No. 5-0679.

14. L. V. Azaroff and M. J. Buerger, The Powder Method in X-ray Crystallography (McGraw-Hill Book co., Inc., New York, 1958), p. 256.

15. L. H. Van Vlack, Elements of Material Science and Engineering Addison-Wesley Publishing Co., Reading, MA, 4th ed., pp. 120-122 (1980).